Abstract

Designing FRP confined concrete columns requires reliable analytical tools that predict the level of performance and ductility enhancement. Finite element investigation is made for the purpose of exploring confinement mechanism of concrete columns wrapped in FRP. Numerical procedure is developed aiming at determining the type and thickness of FRP jacket needed to achieve a certain level of ductility enhancement.

This study presents defining displacement ductility factor of concrete columns subjected to axial load and lateral displacement based on a published recent study which developed a stress strain curve, which was used to obtain moment curvature relationship. Three sets of published experimental tests were used to validate the numerical procedure. Comparisons between predicted results obtained by using the proposed procedure and actual results of experimental tests proved the reliability of the proposed procedure. A Finite Element investigation is conducted through three models to explore confinement mechanism of concrete columns wrapped with FRP.

Acknowledgments

I am using this opportunity to express my gratitude to everyone who supported me throughout my masters. I am thankful for their aspiring guidance, invaluably constructive criticism and friendly advice during the project work. I am sincerely grateful to them for sharing their truthful and illuminating views on a number of issues related to the project.

I express my warm special thanks to **Dr. Mashhour Ghoniem** for his guidance through the production of the thesis and the honor to be under his supervision. Thanks to my supervisor **Dr. Abdelmoniem Yassin Sanad** for his useful instructions and support. A huge thanks and appreciation goes to **Dr. Moustafa Khalifa** for the huge effort, support and advice. No words can describe how grateful I am.

Thanks to all the people who encouraged me my Parents, my wife, my brother and sister and my friends.

Table of contents

Chapter 1 : Introduction 1

1.1 General 2

1.2 Research objectives 3

Chapter 2 : Background 5

2.1 Preamble 6

2.2 Basic structural properties 6

2.3 Seismic effect and design 8

2.4 Retrofit of existing structures with FRP 10

Chapter 3: Confinement Effect on Concrete 12

3.1 Confinement 13

3.2 Basic characteristics of confinement effect on concrete 13

3.3 Passive confinement by ties 14

3.4 Lateral confinement by jacketing 16

3.5 Lateral confinement by FRP jacketing 18

Chapter 4 : Numerical procedure and validation 21

4.1 Introduction 22

4.2 Numerical procedure 22

4.3 Numerical analysis output 29

4.4 Validation of the software 32

Chapter 5 : Parametric Study 43

5.1 Introduction 44

5.2 Parametric Study 45

Chapter 6 : FEA Investigation 75

6.1 Element types 76

6.2 Material properties 77

6.3 Cylinder model wrapped with FRP 77

6.4 Square model wrapped with FRP 79

6.5 Square column subjected to both axial and lateral loads 81

Chapter 7 : Summary and Conclusion 83

7.1 Summary 84

7.2 Conclusion 85

References 88

List of figures

FIG. 2-1 LOAD-DISPLACEMENT CURVE FOR A REINFORCED CONCRETE MEMBER 7
FIG. 2-2 VARIOUS APPLICATIONS OF FRP 11
FIG. 3-1 CONFINING EFFECT ON CONCRETE 13
FIG. 3-2 FULLY CONFINED AND UNCONFINED PARTS AT THE CROSS-SECTION LEVEL AND ALONG THE LENGTH OF THE MEMBER 15
FIG. 3-3 STEEL JACKET FOR CIRCULAR AND RECTANGULAR CROSS SECTION 17
FIG. 3-4 CONCRETE JAKET CROSS SECTION 18
FIG. 3-5- WRAPPING COLUMNS WITH FRP 18
FIG. 3-6 EFFECTIVE CONFINING AREA USED IN MODELLING FRP-CONFINEMENT OF RECTANGULAR RC SECTIONS. (CNR-DT200 2004) 20
FIG. 4-1 FLOW CHART STRESS-STRAIN RELATIONSHIP USING MANDER EQUATION 25
FIG. 4-2 STRAIN AND STRESS DISTRIBUTION AND RESULTANT OF THE INTERNAL FORCES 27
FIG. 4-3 COLUMN GEOMETRY AND DEFORMATION 27
FIG. 4-4 PREDICTION OF DISPLACEMENT DUCTILITY RATIO 29
FIG. 4-5 MOMENT CURVATURE OF CONCRETE COLUMN CONFINED WITH FRP 29
FIG. 4-6 FLEXURAL OVER STRENGTH VARIATION WITH JACKET THICKNESS 31
FIG. 4-7 DISPLACEMENT DUCTILITY FACTORS VARIATION WITH JACKET THICKNESS 31
FIG. 4-8 GEOMETRY AND STEEL CONFIGURATION OF SPECIMENS 33
FIG. 4-9 GEOMETRY AND LATERAL STEEL CONFIGURATION OF SPECIMENS 35
FIG. 4-10 GEOMETRY AND STEEL CONFIGURATION OF SPECIMENS 38
FIG. 4-11 COMPARISON BETWEEN ACTUAL AND PREDICTED VALUES OF $\mu\Delta$ 42
FIG. 5-1 SCHEMATIC FOR SQUARE AND RECTANGULAR SPECIMEN 45
FIG. 5-2 EFFECT OF AXIAL LOAD RATIO ON PLASTIC CURVATURE FOR DIFFRENT ASPECT RATIO AND CONCRETE STRENGTH AT 1 MM THICKNESS 49
FIG. 5-3 EFFECT OF AXIAL LOAD RATIO ON NORMALIZED PLASTIC CURVATURE FOR DIFFRENT ASPECT RATIO AND CONCRETE STRENGTH AT 1 MM THICKNESS 49
FIG. 5-4 EFFECT OF AXIAL LOAD RATIO ON NORMALIZED ULTIMATE CURVATURE FOR DIFFERENT ASPECT RATIO AND CONCRETE STRENGTH AT 1 MM THICKNESS 50
FIG. 5-5 EFFECT OF AXIAL LOAD RATIO ON ULTIMATE CURVATURE FOR DIFFERENT ASPECT RATIO AND CONCRETE STRENGTH AT 1 MM THICKNESS 50
FIG. 5-6 EFFECT OF AXIAL LOAD RATIO ON ULTIMATE MOMMENT FOR DIFFERENT ASPECT RATIO AND CONCRETE STRENGTH AT 1 MM THICKNESS 51
FIG. 5-7 EFFECT OF AXIAL LOAD RATIO ON NORMALIZED ULTIMATE MOMENT FOR DIFFERENT ASPECT RATIO AND CONCRETE STRENGTH AT 1 MM THICKNESS 51
FIG. 5-8 EFFECT OF AXIAL LOAD RATIO ON DISPLACEMENT DUCTILITY FACTOR FOR DIFFERENT ASPECT RATIO AND CONCRETE STRENGTH AT 1 MM THICKNESS. 52
FIG. 5-9 EFFECT OF AXIAL LOAD RATIO ON FLEXURAL OVER STRENGTH FOR DIFFERENT ASPECT RATIO AND CONCRETE STRENGTH AT 1 MM THICKNESS. 52
FIG. 5-10 M-PHI DIAGRAMS FOR DIFFERENT CONCRETE STRENGTH AND CROSS SECTION ASPECT RATIO AT AXIAL LOAD RATIO = 0.2 53
FIG. 5-11 NORMALIZED M-PHI DIAGRAMS FOR DIFFERENT CONCRETE STRENGTH AND CROSS SECTION ASPECT RATIO AT AXIAL LOAD RATIO = 0.2 53
FIG. 5-12 EFFECT OF AXIAL LOAD RATIO ON PLASTIC CURVATURE FOR DIFFERENT ASPECT RATIO AND STEEL REINFORCENEMET PERCENTAGE AT 1 MM THICKNESS. 56
FIG. 5-13 EFFECT OF AXIAL LOAD RATIO ON NORMALIZED PLASTIC CURVATURE FOR DIFFERENT ASPECT RATIO AND STEEL REINFORCEMENT PERCENTAGE AT 1 MM THICKNESS. 56
FIG. 5-14 EFFECT OF AXIAL LOAD RATIO ON NORMALIZED PLASTIC CURVATURE FOR DIFFERENT ASPECT RATIO AND STEEL REINFORCEMENT PERCENTAGE AT 1 MM THICKNESS. 57

FIG. 5-15 EFFECT OF AXIAL LOAD RATIO ON NORMALIZED ULTIMATE CURVATURE FOR DIFFERENT ASPECT RATIO AND STEEL REINFORCEMENT AT 1 MM THICKNESS. 57
FIG. 5-16 EFFECT OF AXIAL LOAD RATIO ON ULTIMATE MOMENT FOR DIFFERENT ASPECT RATIO AND STEEL REINFORCEMENT AT 1 MM THICKNESS. 58
FIG. 5-17 EFFECT OF AXIAL LOAD RATIO ON NORMALIZED ULTIMATE MOMENT FOR DIFFERENT ASPECT RATIO AND STEEL REINFORCEMENT AT 1 MM THICKNESS. 58
FIG. 5-18 EFFECT OF AXIAL LOAD RATIO ON DISPLACEMENT DUCTILITY FACTOR FOR DIFFERENT ASPECT RATIO AND STEEL REINFORCEMENT AT 1 MM THICKNESS. 59
FIG. 5-19 EFFECT OF AXIAL LOAD RATIO ON FLEXURAL OVER STRENGTH FOR DIFFERENT ASPECT RATIO AND STEEL REINFORCEMENT AT 1 MM THICKNESS. 59
FIG. 5-20 M-PHI DIAGRAMS FOR DIFFERENT STEEL REINFORCEMENT PRECENTAGE AND CROSS SECTION ASPECT RATIO AT AXIAL LOAD RATIO = 0.2 60
FIG. 5-21 EFFECT OF AXIAL LOAD RATIO ON PLASTIC CURVATURE FOR DIFFERENT ASPECT RATIO AND FRP THICKNESS. 63
FIG. 5-22 EFFECT OF AXIAL LOAD RATIO ON NORMALAIZED PLASTIC CURVATURE FOR DIFFERENT ASPECT RATIO AND FRP THICKNESS. 63
FIG. 5-23 EFFECT OF AXIAL LOAD RATIO ON ULTIMATE CURVATURE FOR DIFFERENT ASPECT RATIO AND FRP THICKNESS. 64
FIG. 5-24 EFFECT OF AXIAL LOAD RATIO ON NORMALIZED ULTIMATE CURVATURE FOR DIFFERENT ASPECT RATIO AND FRP THICKNESS. 64
FIG. 5-25 EFFECT OF AXIAL LOAD RATIO ON ULTIMATE MOMENT FOR DIFFERENT ASPECT RATIO AND FRP THICKNESS.65
FIG. 5-26 EFFECT OF AXIAL LOAD RATIO ON NORMALIZED ULTIMATE MOMENT FOR DIFFERENT ASPECT RATIO AND FRP THICKNESS. 65
FIG. 5-27 EFFECT OF AXIAL LOAD RATIO ON DISPLACEMENT DUCTILITY FACTOR FOR DIFFERENT ASPECT RATIO AND FRP 66
FIG. 5-28 EFFECT OF AXIAL LOAD RATIO ON FLEXURAL OVER STRENGTH FOR DIFFERENT ASPECT RATIO AND FRP THICKNESS. 66
FIG. 5-29 FIG. 5 20 M-PHI DIAGRAMS FOR DIFFERENT FRP THICKNESS AND CROSS SECTION ASPECT RATIO AT AXIAL LOAD RATIO = 0.2 67
FIG. 5-30 EFFECT OF AXIAL LOAD RATIO ON PLASTIC CURVATURE FOR DIFFERENT ASPECT RATIO AND FRP TYPES AT 1MM THICKNESS. 70
FIG. 5-31 EFFECT OF AXIAL LOAD RATIO ON NORMALIZED PLASTIC CURVATURE FOR DIFFERENT ASPECT RATIO AND FRP TYPES AT 1MM THICKNESS. 70
FIG. 5-32 EFFECT OF AXIAL LOAD RATIO ON ULTIMATE CURVATURE FOR DIFFERENT ASPECT RATIO AND FRP TYPES AT 1MM THICKNESS. 71
FIG. 5-33 EFFECT OF AXIAL LOAD RATIO ON NORMALIZED ULTIMATE CURVATURE FOR DIFFERENT ASPECT RATIO AND FRP TYPES AT 1MM THICKNESS. 71
FIG. 5-34 EFFECT OF AXIAL LOAD RATIO ON ULTIMATE MOMENT FOR DIFFERENT ASPECT RATIO AND FRP TYPES AT 1MM THICKNESS. 72
FIG. 5-35 EFFECT OF AXIAL LOAD RATIO ON NORMALIZED ULTIMATE MOMENT FOR DIFFERENT ASPECT RATIO AND FRP TYPES AT 1MM THICKNESS. 72
FIG. 5-36 EFFECT OF AXIAL LOAD RATIO ON DISPLACEMENT DUCTILITY FACTOR FOR DIFFERENT ASPECT RATIO AND FRP TYPES AT 1MM THICKNESS. 73
FIG. 5-37 EFFECT OF AXIAL LOAD RATIO ON FLEXURAL OVER STRENGTH FOR DIFFERENT ASPECT RATIO AND FRP TYPES AT 1MM THICKNESS. 73
FIG. 5-38 M-PHI DIAGRAMS FOR DIFFERENT FRP TYPES AND CROSS SECTION ASPECT RATIO AT AXIAL LOAD RATIO = 0.2 74
FIG. 6-1 C3D8 3D BRICK ELEMENT STRUCTURE 76
FIG. 6-2 C3D6 3D PRISM ELEMENT 76
FIG. 6-3 CONCRETE CYLINDER WRAPPED WITH FRP BEFORE AND AFTER APPLICATION OF AXIAL LOAD 78
FIG. 6-4 STRESS STRAIN CURVE FOR THE SPECIMEN USED FOR VALIDATION 78

FIG. 6-5 SQUARE COLUMN WRAPPED WITH FRP 79
FIG. 6-6 VERTICAL STRESS DISTRIBUTION FOR (A) CONFINED COLUMN AND (B) UNCONFINED ONE 80
FIG. 6-7 THE SUMMATION OF LATERAL STRESSES ACROSS THE CROSS SECTION (0➔270 MPA) 80
FIG. 6-8 EFFECTIVELY CONFINED CONCRETE IN SQUARE COLUMN [20] 81
FIG. 6-9 COLUMN SUBJECTED TO LATERAL LOAD AND CONFINED WITH FRP 81
FIG. 6-10 M-PHI DEDUCED FROM NUMERICAL AND FE ELEMENT MODELS FOR THE COLUMN 82

List of tables

TABLE 4-1 INPUT VALUES NEEDED BY SOFTWARE FOR CALCULATION 30
TABLE 4-2 PROPERTIES OF FRP COMPOSITES 32
TABLE 4-3 PROPERTIES OF STEEL REINFORCEMENT 33
TABLE 4-4 DETAILS OF TEST SPECIMENS 33
TABLE 4-5 EXPERIMENTAL VALUES AND CALCULATED CAPACITIES 34
TABLE 4-6 MEMBER AND SECTION DUCTILITY VALUES 34
TABLE 4-7 DETAILS OF TEST SPECIMENS 36
TABLE 4-8 MECHANICAL PROPERTIES OF STEEL BARS 36
TABLE 4-9 DETAILS OF TEST COLUMNS 37
TABLE 4-10 HATEM SELIEM DETAILS OF SPECIMEN 38
TABLE 4-11 SUMMARY OF HATEM SEILIM EXPERIMENTAL ANALYSIS 39
TABLE 4-12 SUMMARY OF LACOBUCCI ET AL. EXPERIMENTAL ANALYSIS 40
TABLE 4-13 SUMMARY OF MUHAMMAD S.MEMON ET AL EXPERIMENTAL ANALYSIS 41
TABLE 4-14 COMPARISON OF RESULTS 42
TABLE 5-1 CROSS SECTION CONFIGURATIONS SUMMARY 46
TABLE 5-2 FRP MATERIAL PROPERTIES 47
TABLE 5-3 CROSS SECTION CONFIGURATIONS USED FOR DEMONSTRATING THE EFFECT OF F_{CU} 47
TABLE 5-4 EFFECT OF INCREASING FCU PARAMETER 48
TABLE 5-5 CROSS SECTION CONFIGURATIONS USED TO DEMONSTRATE THE EFFECT OF AS% 54
TABLE 5-6 EFFECT OF AS % PARAMETER 55
TABLE 5-7 CROSS SECTIONS CONFIGURATION USED FOR 61
TABLE 5-8 EFFECT OF INCREASING JACKET THICKNESS ON CONFINED CONCRETE 62
TABLE 5-9 CROSS SECTIONS CONFIGURATION USED FOR 68
TABLE 5-10 FRP SYSTEM PROPERTY INFLUENCE ON CONFINED CONCRETE 69
TABLE 6-1 PROPRTIES OF COLUMN 82

Chapter1

INTRODUCTION

1.1 General

Recent seismic events around the world continue to underline the importance of seismic retrofit and strengthening of existing reinforced concrete structures. There is a demand for a practical and cost effective design approach for the remedial and retrofitting solution.

Confining wraps or jackets to retrofit existing concrete columns represent a principal application of fiber reinforced polymers (FRP). In the last decade, passive confinement of concrete columns was the focus of research and investigation, exploring all the aspects of technique.

Compressive strength and ductility can be enhanced using an FRP jacket with the fibers oriented in the hoop direction to confine the concrete column. To achieve safe and economic designs of the FRP jackets, designers need to have an effective accurate tool to be able to predict and assess the behavior of such columns and then they can recommend the appropriate retrofitting specifications based on knowledge of desired seismic energy to dissipate.

In high seismicity regions, engineers find that FRP jackets can be used in improving the shear strength and ductility capacity of reinforced concrete members, a tempting structural rehabilitation option. When the plastic hinge region in an RC column is wrapped with FRP, development of ductile flexural behavior occurs. This type of behavior is desirable for RC columns subjected to cyclic lateral loads such as those that occur in a seismic event.

In circular sections, applied axial load leads to radial lateral displacement due to Poisson effect meaning that the lateral expansion is the same in all directions around the section. This leads to equal lateral pressure on the jacket and that activates the confining effect of the FRP jacket in the hoop direction and causes radial confining forces or else hydrostatic confining pressure. This pressure results in a stress state which is the same in every point of the section.

In rectangular sections, the confining effect can confine the lateral displacement of corner parts but cannot confine the displacement outside the central part of the sides. This is due to the character of the rectangular section which results in different stress-state in every point of the section. This makes the circular section more efficient if needed to be confined compared to the rectangular section, thus,

there is a need of shape modification of the rectangular sections to get maximum benefit from confinement by FRP jacket.

Confining columns with FRP wraps causes an increase in the confined concrete peak stress with reference to unconfined concrete due to elastic Poisson's lateral stresses, followed by nonlinear dilatational behavior of concrete due to pre-peak cracking. Then, it increases the post peak ductility and ultimate strength of the concrete column developing a pseudo ductile plateau [1].

Ductility is needed regarding seismic retrofitting because it increases lateral displacement (energy dissipation) and allows stress redistribution and provides warning of impending failure. Steel-reinforced concrete beams are under-reinforced by design, so that failure is initiated by yielding of the steel reinforcement (warning), followed, after considerable deformation at no substantial loss of load carrying capacity, by concrete crushing and ultimate failure. This mode of failure is ductile and is guaranteed by designing the tensile reinforcement ratio to be substantially below (ACI 318 requires at least 25 % below) the balanced ratio [2], which is the ratio at which steel yielding and concrete crushing occur simultaneously. The reinforcement ratio thus provides a metric for ductility, and the ductility corresponding to the maximum allowable steel reinforcement ratio provides a measure of the minimum acceptable ductility.

1.2 Research objectives

The objectives of the current research are to investigate the seismic behavior of square and rectangular columns retrofitted with FRP jackets and to present a design approach for such a type of retrofitting based on numerical analysis and validated by experimental results. This thesis includes 6 more chapters added to this chapter. Chapter 2 gives an introduction to seismic action and retrofitting, also it includes the basic structural properties and finally it introduces the FRP as a material. Chapter 3 explains the confinement effect on concrete by ties and FRP on rectangular and circular columns. Finally it gives how confinement can be achieved practically. In chapter 4, introduces the methodology for predicting displacement ductility factor after presenting former work defining stress strain curve and moment curvature diagram .Also the numerical procedure is validated by comparison of the results with experimental work. Chapter 5 is a parametric study using the numerical procedure shown in chapter 4. The studies are used to demonstrate the effect of each design

variable on the cross section's needed FRP wrapping thickness required for ductility enhancement. Chapter 6 is a finite element investigation using ABAQUS [3] through three different models. Chapter 7 includes summary and conclusions for the research.

Chapter 2
BACKGROUND

2.1 Preamble

Many existing structures located in seismic regions are inadequate based on current seismic design codes. In addition, a number of major earthquakes during recent years have underscored the importance of retrofitting and rehabilitation to reduce seismic effect and losses. Seismic retrofitting of existing structures is one of the most effective methods of reducing this effect. In recent years, a significant amount of research has been devoted to the study of various retrofitting techniques to enhance the seismic performance of RC structures. One of these techniques is RC columns confinement with FRP wraps. This chapter presents information related to basic properties of structural elements, a brief explanation of seismic action, its causes and effects, design performance objective and seismic design factors. It also includes a general overview about column retrofitting methods and finally, the FRP material properties are discussed.

2.2 Basic structural properties

2.2.1 Stiffness

Stiffness is a property to be used to quantify and control the deformation under the action of a certain force. Relationships for computing stiffness are readily established from first principles of structural mechanics using member's geometry, material properties, and members end conditions. In reinforced concrete structures, these relationships are not quite simple but can be achieved using some assumptions. A typical relationship between load and displacement, describing the response of a reinforced concrete element subjected to monotonically increasing load, is shown in Fig. 2-1. For design purposes, the real response may be approximated to bilinear relationship, idealized response, where S defines the yield strength of the member. The slope of the idealized linear elastic response, $K=S_y / \Delta_y$, is used to quantify stiffness. This should be based on the effective secant stiffness of the real load-displacement curve at a load of $O.75S_y$ as shown in the figure.

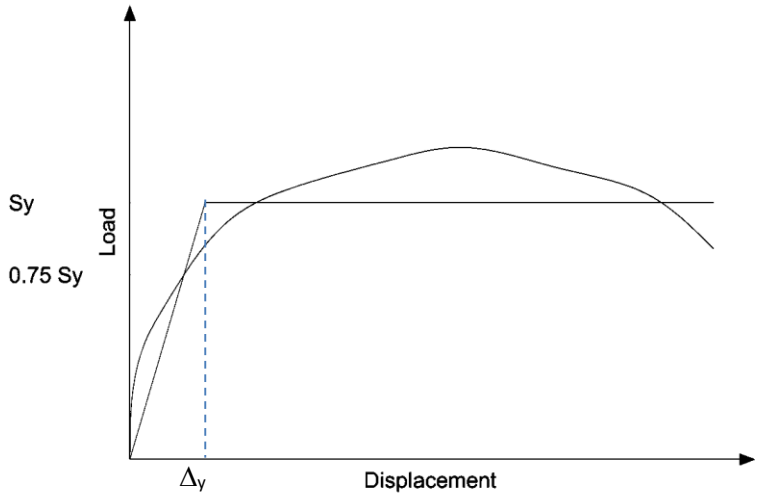

Fig. 2-1 - Load-Displacement curve for a reinforced concrete member

2.2.2 Ductility

Ductility sometimes termed toughness is the property of being able to deform through several cycles of displacements much larger than the yield displacement, without significant strength degradation. If the strength or stiffness degrade excessively, the response displacements increase significantly beyond those corresponding to elastic response and the structure may collapse.

Also ductility is often defined mathematically as the ratio of deformation at a given response level to deformation at yield response. Displacement expected during the design-level earthquake is the maximum expected displacement ductility factor which is defined as

$$\mu_\Delta = \frac{\Delta_m}{\Delta_y} \qquad 2\text{-}1$$

Where μ_Δ is the displacement ductility factor, Δ_m is the maximum displacement, Δ_y is the yield displacement.

Although the ductility ratio defined in equation 2-1 refers to displacements, curvature ductility ratios relating to maximum and yield curvatures at critical sections are also frequently defined. Also other measures of ductility including rotational ductility and strain ductility are sometimes useful indicators of the level of inelastic response.

As discussed in the introduction, ductility increases lateral displacement (energy dissipation) and allows stress redistribution and provides warning of impending failure of seismic action.

2.3 Seismic effect and design

2.3.1 Cause and effect

When the earth shakes, due to movements of plates below the earth's crust, it is known as an earthquake. Earthquakes are natural disasters, which can kill thousands of people in an instant and can destroy cities and countries. The vibrations during an earthquake have the potential to wreak havoc and cause destruction beyond imagination, because they cannot be predicted. Earthquakes are followed by many aftershocks which can be of a low magnitude, and sometimes equally destructive.

When the ground shakes, buildings respond to the accelerations transmitted from the ground through the structure's foundation. The inertia of the building (which wants to stay at rest) can cause shearing of the structure which can concentrate stresses on the weak walls or joints in the structure, resulting in failure or perhaps total collapse. The type of shaking and the frequency of shaking depend on the structure. Tall buildings tend to amplify the motions of longer period motions when compared with short buildings. Each structure has a resonance frequency that is characteristic of the building. Predicting the precise behavior of buildings is complicated.

A typical RC building is made of horizontal members (beams and slabs) and vertical members (columns and walls), and supported by foundations that rest on ground. The system comprising of RC frame participates in resisting the earthquake forces. Earthquake shaking generates inertia forces in the building, which are proportional to the building mass. Since most of the building mass is present at floor levels, earthquake induced inertia forces primarily develop at the floor levels. These forces travel downwards – through slabs and beams to columns and walls, and then to foundations from where they are dispersed to ground. As inertia forces accumulate downwards from the top of the building, the columns and walls at lower story experience higher earthquake- induced forces and are therefore designed to be stronger than those in story above.

2.3.2 Performance design objectives

Serviceability is the basic performance objective in order to prevent impediments to continued functional use. In order to ensure this, the serviceability limit state is selected for the structure. This is the limit state corresponding to the so-called light or no damage levels such that it is possible after an earthquake to have almost no preconditions needed for continued use. The earthquake intensity used for investigating the serviceability limit state is so-called moderate or medium earthquake level, which is likely to be encountered one or more times during the expected service life. Depending on the level of earthquake activity, it is possible to have different levels for each region.

Reparability (Restorability) is one of the performance objectives in order to control the level of damage. The limit state corresponding to this is called the repair limit state, or the damage control limit state. Ideally, this is established by quantifying the damage level of structural and non-structural members such that economically allowable repair is possible, by taking into account the repair costs required after the earthquake. In this manner, the reparability limit state is the objective indicating the ease of restoring the diminished performance caused by the earthquake effects during the building service life as well as restoring the performance after earthquake damage back to the original basic performance objectives (safety and serviceability).

Safety is the performance objective for human life protection, corresponding to the ultimate limit state or the safety limit state of a structure. Therefore, the design objective is to be able to bare loads and not to collapse. In terms of structural damage, the limit state is just before collapse due to severe damage.

2.3.3 Seismic design factors

The following factors affect and are affected by the design of the building. It is important that the design team understands these factors and deal with them prudently in the design phase [4].

Torsion is caused by uneven mass distribution. objects and buildings have a center of mass, a point by which the object (building) can be balanced without rotation occurring. If the mass is uniformly distributed then the geometric center of the floor and the center of mass may coincide. Uneven mass distribution will position the center of mass outside of the geometric center causing "torsion" generating stress

concentrations. A certain amount of torsion is unavoidable in every building design. Symmetrical arrangement of masses, however, will result in balanced stiffness against either direction and keep torsion within a manageable range.

Damping is the rate at which natural vibration is absorbed, buildings in general are poor resonators to dynamic shock and dissipate vibration by absorbing it.

Ductility is the characteristic of a material (such as steel) to bend, flex, or move, but fails only after considerable deformation has occurred.

Strength is a property of a material to resist and bear applied forces within a safe limit. Stiffness of a material is a degree of resistance to deflection or drift (drift being a horizontal story-to-story relative displacement).

Building Configuration defines a building's size and shape, and structural and nonstructural elements. Building configuration determines the way seismic forces are distributed within the structure, their relative magnitude, and problematic design concerns.

Knowledge of the building's torsion, damping, ductility, strength, stiffness, and configuration can help one determine the most appropriate seismic retrofitting techniques used.

2.3.4 Seismic retrofitting

Seismic retrofitting is the modification of existing structures to make them more resistant to seismic activity, ground motion, or soil failure due to occurrence of earthquakes.

Retrofitting of existing structures accounts for a major portion of the total cost of hazard mitigation. Thus, it is of critical importance that the structures that need seismic retrofitting are identified correctly, and an optimal retrofitting is conducted in a cost effective fashion. Once the decision is made, seismic retrofitting can be performed through several methods with various objectives such as increasing the load, deformation, and/or energy dissipation capacity of the structure.

2.4 Retrofit of existing structures with FRP

The retrofit of existing reinforced concrete structures has always been a crucial field where civil engineering has to give solutions. Despite the natural aging and damage of structures and materials, there are many other reasons that make the structural intervention necessary, like the change of use of a structure, the insufficient

initial design or bad performance of design during construction, the environmental effects, the lack of well preservation of the structure and finally and most importantly, random loading like earthquakes or fire or impact effects.

This need for renovation and rehabilitation of structures has led to seeking of new materials which can make the intervention easier and more effective. FRP belongs to this new generation of materials. Generally, we can limit the ways of retrofitting with those materials in two categories. First, are the externally bonded (EBR) FRPs usually in the form of laminates or rovings. And second, the (NSM) FRPs which are the near surface FRP mounted into superficial structural members (grooves) as shown in Fig. 2-2.

NSM **Laminates for flexure** **FRP wraps**

Fig. 2-2 Various applications of FRP

Chapter 3

CONFINEMENT EFFECT ON CONCRETE

3.1 Confinement

Confinement is the prevention of structural element to expand laterally as a result of Poisson ratio, due to axial load or bending moment on structural element. Confinement is desired because it increases strength of element, also it has a great function in increasing ductility thus enhancing the resistance to earthquakes as discussed in the previous chapter. Confinement can be achieved in an active way or passive one, where the first is introducing lateral pressure to the element and the second is letting Poisson's ratio responsible for the lateral pressure. Various techniques to confine columns are sources of research. In this chapter, confinement will be discussed and a comparison between a three types of confinement jackets will be made.

3.2 Basic characteristics of confinement effect on concrete

The stress strain relationship of concrete loaded monotonically under short-term, with increasing uniaxial compressive loading shows gradual degradation in stiffness, caused by development of micro cracks. The failure of concrete is a result of the continuously increasing rate propagation of those cracks. The presence of passive confining reinforcement has a crucial effect on this behavior of concrete. By doing so, it keeps the cracked pieces of concrete together, limits the progress of expansion and therefore it delays the upcoming failure. The result is that concrete can develop high deformations in the direction of loading without loss of strength. Thus, the stress strain curve obtained shows characteristics similar to those of an elasto-plastic material as shown in Fig. 3-1 [1].

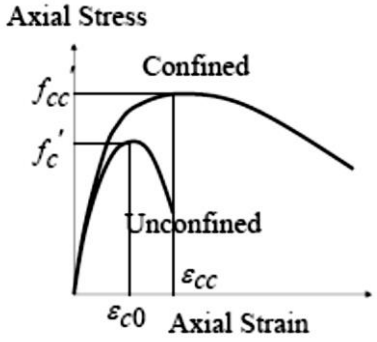

Fig. 3-1 Confining effect on concrete

3.2.1 Behavior under lateral hydraulic pressure

The improvement through confinement is more intense when the transversal compression stresses are applied actively, like for example by hydraulic pressure. Classical experimental study is the research of Richart, et al [5]. The basic result of this research is valid up to nowadays, and has been confirmed theoretically too. The increase in the strength and deformability of concrete under hydrostatic pressure is represented in the following equations:

$$f_{cc} = f_{co} + k_1 . f_1 \quad 3\text{-}1$$

$$\varepsilon_{cc} = \varepsilon_{co} \cdot \left(1 + k_2 \cdot \frac{f_1}{f_{co}}\right) \quad 3\text{-}2$$

where f_{cc} and ε_{cc} are the maximum concrete stress and the corresponding strain respectively, under the lateral fluid pressure f_l . While f_{co} & ε_{co} are unconfined concrete strength and corresponding strain respectively, and k_1 , k_2 are coefficients that are function of the concrete mix and the lateral pressure. Richart et al [5] found that the averaged value of the coefficient k_1 is equal to 4.1 and k_2=5k_1

3.2.2 Behaviour under biaxial stress condition

In the case of bi-directional stress state, concrete compressive strength increases with lateral compressive (confining) stress but decreases with lateral tensile stress [6].

3.3 Passive confinement by ties

In the case of triaxial stress state, the concrete strength and ductility increases. When stirrups are used in combination with the longitudinal reinforcement, both limit the expansion of concrete (passive confinement). This kind of confinement affects the behavior of the material after the appearance of the internal cracking which results in the initiation of expansion.

Confinement with circular spirals is more effective than of that with closed orthogonal or tetragonal ties. This is because circular spirals, due to their shape, create continuous confining pressure in all the application area. On the contrary, the orthogonal or tetragonal ties allow some expansion of concrete due to flexural behaviour of their sides which result in unconfined parts of the section near the central

parts of the sides of the specimen. Same unconfined parts are observed also between two successive stirrups Fig. 3-2 shows various types of confinement using ties.

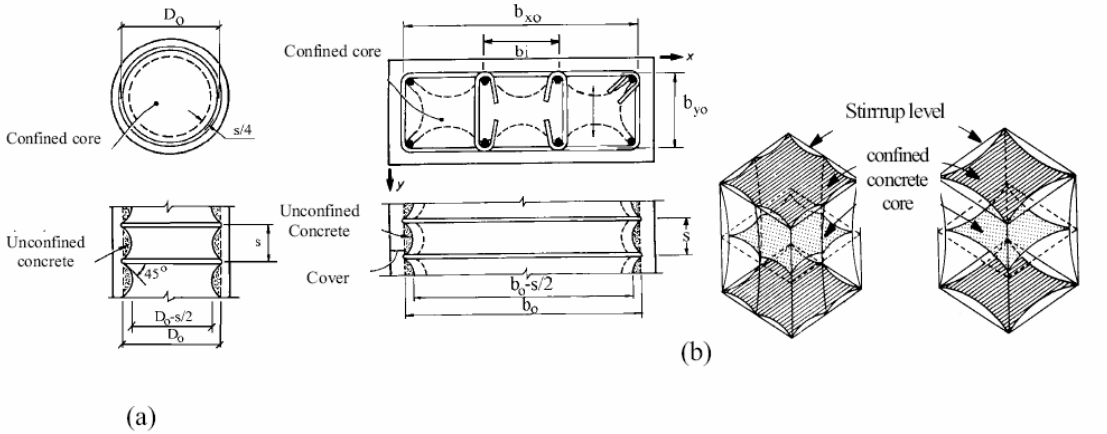

Fig. 3-2 Fully confined and unconfined parts at the cross-section level and along the length of the member a) circular ties b) rectangular ties

3.3.1 Parameters affecting the final shape of stress strain curve of confined concrete

1) The volumetric ratio (ρ_w) where ρ_w is the fraction of the volume of ties to the volume of the confined core of the section (volume of the solid bounded by the external tie).

2) The yield strength of the transversal reinforcement (f_y). Steel stirrups with higher yield strength can impose higher confining forces.

3) Spacing of ties (s). Smaller spacing of stirrups increases the imposed confinement due to reduction of the area of the unconfined part of the member.

4) The shape and the configuration of the stirrups. Depending on the shape and the configuration of the ties used, it is possible to reduce to the minimum the unconfined parts of the section which results in increase in the final strength and ductility.

5) The longitudinal reinforcement which also contributes to the development of confinement (raise resistance to the lateral expansion of the confined core). This contribution is proportional to the volumetric percentage of the longitudinal reinforcement (ρ_l) and the diameter of the steel bars (Φ_l).

6) Concrete strength (f_c). Low strength concrete appears to be more ductile as a material compared to higher strength concrete.

7) The type and the rate of loading. [1]

3.4 Lateral confinement by jacketing

Confinement can be achieved by jacketing, which is wrapping the column with another material that prevents it from expanding. This induces lateral passive pressure due to Poisson ratio. Jackets can be made from concrete, steel or FRP [7].

3.4.1 Steel Jacketing.

The procedure was originally developed for circular columns. Two half shells of steel plate rolled to a radius of 12.5 to 25 mm larger than the column radius are positioned over the area to be retrofitted and are site-welded to provide a continuous tube with a small annular gap around the column. This gap is grouted with a pure cement grout, after flushing with water. Typically, a space of about 50 mm is provided between the jacket and any supporting member (footing or cap beam), to avoid the possibility of the jacket acting as compression reinforcement by bearing against the supporting member at large drift angles. This is to avoid excessive flexural strength enhancement of the plastic hinge region, which could result in increases in moments and shears in footings and cap beams under seismic response. The jacket is effective in passive confinement. The level of confinement induced depends on the hoop strength and stiffness of the steel jacket.

For rectangular columns, the recommended practice is to use an elliptical jacket that provides a continuous confining action similar to that for a circular column but with a confining stress potential that varies around the circumference because of the continuously changing curvature of the jacket. The space between the jacket and column is filled with normal unmodified concrete rather than grout. Fig. 3-3 shows steel jacket for circular and rectangular cross sections.

Rectangular steel jackets on rectangular columns are not recommended. Although these can be expected to be fully effective for shear strength enhancement, a column retrofitted for shear will normally also require enhanced flexural ductility, which will not be provided by the steel jacket except at the corners, since there will be little restraint of lateral dilation of the core provided by bending of the jacket. Thus confinement for enhanced compression strain capacity or improved lap-splice performance is unlikely to be effective. Tests on various designs of stiffened rectangular jackets have shown them to be significantly less effective than elliptical jackets [8].

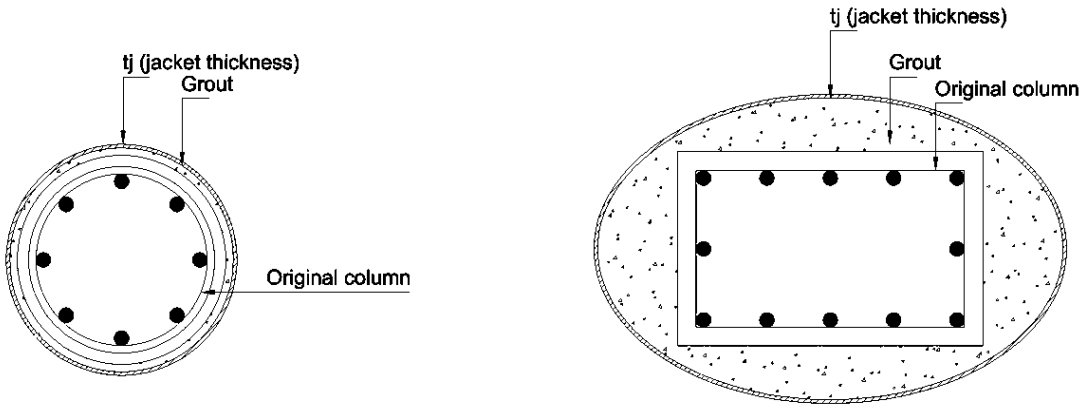

Figure 3-3 steel jacket for circular and rectangular cross section

3.4.2 Concrete Jacketing.

Addition of a relatively thick layer of reinforced concrete in the form of a jacket around the columns can be used to enhance flexural strength, ductility and shear strength of columns. By doweling the longitudinal reinforcement of the jacket into the footing with sufficient anchorage length to develop the reinforcement strength, the column flexural strength can be enhanced, although this must generally be accompanied by footing retrofit measures to enhance footing flexural and shear strength sufficiently to ensure that plastic hinging develops in the column.

Enhanced confinement of circular columns is relatively easy to achieve with a concrete jacket, by use of close-spaced hoops or a spiral of small pitch. However, unless the concrete jacket is made of elliptical or circular shape, it is difficult to achieve effective confinement by a rectangular concrete jacket. Longitudinal bars in the midregion of each face will be susceptible to buckling, and only the concrete near the corners will be effectively confined. The situation can be improved by chipping the corners of the existing concrete column back to the corner bars and using hoops for the concrete jacket which include 45° corner bends, alternately with full peripheral hoops, The use of midside links in holes drilled through the core of the existing column, is likely to be expensive, and the links will be difficult to place because of the need to bend the hook at one end in place after threading through the hole. Fig. 3-4 shows concrete jacket cross section detail.

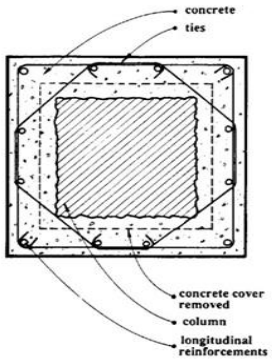

Fig. 3-4 - Concrete jacket cross section

3.4.3 Composite-Materials Jackets.

There has been a considerable research [9] [10] [11] performed to establish the effectiveness of column retrofit using jackets of composite materials such as fiberglass, carbon fiber, and kevlar, generally bonded together and to the column with epoxy. Fig. 3-5 shows two forms of application, one involving the hand layup of a jacket made from layers of epoxy-impregnated fiberglass fabric, and the second, and wrapping of a column with carbon fiber tows, also impregnated with epoxy. Because of the greater strength and stiffness of the carbon fiber, lesser thicknesses are needed than for the less expensive but more flexible and weaker fiberglass jacket.

In both cases, the techniques are most suitable for circular columns, since obtaining full confinement for rectangular columns requires placing concrete bolsters or other means of section shape modification to enable the jacket to be placed over a continuously curved surface. However, it has been found that reasonable enhancement of ductility has been achieved for rectangular carbon fiber or fiberglass-epoxy jackets on rectangular columns [12] [13].

Fig. 3-5 - Wrapping columns with FRP

3.5 Lateral confinement by FRP jacketing

The use of FRP in place of steel for this application offers several advantages. First of all, they have much higher strength (especially the carbon fiber sheets) and they keep imposing confining lateral pressure up to rupture due to their elastic behaviour up to failure contrary to the elasto-plastic behaviour of steel. If the ratio of circumferential to axial fibers is large, the FRP axial modulus is small, allowing the concrete to take essentially the entire axial load; the tensile strength in the circumferential direction is very large and essentially independent from the value of the axial stress; ease and speed of application result from their light weight; their minimal thickness does not produce any change in the shape and size of the strengthened elements; and the good corrosion behaviour of FRP materials makes them suitable for use in coastal and marine structures.

3.5.1 FRP-confined concrete in circular sections

In circular sections, the induced radial displacement by the applied axial load (meaning the same displacement around the circumference of the section) activates the confining device and causes radial confining forces or else hydrostatic confining pressure. This pressure results in stress state which is the same in every point of the section as mentioned before. It is worthy underlying also that at every point of the circumference, the lateral expansion of concrete is equal to the deformation of FRP.

3.5.2 FRP-confined concrete in rectangular sections

Rectangular sections confined with FRP are not efficiently confined as the circular sections as discussed. Only displacement of corners can be confined, but cannot confine the displacement outside the central part of the sides from character of the rectangular section, which results in different stress-state in every point of the section.

Rounded corners shown in the Fig. 3-6 are introduced in the case of FRP confinement to improve the effectiveness of FRP jacket. However, due to the presence usually of internal reinforcement, the radius of the rounded corner is generally limited to small values.

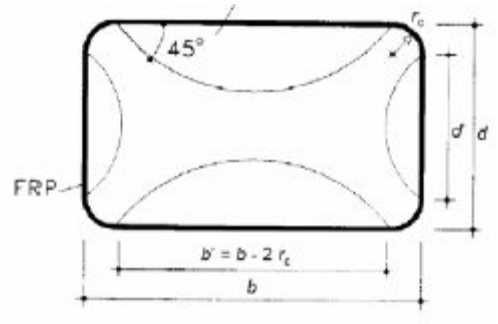

Fig. 3-6 Effective confining area used in modelling FRP-confinement of rectangular RC sections. (CNR-DT200 2004)

Chapter 4

NUMERICAL PROCEDURE AND VALIDATION

4.1 Introduction

Designing FRP confined concrete columns requires analytical tools that predict the level of performance and ductility enhancement for concrete columns. Therefore, a new design approach enables user to do this prediction using software based on confinement model.

Previous study defining stress strain curve and M-phi diagram is introduced [14] then the methodology predicting displacement ductility factor is explained. Also the numerical procedure is validated by comparison of the results with experimental work

4.2 Numerical procedure

4.2.1 Defining the stress strain curve

Mander et al. (1988a) proposed a unified stress-strain approach for confined concrete applicable to both circular and rectangular shaped transverse reinforcement. The model was based on an equation suggested by Popvics (1973). In this approach the relationship between longitudinal compressive concrete stress fc and longitudinal compressive strain ε_c takes the forms:

$$f_c = \frac{f'_{cc}\, x\, g}{g-1+x^g} \quad 4\text{-}1$$

$$x = \frac{\varepsilon_c}{\varepsilon_{cc}} \quad 4\text{-}2$$

$$\varepsilon_{cc} = \varepsilon_{co}\left[1+5\left(\frac{f'_{cc}}{fc'}-1\right)\right] \quad 4\text{-}3$$

$$g = \frac{E_c}{E_c - E_{Sec}} \quad 4\text{-}4$$

$$E_{Sec} = \frac{f'_{cc}}{\varepsilon_{cc}} \quad 4\text{-}5$$

Where f'_{cc} is compressive strength of confined concrete, ε_{cc} is the corresponding strain, ε_c is the longitudinal compressive concrete strain, f_c' is the unconfined compressive strength of concrete and ε_{co} is the corresponding strain (generally ε_{co}=0.002 can be assumed), and E_c=5000$\sqrt{f_c'}$($\frac{N}{mm^2}$).

In his model Mander expressed the compressive strength of confined concrete f'_{cc} by

$$f'_{cc} = \alpha_1 \alpha_2 f_c' \quad 4\text{-}6$$

In which α_1 is a strength enhancement factor that considers the concrete to be subjected to a tri-axial stress state with bi-equal confining stresses, and α_2 is a reduction factor that considers any deviation from the bi-equal confining stress concept.

The factors α_1 and α_2 were proposed by Mander et al. [15] and by Wang and Restrepo, as follows [16] :

$$\alpha_1 = 1.25\left(1.8\sqrt{1+7.94\frac{F_l}{f_c'}} - 1.6\frac{F_l}{f_c'} - 1\right) \quad 4\text{-}7$$

$$\alpha_2 = \left(1.4\frac{f_l}{F_l} - 0.6\left(\frac{f_l}{F_l}\right)^2 - 0.8\right)\sqrt{\frac{F_l}{f_c'}} + 1 \quad 4\text{-}8$$

where F_l and f_l are the maximum and minimum confining stresses in x and y directions respectively. The lateral confining stresses due to the FRP jacket in x and y directions ($f_{l,jx}$ and $f_{l,jy}$) are given for rectangular section by :

$$f_{l,jx} = \rho_{jx} f_j \quad 4\text{-}9$$

$$f_{l,jy} = \rho_{jy} f_j \quad 4\text{-}10$$

where f_j is the confining stress and is obtained from

$$f_j = E_j \varepsilon_j \quad 4\text{-}11$$

For $\left(0 \le \varepsilon_j \le \varepsilon_{ju}\right)$

$f_j = 0$

For $\left(\varepsilon_j \le \varepsilon_{ju}\right)$

where E_j and ε_{ju} are the modulus of elasticity and the ultimate strain of the jacket material respectively, and ε_j is the circumferential strain in the jacket.

The ratios ρ_{jx} and ρ_{jy} are defined as:

$$\rho_{jx} = 2\frac{t_j}{t_y} \quad 4\text{-}12$$

$$\rho_{jy} = 2\frac{t_j}{t_x} \quad 4\text{-}13$$

where t_j is the jacket thickness and t_y and t_x are the overall cross-sectional dimensions.

Similarly the confining stresses due to the steel hoops in the x and y directions take the forms:

$$f_{l,sx} = \rho_{sx} f_{sh} \quad 4\text{-}14$$

$$f_{l,sy} = \rho_{sy} f_{sh} \quad 4\text{-}15$$

where f_{sh} is the confining stress in the hoops and is obtained as:

$$f_{sh} = E_s \varepsilon_t \quad \text{For } (\varepsilon_t < \varepsilon_y) \tag{4-16}$$

$$f_{sh} = f_{sy} \quad \text{For } (\varepsilon_t > \varepsilon_y) \tag{4-17}$$

E_s is the modulus of elasticity of steel reinforcement and ε_y and f_{sy} are the yield strain and yield stress of the steel reinforcement, respectively.

The confinement reinforcement ratios ρ_{sx} and ρ_{sy} are defined as:

$$\rho_{sx} = \frac{A_{t,x}}{s d_y} \tag{4-18}$$

$$\rho_{sx} = \frac{A_{t,y}}{s d_x} \tag{4-19}$$

in which d_x and d_y are the distances between the centerlines of the perimeter hoop in the x and y directions, respectively; $A_{t,x}$ and $A_{t,y}$ are areas of transverse steel parallel to the x and y axis, respectively; and (s) is the spacing between sets of hoops.

The lateral confining stress f_l acting upon the area confined by both the jacket and the steel hoops is the summation of the lateral confining stress due to steel hoops $f_{l,s}$ and the lateral confining stress due to jacket $f_{l,j}$

$$f_l = f_{l,s} + f_{l,j} \tag{4-20}$$

In recent years, researchers have attempted to extend Mander's model to predict the behavior of concrete, accounting for the effect of confinement provided by elastic FRP jackets. A major obstacle of the model is due to the use of constant value for confining pressure throughout the loading history. FRP behaves elastically until failure, and the inward pressure increases continuously, so this assumption is not appropriate. Based on Pantazopoulu and Mills [17] constitutive model for unconfined concrete under uniaxial loading, Spoelstra and Monti [18] proposed the equation that explicitly shows the dependence of concrete f_c and lateral strain ε_l on the current strain ε_c and the confining pressure f_l

$$\varepsilon_l(\varepsilon_c, f_l) = \frac{E_c \varepsilon_c - f_c(\varepsilon_c, f_l)}{2 \beta f_c(\varepsilon_c, f_l)} \tag{4-21}$$

$$\beta = \frac{5700}{\sqrt{f_c}} - 500 \tag{4-22}$$

It is assumed that under concentric compressive loading, the transverse strain in the concrete surface of the column ε_l, the strain in the jacket ε_j, and the strain in the steel hoops ε_s are all equal that is

$$\varepsilon_l = \varepsilon_j = \varepsilon_s \tag{4-23}$$

This model represents an incremental approach to define the stress and strain curve Fig. 4-1.

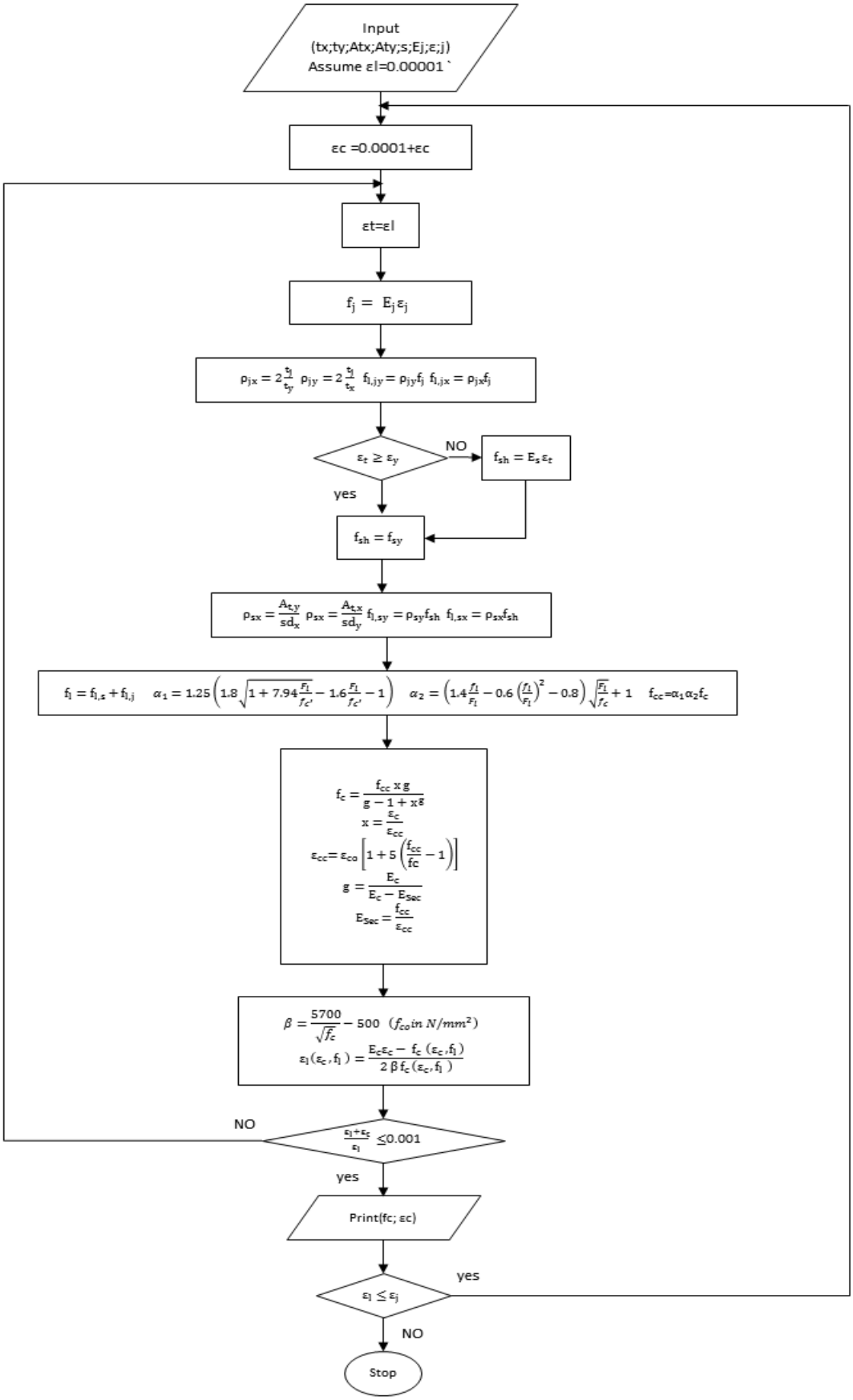

Fig. 4-1 Flow chart stress-strain relationship using Mander equation

4.2.2 Numerical procedure for moment curvature diagram

- **Assumptions**

In developing moment curvature diagram for concrete sections confined with FRP, the following assumptions are taken into consideration. Stress strain relationship proposed by the selected model is taken as a stress block, concrete tensile strength is neglected, the variation of the strain up to failure is assumed to be linear, steel is perfectly bonded with concrete and axial force which is applied to the section is assumed to be applied first and held constant while moment is increased to their failure values.

- **Material constitutive law**

Confining concrete columns with a certain thickness of FRP wraps causes an increase in the confined concrete peak stress with reference to unconfined concrete strength. This is due to elastic Poisson's lateral stresses followed by nonlinear dilatational behavior of concrete due to pre-peak cracking. Then, it increases the post peak ductility and ultimate strength of the concrete column developing a pseudo ductile plateau. Increasing thickness of FRP jacket enhances compressive capacity of concrete columns.

- **Numerical procedure**

The column cross-section is divided into small filaments and for each filament stresses and strains are calculated, utilizing a numerical procedure for obtaining stress strain relationship of concrete columns subjected to axial force and lateral load. Resultant forces and moments can be computed as illustrated in Fig. (4-2) .The moment curvature diagram is developed by incrementing the curvature. For a particular curvature, strain is computed for concrete and steel. Stress corresponding to this strain is obtained as mentioned in section 4.2.1. Neutral axis length is altered until the sum of internal compression and tension forces in the section are equal to the desired axial force. Once the forces are balanced, moment is calculated and thus one point of the moment curvature diagram is determined. The curvature is then incremented and the forgoing procedure of balancing the forces and calculating the moment is repeated. This is continued until either the concrete compressive strain

reaches 0.01 or the peak moment is reached. This point at the diagram represents ultimate curvature and ultimate moment.

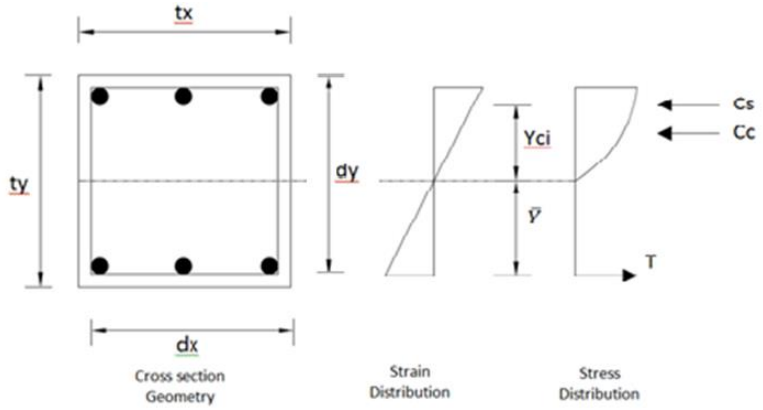

Fig. 4-2 Strain and stress distribution and resultant of the internal forces

The input data needed for the model includes modulus of elasticity of FRP (E_j), modulus of elasticity of steel (E_s), concrete compressive strength (F_{cu}), rupture strain of FRP (e_{ju}), column thickness in x direction (t_x), column thickness in y direction (t_y), spacing between stirrups in the longitudinal direction (s), perimeter hoop side length in X direction (d_x), perimeter hoop side length in Y direction (d_y), yield strain of longitudinal steel (e_y), yield stress of steel used for stirrups (f_{sy}), area of steel of hoops in X direction (A_{tx}), area of steel in Y direction (A_{ty}), longitudinal area of steel (A_s), axial force applied on the column (P), yield stress of longitudinal steel (f_y), height of column (H), plastic hinge height (L_p), and thickness of FRP jacket (t_j).

4.2.3 Predicting displacement ductility Ratio

Referring to Fig. 4-3, displacement ductility ratio μ_Δ is a measure of the level of ductility enhancement of reinforced concrete rectangular columns where it is defined as:

$$\mu_\Delta = \frac{\Delta_p}{\Delta_y} \qquad 4\text{-}24$$

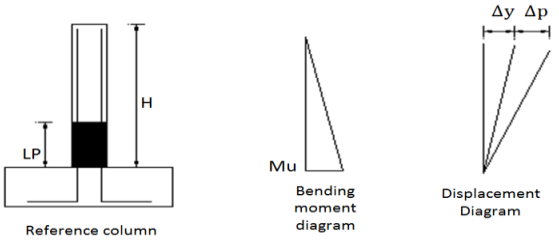

Fig. 4-3 Column geometry and deformation

Where Δ_y is the yield displacement and Δ_p is the plastic displacement. The yield displacement Δ_y can be obtained from the equation

$$\Delta_y = \phi_y \times \frac{1}{3} \times H^2 \quad 4\text{-}25$$

The yield curvature $Ø_y$ can be found by using the numerical procedure generating the moment curvature diagram as the curvature corresponding to yielding of the longitudinal steel. The distance H is measured from the critical section of plastic hinge to the point of contra flexure.

Δ_p is the plastic displacement corresponding to the rotational capacity of the column hinge θ_p where:

$$\Delta_p = \theta_p \times H \quad 4\text{-}26$$

The plastic rotation θ_p is defined as:

$$\theta_p = L_p Ø_p = L_p (Ø_u - Ø_y) \quad 4\text{-}27$$

According to Priestly et al. [7] a reasonable estimate for the plastic hinge length Lp formed against a supporting member is given by:

$$L_p = 0.08H + 0.022 f_{ye} d_{bl} \geq 0.044 f_{ye} d_{bl} \quad 4\text{-}28$$

The plastic curvature $Ø_p$ is the difference between ultimate curvature $Ø_u$ corresponding to the limit compression strain ε_{cu} and the yield curvature $Ø_y$ thus

$$Ø_p = Ø_u - Ø_y \quad 4\text{-}29$$

The plastic curvature is assumed to be constant over the plastic hinge length Lp which is calibrated to give the same plastic rotation as occur in the real structure. This numerical procedure is explained in the flow chart shown in Fig. 4-4.

The ultimate curvature $Ø_u$ can be found utilizing the technique explained in the previous section in generating the moment curvature diagram.

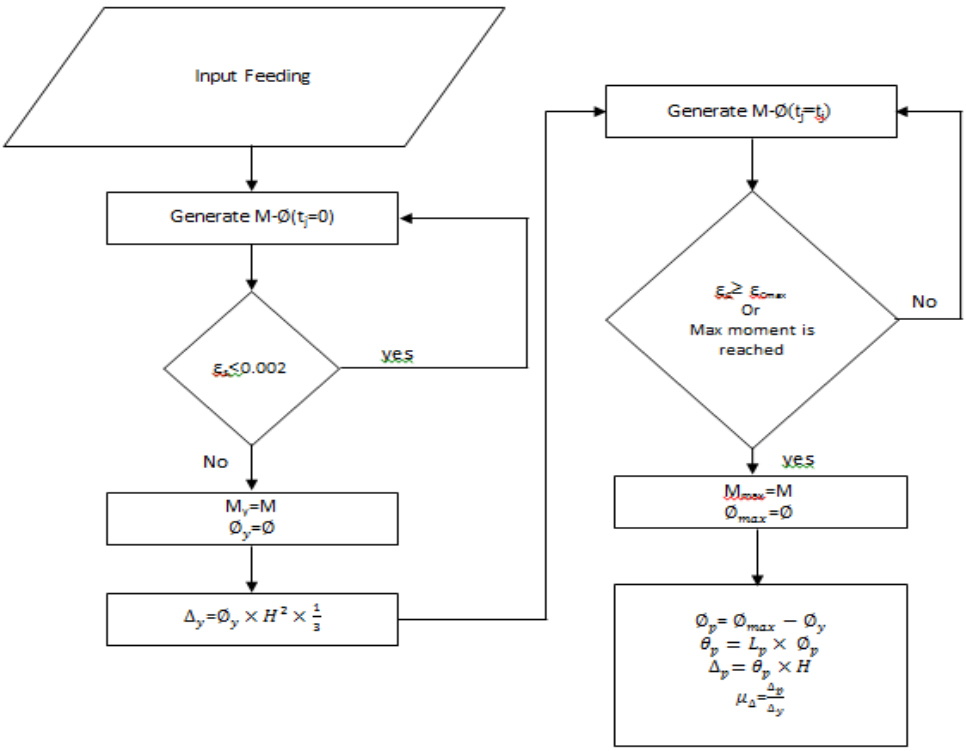

Fig. 4-4 Prediction of displacement ductility ratio

4.3 Numerical analysis output

A computer program is developed with source code using C language with Borland C compiler to generate a moment-curvature diagram for concrete rectangular or square columns confined with steel or FRP or both of them at the same time, subjected to bending moment and axial force. A text file is produced by the program, easily adapted for Excel sheet format to be used for drawing charts and comparing results. Fig. 4-5 shows M-phi diagram for a concrete column confined with FRP and steel hoops, where details of these columns are stated in table 4-1.

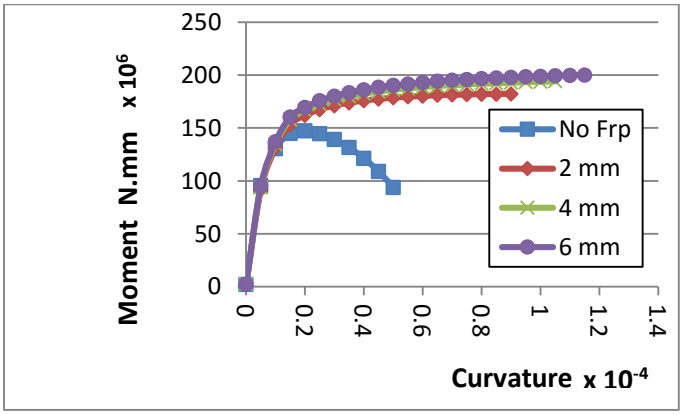

Fig. 4-5 Moment curvature of concrete column confined with FRP

Table 4-1 Input values needed by software for calculation

Input	Value	Unit
FRP modulus	76350	N/mm^2
Steel modulus	202170	N/mm^2
Compressive strength of concrete	36.5	N/mm^2
Ultimate strain of FRP	0.0126	
Column width	300	mm
Column length	300	mm
Spacing	300	mm
Distance between premiter hoops X	265	mm
Distance between premiter hoops Y	265	mm
Ultimate strain of steel stirrups	0.0022	
Stirrups yield stress	280	N/mm^2
Transverse steel X	56.5	mm^2
Transverse steel Y	56.5	mm^2
Long. steel	402	mm^2
Axial load	1500000	N
Long. steel yield strain	0.0022	
Diameter of long steel	16	mm
Height of column	2000	mm
Plastic hinge	399	mm

These analyses are used to determine the Yield Moment M_y, Yield Curvature $\emptyset_y$, Ultimate Moment M_u and Ultimate Curvature $\emptyset_u$, which are then used to calculate the Section Plastic Curvature, Section Curvature Ductility, Flexural Over Strength (ratio between M_u over M_y) and Displacement Ductility Factor of each cross section as in Fig.4-6 and Fig.4-7.

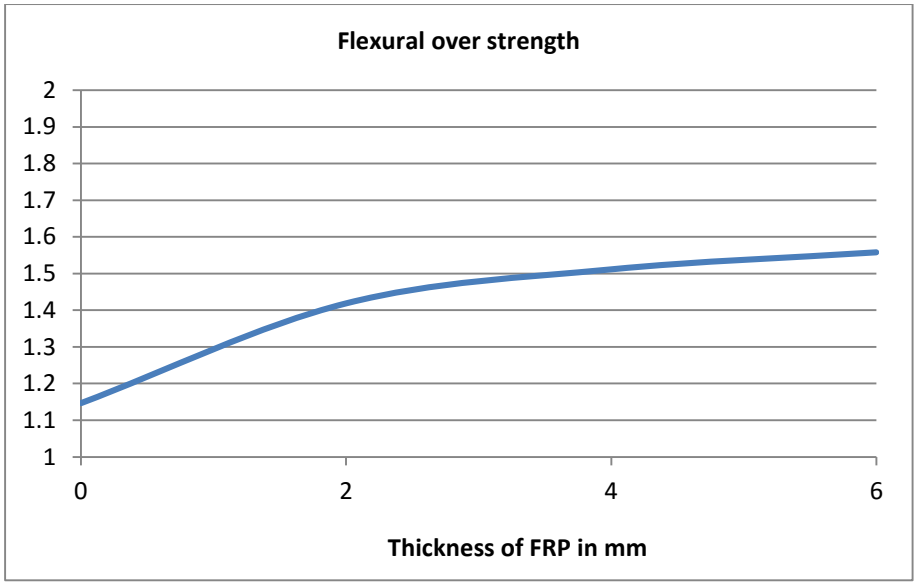

Fig. 4-6 Flexural over strength variation with jacket thickness

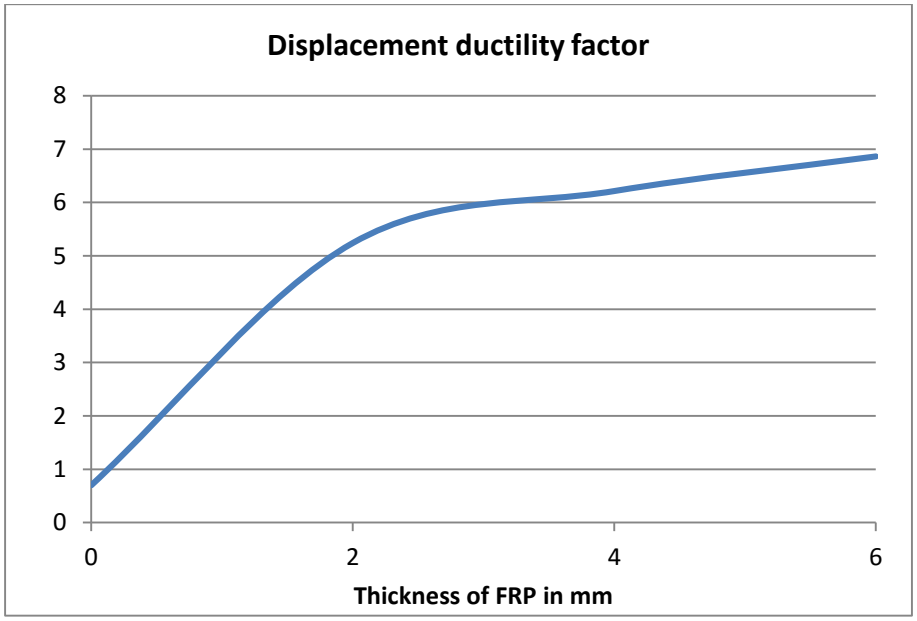

Fig. 4-7 Displacement ductility factors variation with jacket thickness

4.4 Validation of the software

Three sets of published experimental results by Richard et al [11] Muhammad S. Memon et al [10], Hatem Abdelaal Seliem [9] were considered to validate the numerical model. A summary of the material properties dimensions and steel used for the specimens from the experiments conducted is given later.

4.4.1 Richard D. Iacobucci, Shamim A. Sheikh, and Oguzhan Bayrak

Large-scale columns were designed with no seismic transverse steel detailing. The main variables studied were the number of CFRP layers in the test zone, the presence of column damage, and the level of applied axial load. Retrofitted and control specimens were tested under a constant axial load with cyclic flexural and shear loads.

Each specimen was comprised of a 305 x 305 x 1473 mm column connected to a 508 x 762 x 813 mm stub. The corners of all columns were rounded using concave wood sections, with a 16 mm radius, placed inside the forms during casting to facilitate FRP wrapping. The columns were characteristic of field members located in multistory building frames or in bridges between the points of maximum moment and contra flexure. Each stub was adjacent to the site of maximum moment and served as a discontinuity such as a column-footing junction or a beam-column interface. All specimens contained eight 20M longitudinal bars uniformly distributed around the column core creating a core area that was 77% of the gross column area. Perimeter hoops laterally supported the four corner bars and internal hoops enclosed the four middle bars. Properties of FRP and steel reinforcement are listed in tables 4-2 and 4-3 respectively. Details of the specimens are listed in Table 4-4. Fig. 4-8 shows geometry of specimens.

Table 4-2 Properties of FRP composites

Composite	Thickness, mm	Tensile strength/ unit width (N/mm/layer)	Strain at rupture	Elastic modulus,* MPa
CFRP	1.00	962	0.0126	76,350
GFRP	1.25	563	0.0211	21,346

Table 4-3 Properties of steel reinforcement

Bar size	Stress-strain characteristics						
	f_y, MPa	ε_y	E_s, MPa	ε_{sh}	f_u, MPa	ε_u	ε_r
U.S. No. 3	457	0.0022	207,730	0.0070	739	0.1050	0.1435
20M	465	0.0023	202,170	0.0113	640	0.1288	0.2038
10M	505	0.0028	180,360	0.0133	680	0.1413	0.2163

Table 4-4 Details of test specimens

Specimen	f'_c, MPa	Layers of CFRP	Lateral steel				Axial load	
			Size at spacing, mm	ρ_s, %	f_y, MPa	$A_{sh}/A_{sh(ACI)}$	P/f'_cA_g	P/P_o
AS-1NS	31.4	0	U.S. No. 3 at 300	0.61	457	0.49	0.40	0.33
ASC-2NS	36.5	1	U.S. No. 3 at 300	0.61	457	0.42	0.38	0.33
ASC-3NS	36.9	2	U.S. No. 3 at 300	0.61	457	0.42	0.65	0.56
ASC-4NS	36.9	1	U.S. No. 3 at 300	0.61	457	0.42	0.65	0.56
ASC-5NS	37.0	3	U.S. No. 3 at 300	0.61	457	0.42	0.65	0.56
ASC-6NS	37.0	2	U.S. No. 3 at 300	0.61	457	0.42	0.38	0.33
AS-7NS	37.0	0	U.S. No. 3 at 300	0.61	457	0.42	0.38	0.33
ASCR-7NS	37.0	1	U.S. No. 3 at 300	0.61	457	0.42	0.38	0.33
AS-8NS	42.3	0	U.S. No. 3 at 300	0.61	4.57	0.36	0.62	0.56
ASCR-8NS	42.3	3	U.S. No. 3 at 300	0.61	457	0.36	0.62	0.56
AS-3*	33.2	0	U.S. No. 3 at 108	1.68	507	1.43	0.60	0.50
AS-19*	32.3	0	U.S. No. 3/ 6 mm at 108	1.30	507/ 462	1.12	0.47	0.39

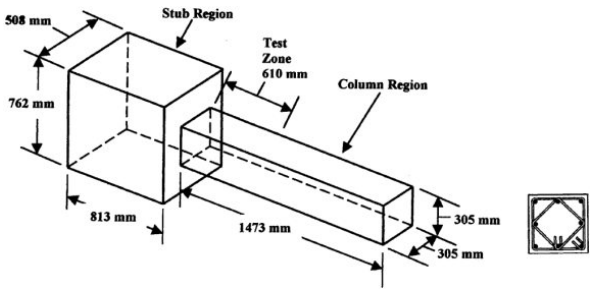

Fig. 4-8 Geometry and steel configuration of specimens

Each specimen was tested horizontally in a loading frame under a constant axial load and applied lateral cyclic displacement excursions simulating earthquake forces. A hydraulic jack with a capacity of 4450 kN provided the axial force that was measured using a load cell of similar capacity. Special hinges permitted in-plane rotation of each specimen end allowing the loading path to remain constant throughout the test. Engineering levels were used to initially align each specimen in both the vertical and horizontal planes. The specimen was axially loaded in 200 kN increments up to 50% of the specified test load and readings from instrumentation

were checked at each stage. If an adjustment was required to obtain the necessary alignment, the specimen was unloaded and repositioned. The process was repeated until the column was properly aligned in the test frame, although most specimens required minimal adjustment. After alignment, the predetermined axial load was applied and the 1000 kN actuator was connected to the stub adjacent to the interface with the column. The specimen was then subjected to transverse displacement excursions using a displacement-control mode of loading Tables 4-5 and 4-6 shows the Experimental values and calculated capacities.

Table 4-5 Experimental values and calculated capacities

Specimen	Layers of CFRP	P/P_o	V_{max}, kN	V_r, kN	M_{smax}, kN · m	M_{max}, kN · m	M_{pr}, kN · m	Damage zone, mm
AS-1NS	0	0.33	108.2	111.0	200.3	180.4	200.3	185
ASC-2NS	1	0.33	127.5	113.2	252.4	228.8	214.6	175
ASC-3NS	2	0.56	126.4	113.3	255.9	233.2	177.1	180
ASC-4NS	1	0.56	120.7	113.3	236.9	218.2	177.1	185
ASC-5NS	3	0.56	131.3	113.4	281.3	260.1	177.6	195
ASC-6NS	2	0.33	129.6	113.4	262.3	245.8	216.2	125
AS-7NS	0	0.33	117.2	113.4	230.0	208.4	216.2	190
ASCR-7NS	1	0.33	118.1	113.4	237.4	215.8	216.2	180
AS-8NS	0	0.56	105.7	115.4	210.3	167.6	189.7	460
ASCR-8NS	3	0.56	113.4	115.4	242.2	198.0	189.7	415
AS-3*	0	0.50	97.0	286.9	204.0	192.9	170.0	140
AS-19*	0	0.39	108.5	213.1	219.6	202.1	185.7	114

Table 4-6 Member and section ductility values

	Ductility factors			Ductility ratios				Energy indicators			
Specimen	$\mu_{\Delta 80}$	$\mu_{\phi 80}$	$\mu_{\phi 90}$	$N_{\Delta 80}$	$N_{\Delta t}$	$N_{\phi 80}$	$N_{\phi t}$	W_{80}	W_t	E_{80}	E_t
AS-1NS	3.7	5.3	4.1	9.5	18.4	8.4	23.9	10.2	25.3	10.8	66.2
ASC-2NS	6.1	11.6	9.1	33.3	61.1	61.2	72.8	110.5	254.6	352.1	465.8
ASC-3NS	5.6	+	+	23.6	34.5	+	56.0	80.9	130.9	+	326.2
ASC-4NS	5.2	+	+	15.9	21.6	+	24.3	41.4	57.1	+	79.2
ASC-5NS	7.1	+	+	44.5	59.2	+	109.3	260.6	392.1	+	1083.2
ASC-6NS	8.2	+	15.4	59.2	104.4	+	160.5	306.7	621.9	+	1328.1
AS-7NS	+*	+	+	+	12.0	+	9.9	+	13.5	+	7.7
ASCR-7NS	5.4	+	+	35.3	41.4	+	55.9	127.3	139.9	+	214.7
AS-8NS	+	+	+	+	7.3	+	5.4	+	5.4	+	7.9
ASCR-8NS	+	+	+	+	30.7	+	27.9	+	145.4	+	101.7
AS-3†	4.7	+	+	23.0	32.0	+	74.0	84.0	127.0	+	753.0
AS-19†	4.0	19.0	10.0	18.0	44.0	85.0	129.0	33.0	130.0	631.0	1230.0

4.4.2 Muhammad S. Memon and Shamim A. Sheikh

Large-scale reinforced concrete columns were constructed using typical lateral steel detailing from the pre-1971 design codes. Seven of these columns were strengthened or repaired with GFRP wraps. One unwrapped column from this program and one from an earlier study were used as control specimens to evaluate the

benefits of FRP retrofitting. All the specimens were tested under constant axial load and cyclic lateral excursions simulating seismic loading conditions. The main variables of the study were the number of GFRP layers in the potential plastic hinge region, the level of applied axial load, and the presence of column damage.

Each specimen consisted of a square column of dimensions 305 x 305 x 1473 mm cast integrally with a stub of dimensions 508 x 762 x 813 mm. The column represented a portion of a column in a bridge or a building between the section of maximum moment and the point of contra flexure. The stub represented the discontinuity similar to a footing or a beam column joint. The total core area was approximately equal to 77% of the gross area of the column. All columns contained eight 20M longitudinal bars uniformly distributed around the core. Perimeter ties laterally supported the four corner bars and internal ties enclosed the four middle bars. The corners of columns were rounded to facilitate GFRP wrapping using concave wood sections, with a 16 mm radius, placed inside the forms. Details of the specimens and reinforcing steel properties are given in Tables 4-7, 4-8 and Fig.4-9.

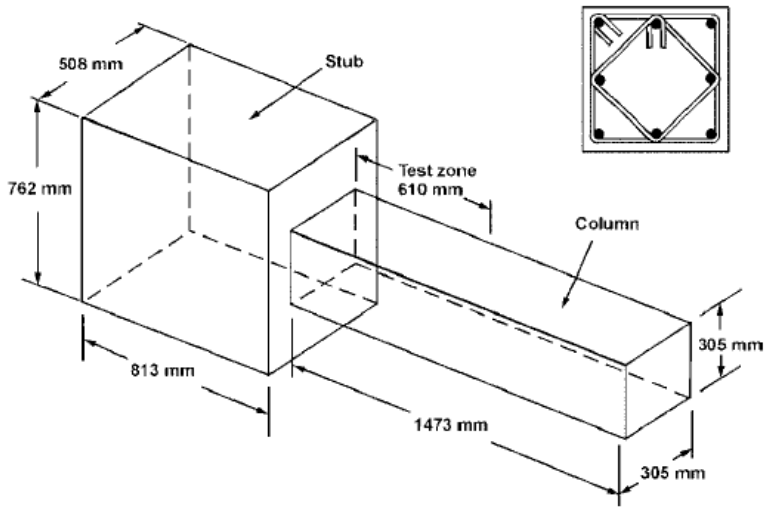

Fig. 4-9 Geometry and lateral steel configuration of specimens

Table 4-7 Details of test specimens

Specimen	f_c', MPa	GFRP treatment	Axial load P/P_o	Lateral steel			Longitudinal steel	
				Size at spacing s, mm	ρ_s, %	$A_{sh}/A_{sh(ACI)}$	No. of bars and size	ρ_g, %
AS-1NSS	42.4	None	0.56	U.S. No. 3 at 300	0.61	0.36	Eight-20M	2.58
ASG-2NSS	42.5	Two layers	0.33	U.S. No. 3 at 300	0.61	0.36	Eight-20M	2.58
ASG-3NSS	42.7	Four layers	0.56	U.S. No. 3 at 300	0.61	0.36	Eight-20M	2.58
ASG-4NSS	43.3	Two layers	0.56	U.S. No. 3 at 300	0.61	0.35	Eight-20M	2.58
ASG-5NSS	43.7	One layer	0.33	U.S. No. 3 at 300	0.61	0.35	Eight-20M	2.58
ASG-6NSS	44.2	Six layers	0.56	U.S. No. 3 at 300	0.61	0.34	Eight-20M	2.58
ASGR-7NSS	44.2	Two layers	0.33	U.S. No. 3 at 300	0.61	0.34	Eight-20M	2.58
ASGR-8NSS	44.2	Six layers	0.56	U.S. No. 3 at 300	0.61	0.34	Eight-20M	2.58
AS-3[9]	33.2	None	0.50	U.S. No. 3 at 108	1.68	1.43	Eight No. 6	2.44
AS-19[9]	32.3	None	0.39	U.S. No. 3/6 mm at 108	1.30	1.12	Eight No. 6	2.44

Table 4-8 Mechanical properties of steel bars

Bar type	Diameter, mm	Area, mm^2	Modulus E_s, MPa	Yield stress f_y, MPa	Yield strain ε_y	Ultimate stress f_{ult}, MPa	Ultimate strain ε_{ult}
20M	19.5	300	202,170	465	0.0023	640	0.2021
10M	11.3	100	180,360	505	0.0028	680	0.2151
U.S. No. 3	9.5	71	207,730	457	0.0022	739	0.1411

The specimens were tested horizontally in a testing frame. The axial load was applied through a hydraulic jack having the capacity of 4450 kN and was measured using a load cell of similar capacity. Special hinges were used at the ends of the specimen to allow in-plane rotation and to keep the loading path constant throughout the test. To apply reverse lateral load, an actuator with a load capacity of 1000 kN and a stroke capacity of ±150 mm was used.

The displacement control feature of the actuator was used in all the tests to apply predefined displacement history .The hinges at both ends of the actuator were adjusted to allow in-plane rotation at the lower end of the actuator.

The specimen was aligned in the vertical plane using engineering levels. In the horizontal plane, plumb-bobs were used to match the centerline of the specimen with the line of action of the axial load. After the external instrumentation was installed, the specimen was loaded up to 50% of the predetermined axial load in 200 kN increments. The deformations at the four corners of the specimen were recorded using four LVDTs. If the difference between the average reading and the maximum or minimum displacement reading was more than 5%, the specimen was unloaded and necessary adjustments were made. The process was repeated until the specimen was properly aligned. The strain gauge readings were also used to confirm the alignment.

4.4.3 Hatem Seliem

Full scale cantilever columns under constant axial force and reversed cyclic lateral load that simulated forces from an earthquake all columns were instrumented to obtain much information as possible about their behavior at each stage of loading. Table 4-9 shows details of tested columns.

Table 4-9 Details of Test columns

Column		Treatment of The Plastic Hinge Zone	Transverse Rft Volumetric Ratio ρ_s	Axial Load Level P/(f_cA_g)	Concrete Strength (MPa) Cube	cylinder
First Group	C1As	As built	0.0051	0.31	37.8	28.5
	C1RG2	Retrofitted with 2 layers of 1.3 mm GFRP		0.27	42	32.7
	C1RG2'	Retrofitted with 2 layers of 1.3 mm CFRP		0.26	42.1	33.7
	C1RC2'	Retrofitted with 2 layers of 1 mm GFRP		0.26	45.6	30
Second Group	C2AS	As built	0.0042	0.29	40.7	30
	C2RG2	Retrofitted with 2 layers of 1.3 mm GFRP		0.28	39.1	30.2
	C2RC1	Retrofitted with 1 layers of 1 mm CFRP		0.29	41.2	30.2
	C2RC2	Retrofitted with 2 layers of 1 mm CFRP		0.28	43.7	31.6

Columns are subjected to cyclic horizontal loads in a single curvature as shown in Fig.4-10 the column was well anchored to the laboratory strong floor using 40 mm diameter anchors, in order to achieve full fixity at footing level, the anchors were tightened using a prestressing piston to insure preventing any sliding of the footing against laboratory floor. Lateral cyclic load was applied using a 500kN reversible hydraulic jack mounted on a stiff reaction steel frame, a quasi-static

displacement control technique is used to test the columns. Specimens details are mentioned in Table 4-10.

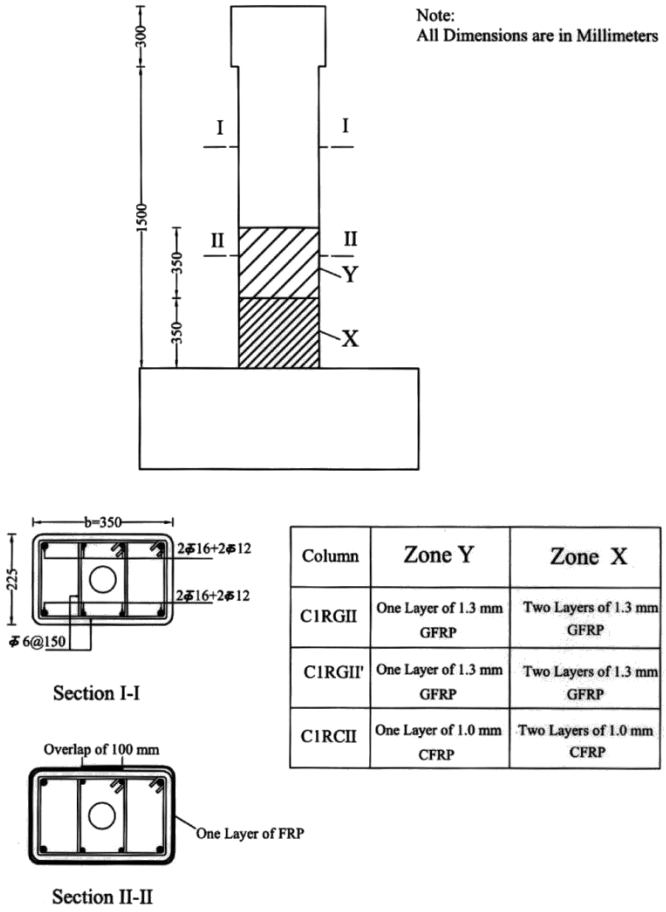

Column	Zone Y	Zone X
C1RGII	One Layer of 1.3 mm GFRP	Two Layers of 1.3 mm GFRP
C1RGII'	One Layer of 1.3 mm GFRP	Two Layers of 1.3 mm GFRP
C1RCII	One Layer of 1.0 mm CFRP	Two Layers of 1.0 mm CFRP

Fig. 4-10 Geometry and steel configuration of specimens

Table 4-10 Hatem Seliem details of specimen

	Column	Displacement Ductility Ratio μ_Δ	Strength Decay Rate SDR (KN/mm)	Elastic Stiffness At Yield Displacement K_y	Drift Index (%)	Energy Indicator I_{E85}	Ultimate Loa (KN)
First Group	C1AS	3.2	1.11	5.55	2.50	104	96.77
	C1RGII	10.0	0.23	6.71	6.30	1539	106.45
	C1RCII	11.5	0.16	6.95	7.90	2297	103.98
Second Group	C2AS	3.3	1.06	7.70	2.27	99	108.91
	C2RGII	9.8	0.42	8.60	6.40	1149	116.11
	C2RCI	7.1	0.34	8.00	4.93	736	116.43
	C2RCII	11.3	0.38	9.45	7.11	2676	127.24

Table 4-11 Summary of Hatem Seilim experimental analysis

Hatem seliem specimens

Property	C1As	C1RGII	C1RCII	C2AS	C2RGII	C2RCI	C2RCII
Frp modulus of elasticity	-	26100	72400	-	26100	72400	72400
Steel modulus of elasticity	200000	200000	200000	200000	200000	200000	200000
Concrete modulus of elasticity	30000	30000	30000	30000	30000	30000	30000
Concrete strength	37.8	42	45.6	40.7	39.1	41.2	43.7
Frp Ultimate strain	-	0.022	0.0121	-	0.022	0.0121	0.0121
Dimension (tx)	350	350	350	400	400	400	400
Dimension (ty)	225	225	225	200	200	200	200
Hoop Spacing	150	150	150	150	150	150	150
Perimeter hoop (dx)	175	175	175	150	150	150	150
Perimeter hoop (dy)	300	300	300	350	350	350	350
stirrups yield strain	0.002	0.002	0.002	0.002	0.002	0.002	0.002
stirrups yield strength	280	280	280	280	280	280	280
Area stirrups in x direction	56	113	113	113	113	113	113
Area stirrups in y direction	113	113	113	113	113	113	113
Longitudinal steel area	580	580	580	580	580	580	580
Axial load	700000	700000	700000	700000	700000	700000	700000
Longitudinal steel yield strength	460	460	460	460	460	460	460
Diameter of longitudinal steel	16	16	16	16	16	16	16
Displacement capacity	3.2	10	11.5	3.3	9.8	7.1	11.3
Height of column	1500	1500	1500	1500	1500	1500	1500
Plastic hinge	350	350	350	350	400	400	400
FPR thickness	0	2.6	2	0	2.6	1	2

Table 4-12 Summary of Lacobucci et al. Experimental analysis

	Iacobucci et al. Specimens									
Property	AS-1NS	**ASC-2NS**	ASC-3NS	ASC-4NS	ASC-5NS	ASC-6NS	AS-7NS	**ASCR-7NS**	AS8NS	ASCR-8NS
Frp modulus of elasticity	76350	**76350**	76350	76350	76350	76350	76350	**76350**	76350	76350
Steel modulus of elasticity	202170	**202170**	202170	202170	202170	202170	202170	**202170**	202170	202170
Concrete modulus of elasticity	30000	**30000**	30000	30000	30000	30000	30000	**30000**	30000	30000
Concrete strength	31.4	**36.5**	36.9	36.9	37	37	37	**37**	42.3	42.3
Frp Ultimate strain	0.0126	**0.0126**	0.0126	0.0126	0.0126	0.0126	0.0126	**0.0126**	0.0126	0.0126
Dimension (tx)	305	**305**	305	305	305	305	305	**305**	305	305
Dimension (ty)	305	**305**	305	305	305	305	305	**305**	305	305
Hoop Spacing	300	**300**	300	300	300	300	300	**300**	300	300
Perimeter hoop (dx)	265	**265**	265	265	265	265	265	**265**	265	265
Perimeter hoop (dy)	265	**265**	265	265	265	265	265	**265**	265	265
stirrups yield strain	0.0022	**0.0022**	0.0022	0.0022	0.0022	0.0022	0.0022	**0.0022**	0.0022	0.0022
stirrups yield strength	457	**457**	457	457	457	457	457	**457**	457	457
Area stirrups in x direction	284	**284**	284	284	284	284	284	**284**	284	284
Area stirrups in y direction	284	**284**	284	284	284	284	284	**284**	284	284
Longitudinal steel area	900	**900**	900	900	900	900	900	**900**	900	900
Axial load	1307336.3	**1459858.1**	2497635	2497635	2502710	1474811.3	1474811.3	**1474811.3**	2771685	2771685
Longitudinal steel yield strength	465	**465**	465	465	465	465	465	**465**	465	465
Diameter of longitudinal steel	19.5	**19.5**	19.5	19.5	19.5	19.5	19.5	**19.5**	19.5	19.5
Displacement capacity	3.7	**6.1**	5.6	5.2	7.1	8.2	+	**5.4**	+	+
Height of column	1473	**1473**	1473	1473	1473	1473	1473	**1473**	1473	1473
Plastic hinge	388	**388**	388	388	388	388	388	**388**	388	388
FPR thickness	0	**1**	2	1	3	2	0	**1**	0	3

Table 4-13 Summary of Muhammad S.Memon et al experimental analysis

Muhammad S. Memon and Shamim A. Sheikh specimens								
Property	AS-1NSS	*ASG-2NSS*	ASG-3NSS	ASG-4NSS	ASG-5NSS	**ASG-6NSS**	*ASGR-7NSS*	**ASGR-8NSS**
Frp modulus of elasticity	21346	*21346*	21346	21346	21346	**21346**	*21346*	**21346**
Steel modulus of elasticity	202170	*202170*	202170	202170	202170	**202170**	*202170*	**202170**
Concrete modulus of elasticity	30000	*30000*	30000	30000	30000	**30000**	*30000*	**30000**
Concrete strength	42.4	*42.5*	42.7	43.3	43.7	**44.2**	*44.2*	**44.2**
Frp Ultimate strain	0.0211	*0.0211*	0.0211	`0.0211	0.0211	**0.0211**	*0.0211*	**0.0211**
Dimension (tx)	305	*305*	305	305	305	**305**	*305*	**305**
Dimension (ty)	305	*305*	305	305	305	**305**	*305*	**305**
Hoop Spacing	300	*300*	300	300	300	**300**	*300*	**300**
Perimeter hoop (dx)	265	*265*	265	265	265	**265**	*265*	**265**
Perimeter hoop (dy)	265	*265*	265	265	265	**265**	*265*	**265**
stirrups yield strain	0.0022	*0.0022*	0.0022	0.0022	0.0022	**0.0022**	*0.0022*	**0.0022**
stirrups yield strength	457	*457*	457	457	457	**457**	*457*	**457**
Area stirrups in x direction	284	*284*	284	284	284	**284**	*284*	**284**
Area stirrups in y direction	284	*284*	284	284	284	**284**	*284*	**284**
Longitudinal steel area	900	*900*	900	900	900	**900**	*900*	**900**
Axial load	2776760	*1639295.625*	2791985	2822435	1675183.125	**2868110**	*1690136.25*	**2868110**
Longitudinal steel yield strength	465	*465*	465	465	465	**465**	*465*	**465**
Diameter of longitudinal steel	19.5	*19.5*	19.5	19.5	19.5	**19.5**	*19.5*	**19.5**
Displacement capacity	2.9	*5.9*	5.2	4.7	5.1	**6.8**	*5*	**5.1**
Height of column	1454	*1454*	1454	1454	1454	**1454**	*1454*	**1454**
Plastic hinge	388	*388*	388	388	388	**388**	*388*	**388**
FPR thickness	0	*2.5*	5	2.5	1.25	**7.5**	*2.5*	**7.5**

Table 4-14 shows calculated and actual displacement capacity of specimens and the ratio between them is shown in Fig. 4-11 with average value of 1.04 and standard deviation of 0.246 which indicates that the new tool is reliable in the determination of displacement ductility ratio enhancement.

Table 4-14 Comparison of results

	Hatem seliem					Iacobucci et al.						Muhammad S. Memon and Shamim A. Sheikh						
Column	C1RGII	C1RCII	C2RGII	C2RCI	C2RCII	ASC-2NS	ASC-3NS	ASC-4NS	ASC-5NS	ASC-6NS	ASCR-7NS	ASG-2NSS	ASG-3NSS	ASG-4NSS	ASG-5NSS	ASG-6NSS	ASGR-7NSS	ASGR-8NSS
$\mu\Delta$ test	10	11.5	9.8	7.1	11.3	6.1	5.6	5.2	7.1	8.2	5.4	5.9	5.2	4.7	5.1	6.8	5	5.1
$\mu\Delta$ predicted	9.4	14.8	9.6	10	13.9	7.7	4.6	4.14	5	8.6	7.7	6	4.2	3.3	5.1	4.6	6.4	4.6
$\frac{\mu\Delta \text{ test}}{\mu\Delta predicted}$	1.06	0.78	1.02	0.71	0.81	0.79	1.22	1.26	1.42	0.95	0.7	0.98	1.24	1.42	1	1.48	0.78	1.11

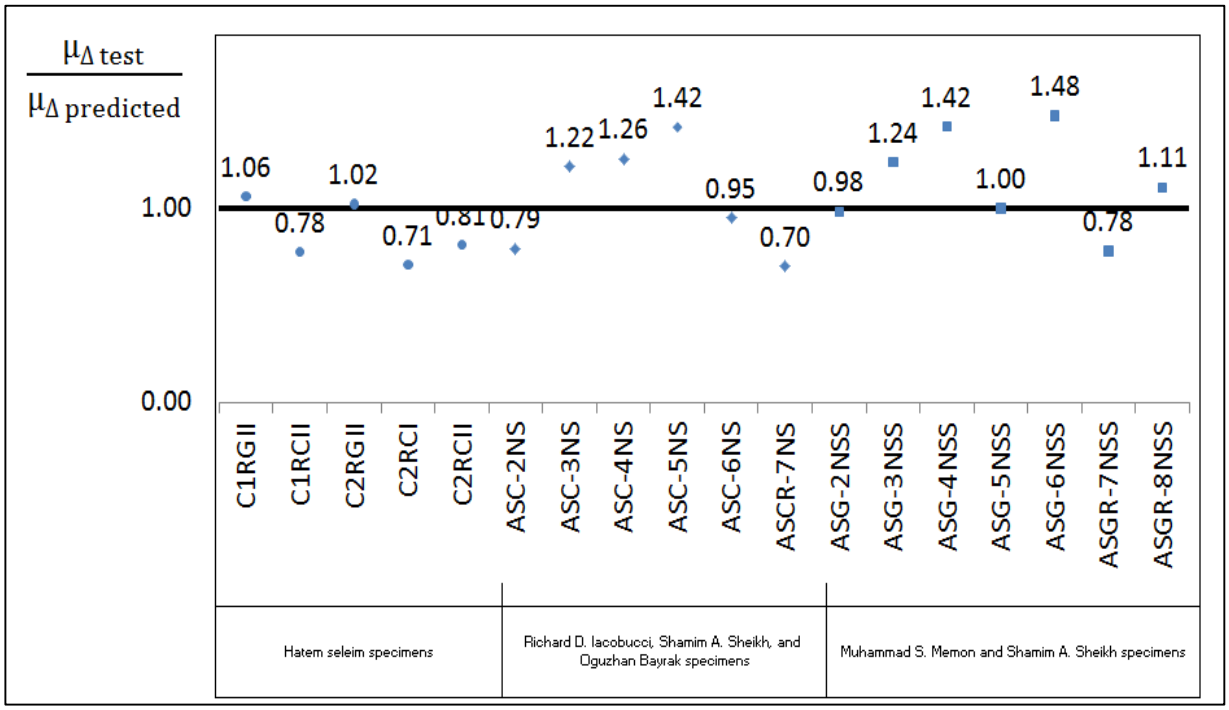

Fig. 4-11 Comparison between actual and predicted values of $\boldsymbol{\mu_\Delta}$

Chapter 5

PARAMETRIC STUDY

5.1 Introduction

In this chapter, a parametric study is conducted to investigate the effects of some design parameters on the behavior of columns retrofitted for earthquake resistance. The parameters are:

1) Concrete compressive strength
2) Columns cross sectional shape (square-rectangular)
3) Thickness of the jacket
4) Longitudinal reinforcement ratio
5) Axial load level
6) Type of FRP (CFRP or GFRP)

Moment-Curvature analyses are used to determine the Yield Moment M_y, Yield Curvature $\emptyset_y$, Ultimate Moment M_u and Ultimate Curvature $\emptyset_u$ which are then used to calculate the Section Plastic Curvature$\emptyset_p$, and Section Over strength Factor Ω_o of each cross section at Axial Load Ratios between 0.1, 0.2 and 0.5. The Axial Load Ratio P_r , as defined in equation 5.1, is the ratio between the cross section's Axial Load P and the product of the cross section's Unconfined Concrete Compressive Strength f_c' and the Gross Cross Section Area A_g.

$$P_r = \frac{P}{A_g \times f_c'} \qquad 5\text{-}1$$

The Section flexural over strength measures M_u relative to M_y, where M_u is defined as the moment corresponding to $\emptyset_u$ and M_y is defined as the moment corresponding to $\emptyset_y$. Thus, it measures the ability of a cross section to maintain flexural strength when inelastically loaded, directly relating to member and structure ductility.

$$\Omega_o = \frac{Mu}{My} \qquad 5\text{-}2$$

Moment-curvature diagrams are also used to analyze how the different confinement types and parameters affect cross section flexural strength. To do this, moment-curvature diagrams for the different cross sections with an applied Axial Load Ratio of 0.2 are presented. The different moment capacities of the various cross sections are then compared to demonstrate how the confinement type or parameter influences the cross section flexural strength.

Additionally, the curvatures, moments, and axial loads determined in the moment-curvature which is normalized and analyzed to determine the no dimensional effects of each parameter. Curvatures are normalized by multiplying them by the cross side length (in mm) as demonstrated in equation 5.3. Equation 5.4 normalizes the moments by dividing them by the product of the unconfined concrete strength, the gross cross section area, and the section side length. Analyzing normalized moments allows the relative effects of a parameter and the efficiency of each cross section to be measured.

$$\emptyset_N = \emptyset \times t_x \quad 5\text{-}3$$

$$M_N = \frac{M}{f_{cu}\, A_g t_x} \quad 5\text{-}4$$

5.2 Parametric Study

Table 5-1 summarizes the details of the specimens used in the parametric study the behavior of each specimen is investigated for axial load ratio of 0.1, 0.2 and 0.5. Fig. 5-1 shows a schematic for square and rectangular columns.

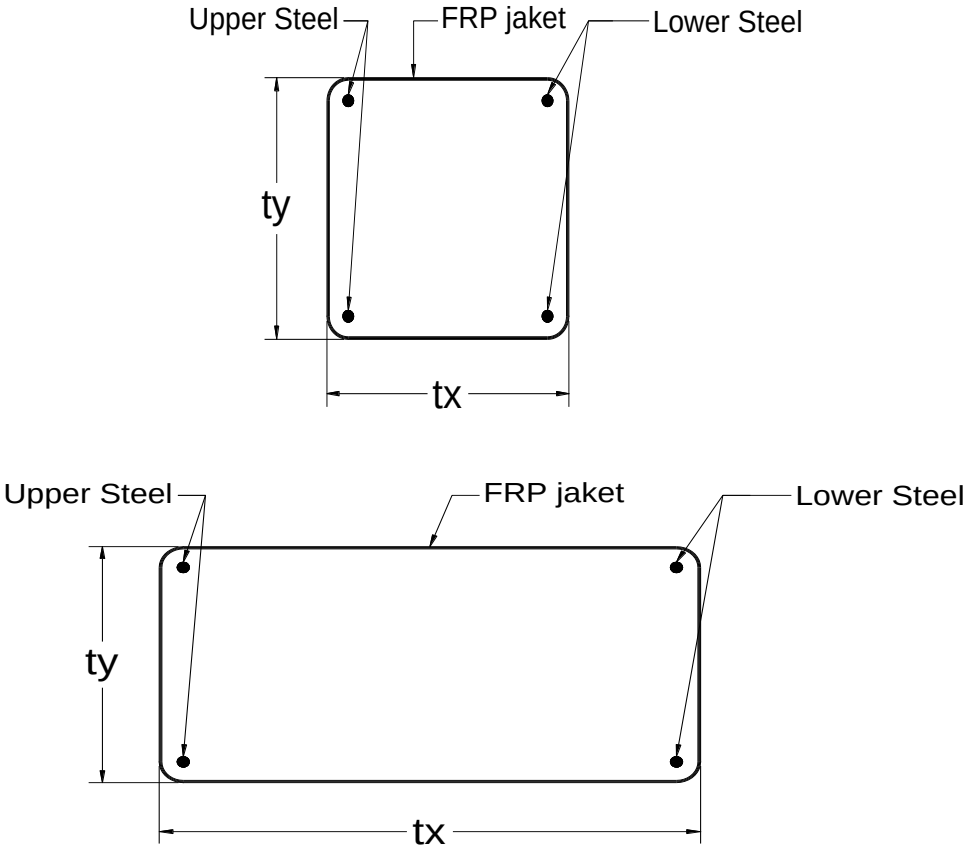

Fig. 5-1 Schematic for square and rectangular specimen

As shown in Table 5-2, two types of FRP are utilized which are carbon and glass fibers. Two values of concrete compressive strengths are used (30 N/mm^2, 50 N/mm^2) .The longitudinal steel reinforcement ratio used is 1% and 2.5%. And the jacket thickness used for confinement is none, 1 and 3.

Table 5-1 Cross Section Configurations Summary

Shape	t_x mm	t_y mm	f_{cu} N/mm^2	t_j mm	$A_{S\%}$	**System**	**Stirrups**
Square	350	350	30	0	1	CFRP	no
Square	350	350	30	1	1	CFRP	no
Square	350	350	30	3	1	CFRP	no
Rec 1:2	350	700	30	0	1	CFRP	no
Rec 1:2	350	700	30	1	1	CFRP	no
Rec 1:2	350	700	30	3	1	CFRP	no
Rec 1:3	350	1050	30	0	1	CFRP	no
Rec 1:3	350	1050	30	1	1	CFRP	no
Rec 1:3	350	1050	30	3	1	CFRP	no
Square	350	350	50	1	1	CFRP	no
Rec 1:2	350	700	50	1	1	CFRP	no
Rec 1:3	350	1050	50	1	1	CFRP	no
Square	350	350	30	1	2.5	CFRP	no
Rec 1:2	350	700	30	1	2.5	CFRP	no
Rec 1:3	350	1050	30	1	2.5	CFRP	no
Square	350	350	30	1	2.5	GFRP	no
Rec 1:2	350	700	30	1	2.5	GFRP	no
Rec 1:3	350	1050	30	1	2.5	GFRP	no

Table 5-2 FRP material properties

FRP system	Glass	Carbon
FRP modulus of elasticity	26100	72400
Ultimate elongation of FRP	0.0211	0.0121

5.2.1 Effect of concrete compressive strength

Tables 5-3, 5-4 and figures 5-1 to 5-10 demonstrate the effect of concrete compressive strength on the seismic behavior of retrofitted columns. Cross sections with low concrete compressive strength showed higher ultimate and plastic curvature compared to cross sections with high concrete compressive strength which means that member ductility is reduced. It is also noticed that at higher axial load levels, ductility decreases even more significantly.

Analysis also showed that cross sections with high concrete compressive strength showed larger flexural resistance than others with low concrete compressive strength. However, normalized ultimate moment is inversely affected, meaning that the cross section is less efficient with high concrete compressive strengths. This occurs because only the compressive strength of concrete was increased, not the confinement of the cross section. Since there is no increase in confinement, the added strength of the cross section is attributed solely to the increase in concrete compressive strength. Higher axial loads showed positive effect of concrete flexural capacity.

It is also noticed that flexural capacity of cross sections with high concrete compressive strength and flexural capacity of cross sections with low concrete compressive strength are enhanced equally when increasing their jacket thickness. And the same is noticed regarding their ductility.

Table 5-3 Cross section configurations used for demonstrating the effect of f_{cu}

Shape	t_x mm	t_y mm	f_{cu} N/mm^2	t_j mm	$A_{S\%}$	System	Stirrups
Square	350	350	30	1	1	CFRP	no
Rec 1:2	350	700	30	1	1	CFRP	no
Rec 1:3	350	1050	30	1	1	CFRP	no
Square	350	350	50	1	1	CFRP	no
Rec 1:2	350	700	50	1	1	CFRP	no
Rec 1:3	350	1050	50	1	1	CFRP	no

Table 5-4 Effect of increasing fcu parameter

Section Property	Effect on square	Effect on 1:2 Rec	Effect on 1:3 Rec	Special notes
Plastic Curvature	Large Decrease	Moderate Decrease	Small Decrease	The influence decreases significantly as axial loads increase
Normalized Plastic Curvature	Large Decrease	Moderate Decrease	Small Decrease	The influence decreases significantly as axial loads increase
Ultimate moment	Small Increase	Moderate Increase	Large Increase	The influence increases significantly as axial loads increase
Normalized Ultimate moment	Small Increase	Small Increase	Small Increase	The influence constant significantly as axial loads increase
Ultimate Curvature	Large Decrease	Moderate Decrease	Small Decrease	The influence decreases significantly as axial loads increase
Normalized Ultimate Curvature	Large Decrease	Moderate Decrease	Small Decrease	The influence decreases significantly as axial loads increase
Flexural Over strength	No Change	No Change	No Change	
Displacement ductility factor	Large Decrease	Moderate Decrease	Small Decrease	Nearly no influence at higher Axial loads

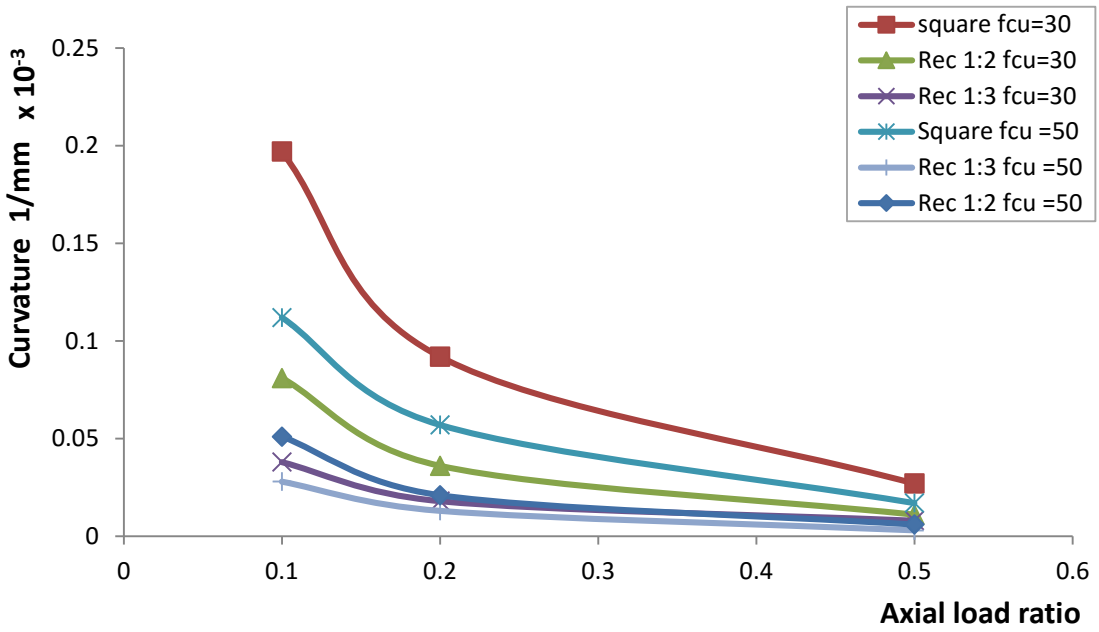

Fig. 5-2 Effect of axial load ratio on plastic curvature for diffrent aspect ratio and concrete strength at 1 mm thickness

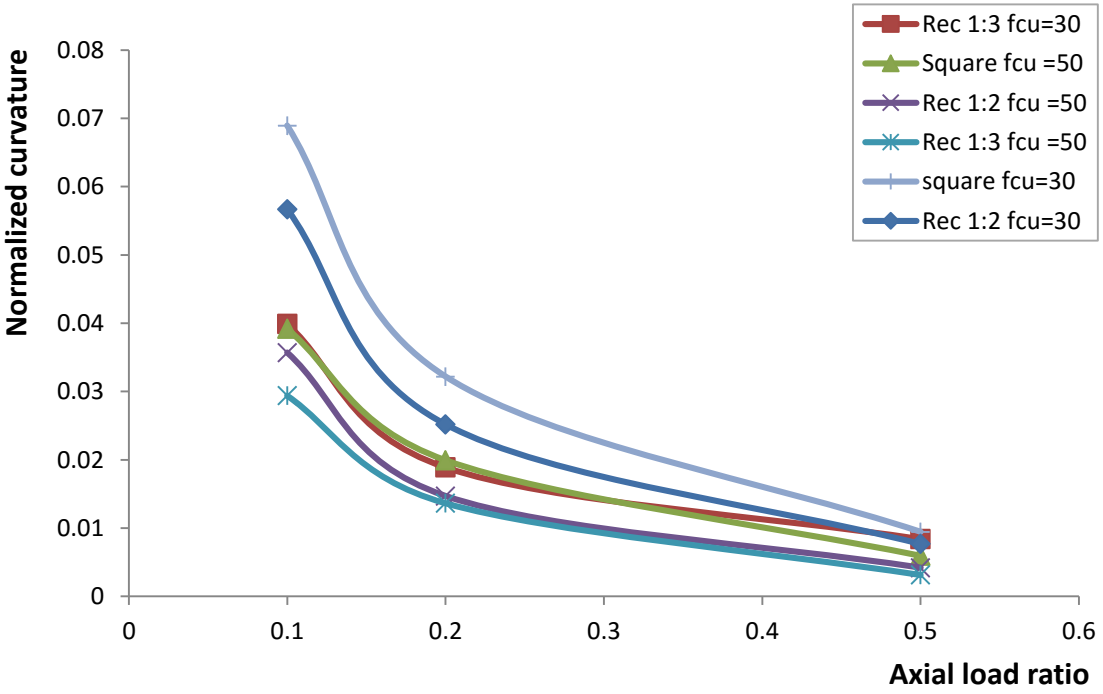

Fig. 5-3 Effect of axial load ratio on Normalized plastic curvature for diffrent aspect ratio and concrete strength at 1 mm thickness

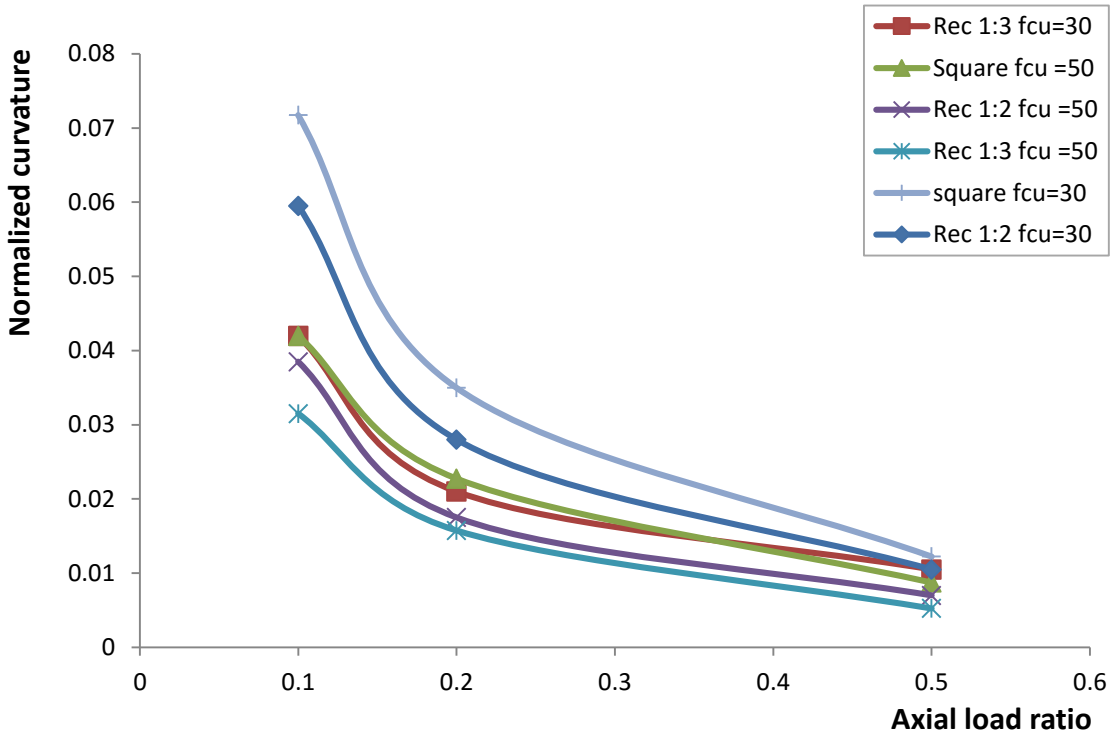

Fig. 5-4 Effect of axial load ratio on normalized ultimate curvature for different aspect ratio and concrete strength at 1 mm thickness

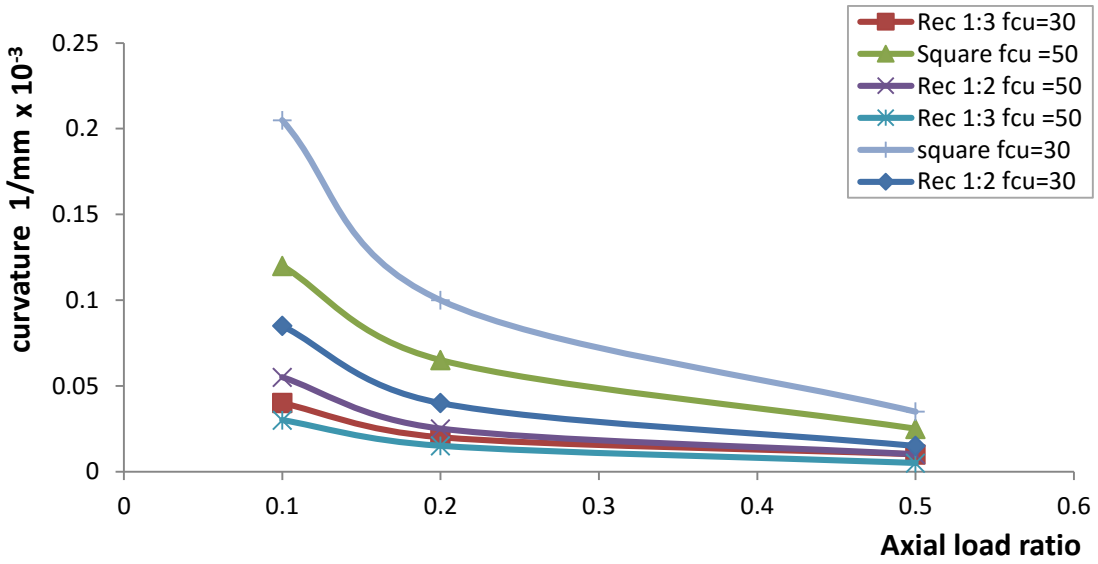

Fig. 5-5 Effect of axial load ratio on ultimate curvature for different aspect ratio and concrete strength at 1 mm thickness

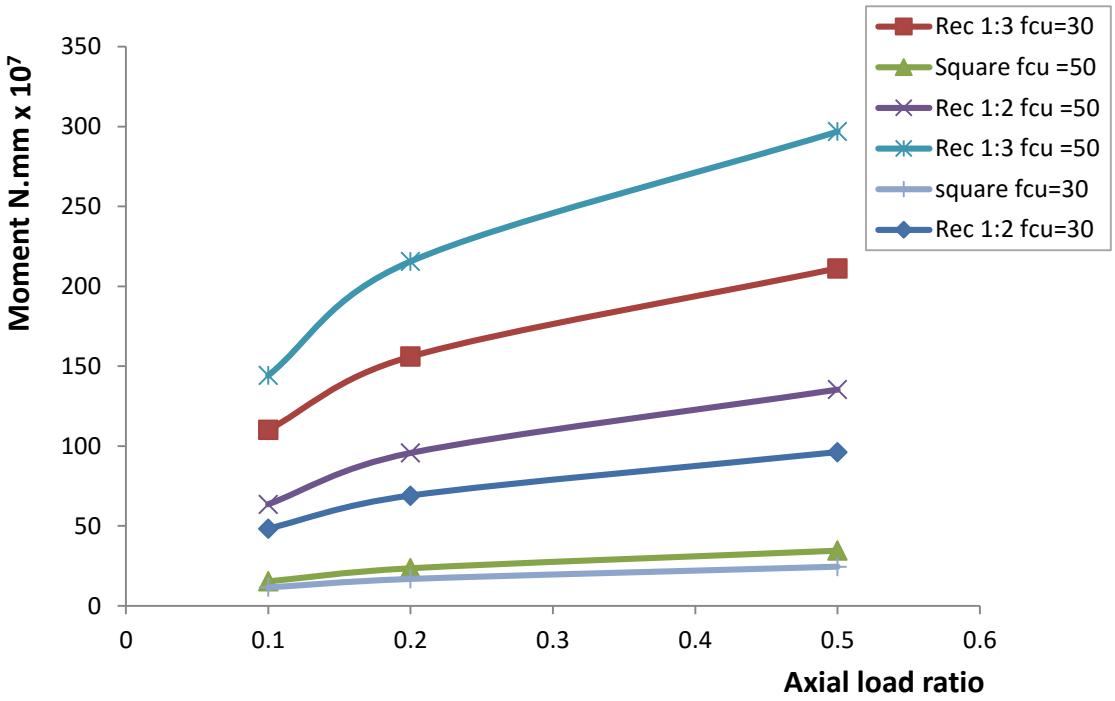

Fig. 5-6 Effect of axial load ratio on ultimate momment for different aspect ratio and concrete strength at 1 mm thickness

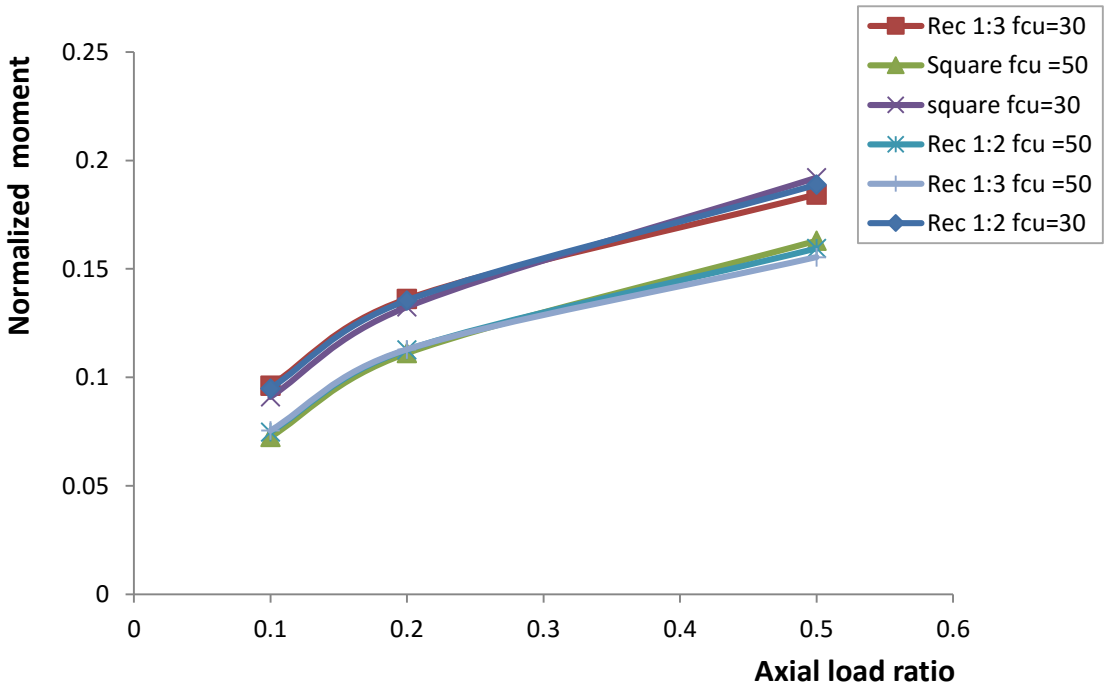

Fig. 5-7 Effect of axial load ratio on normalized ultimate moment for different aspect ratio and concrete strength at 1 mm thickness

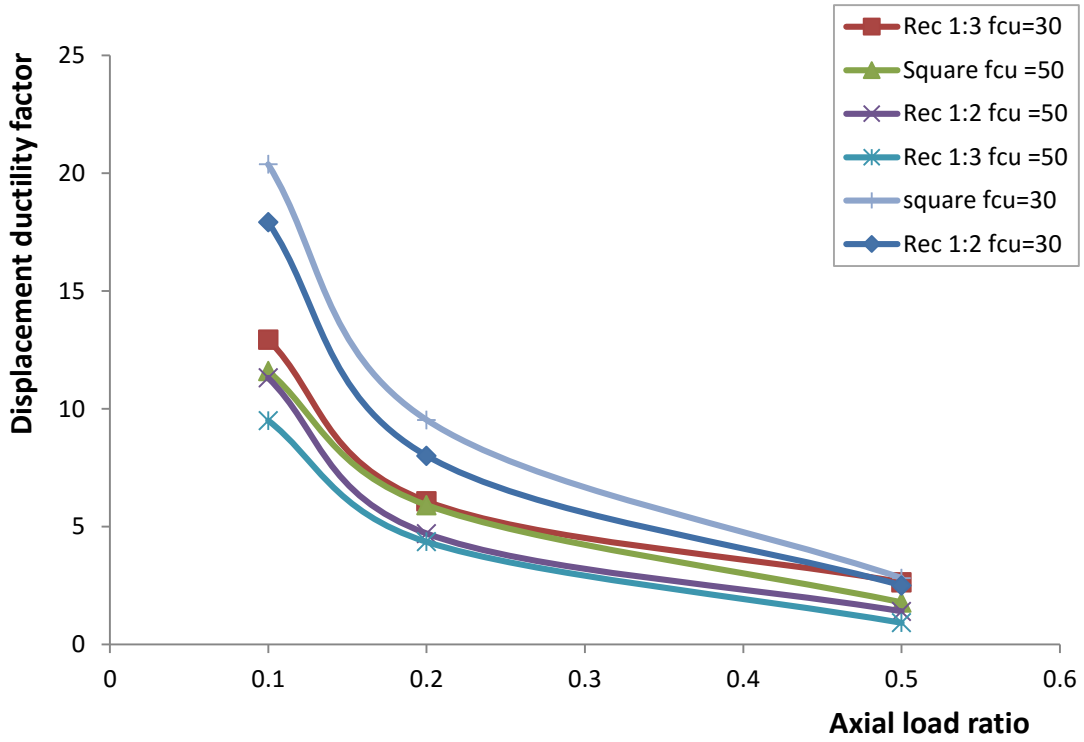

Fig. 5-8 Effect of axial load ratio on displacement ductility factor for different aspect ratio and concrete strength at 1 mm thickness.

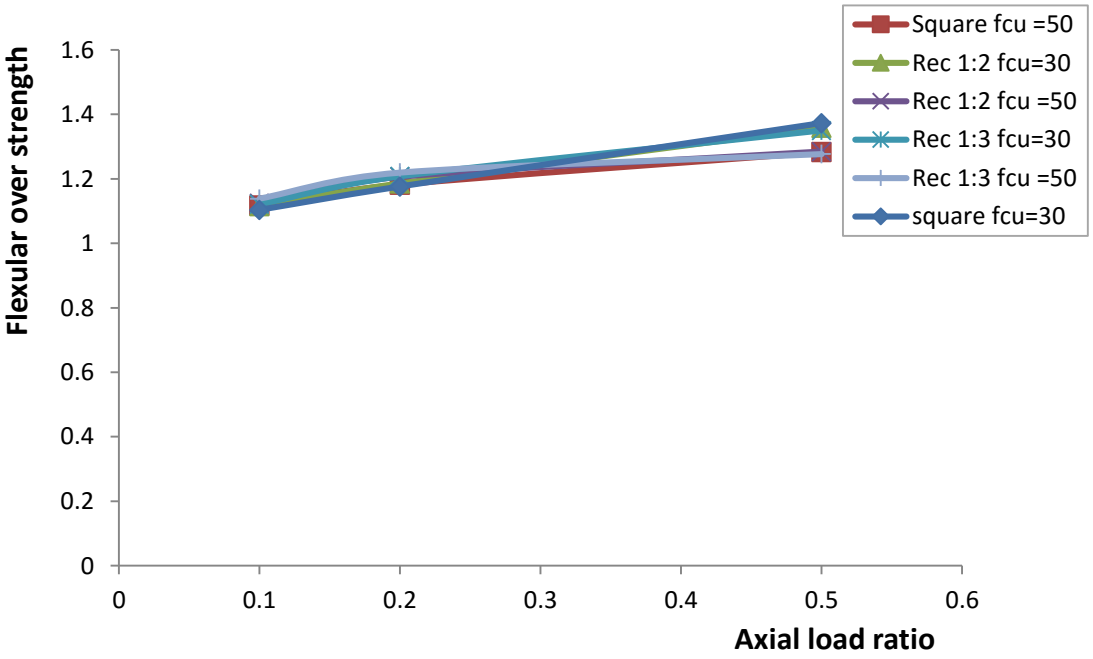

Fig. 5-9 Effect of axial load ratio on flexural over strength for different aspect ratio and concrete strength at 1 mm thickness.

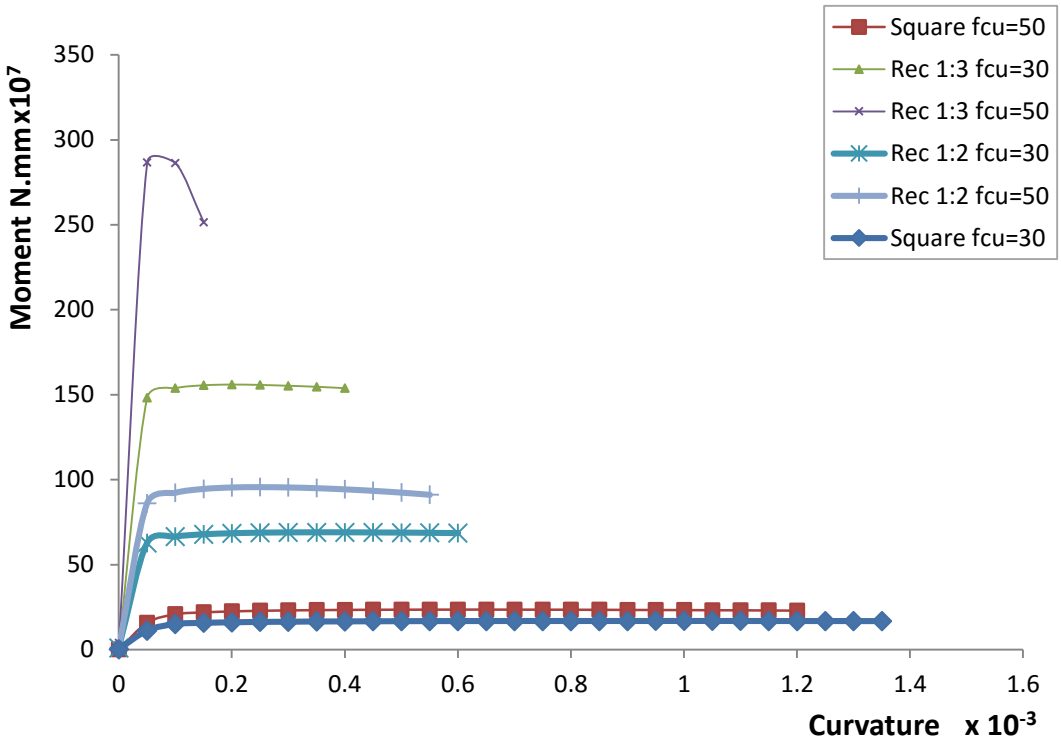

Fig. 5-10 M-phi Diagrams for different concrete strength and cross section aspect ratio at axial load ratio = 0.2

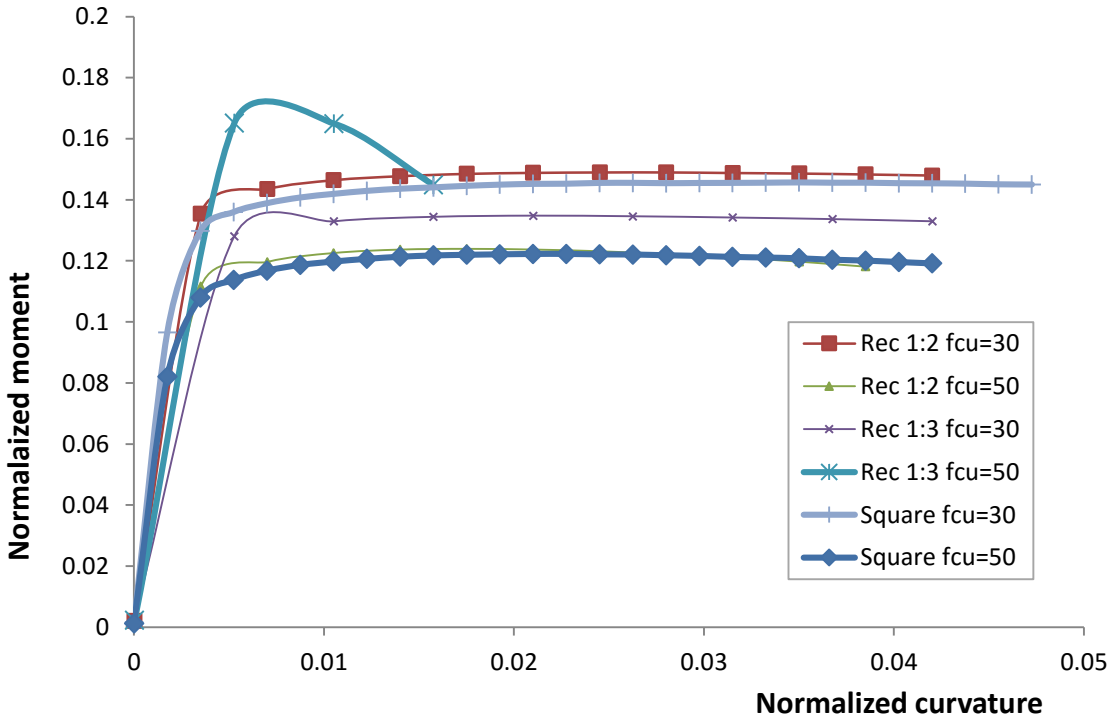

Fig. 5-11 Normalized M-phi Diagrams for different concrete strength and cross section aspect ratio at axial load ratio = 0.2

5.2.2 Effect of longitudinal steel ratio

Tables 5-5, 5-6 and figures 5-11 to 5-19 demonstrate the effect of the longitudinal steel reinforcement ratio on the seismic behavior of retrofitted columns. Cross section with higher longitudinal steel ratio showed lower ultimate and plastic curvature which means that ductility is reduced. This occurs because as a cross section becomes over-reinforced, the depth of the neutral axis increases causing failure of the extreme concrete compression fiber to occur at smaller curvatures.

Ultimate moment as well as its normalized values is high in cross sections with higher longitudinal reinforcement ratio which means that flexural strength is enhanced. In seismic design, the amount of longitudinal reinforcement used should be selected to balance member flexural strength and efficiency with the necessary member displacement capacity and ductility. Flexural over strength is not affected; this is because Yield and Ultimate moments are equally affected by the increase in longitudinal steel ratio.

It is also noticed that flexural capacity of cross sections with high longitudinal steel reinforcement ratio and flexural capacity of cross sections with low longitudinal steel reinforcement ratio are enhanced equally when increasing their jacket thickness. The same is noticed regarding their ductility.

Table 5-5 Cross section configurations used to demonstrate the effect of As%

Shape	t_x mm	t_y mm	f_{cu} N/mm^2	t_j mm	$A_{S\%}$	**System**	**Stirrups**
Square	350	350	30	1	1	CFRP	no
Rec 1:2	350	750	30	1	1	CFRP	no
Rec 1:3	350	1050	30	1	1	CFRP	no
Square	350	350	30	1	2.5	CFRP	no
Rec 1:2	350	750	30	1	2.5	CFRP	no
Rec 1:3	350	1050	30	1	2.5	CFRP	no

Table 5-6 effect of $A_{s\,\%}$ parameter

Section Property	Effect on square	Effect on 1:2 Rec	Effect on 1:3 Rec	Special notes
Plastic Curvature	Large Decrease	Moderate Decrease	Small Decrease	The influence decreases significantly as axial loads increase
Normalized Plastic Curvature	Large Decrease	Moderate Decrease	Small Decrease	The influence decreases significantly as axial loads increase
Ultimate moment	Large Decrease	Moderate Decrease	Small Decrease	The influence decreases significantly as axial loads increase
Normalized Ultimate moment	Large Decrease	Moderate Decrease	Small Decrease	The influence decreases significantly as axial loads increase
Ultimate Curvature	Small Increase	Moderate Increase	Large Increase	The influence slightly decreases as axial loads increase
Normalized Ultimate Curvature	Small Increase	Moderate Increase	Large Increase	The influence slightly decreases as axial loads increase
Flexural Over strength	No Change	No Change	No Change	
Displacement ductility factor	Decrease	Decrease	Decrease	Nearly no influence at higher Axial loads

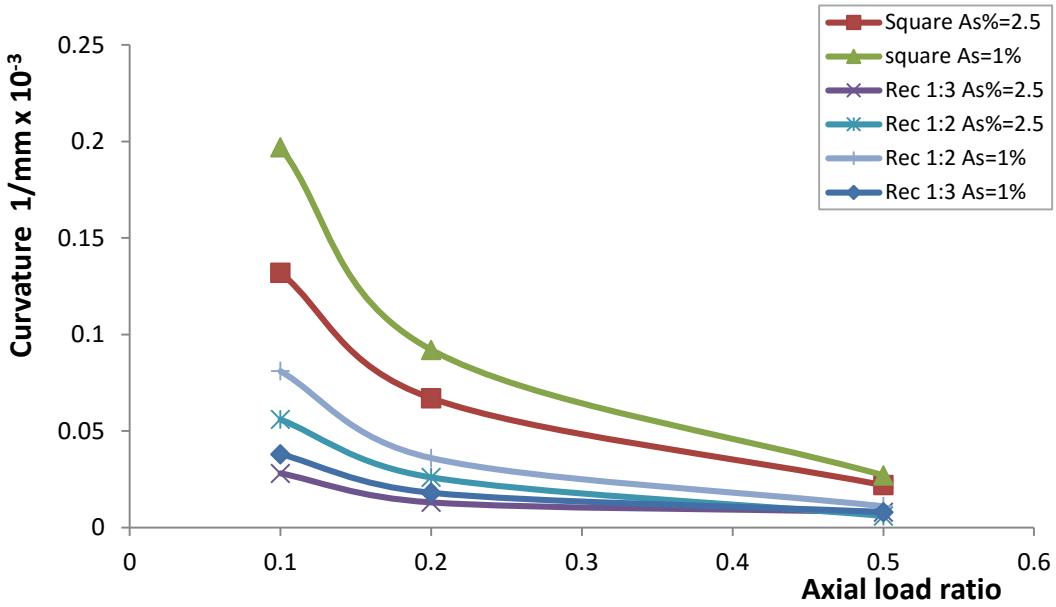

Fig. 5-12 Effect of axial load ratio on plastic curvature for different aspect ratio and steel reinforcenemet percentage at 1 mm thickness.

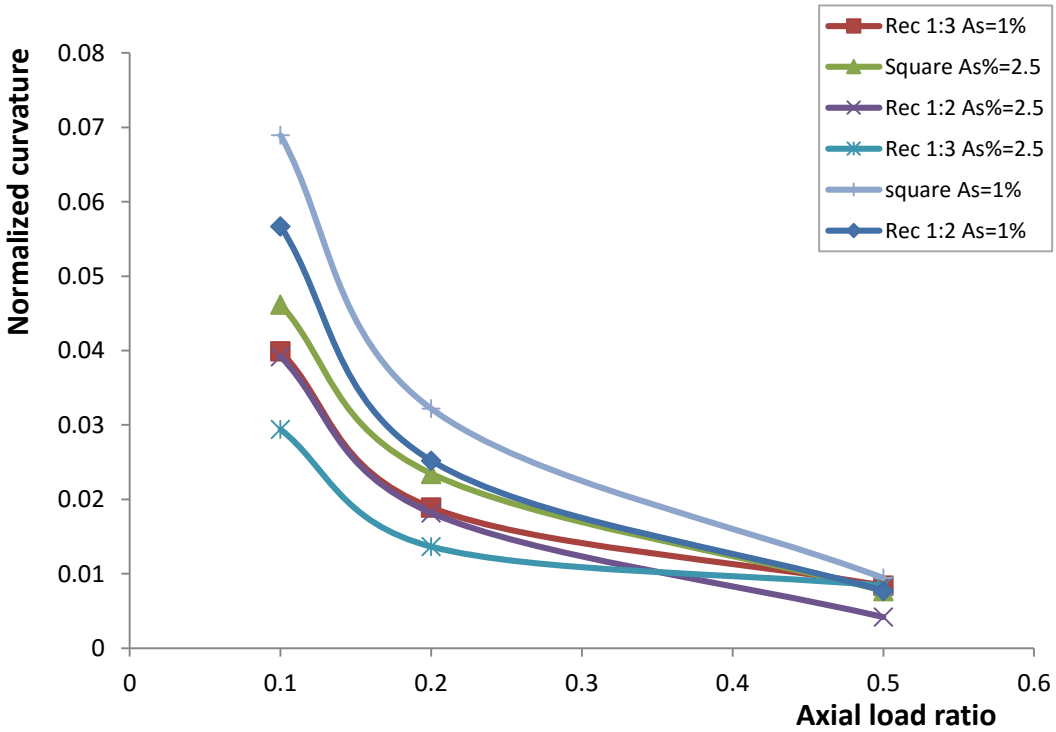

Fig. 5-13 Effect of axial load ratio on normalized plastic curvature for different aspect ratio and steel reinforcement percentage at 1 mm thickness.

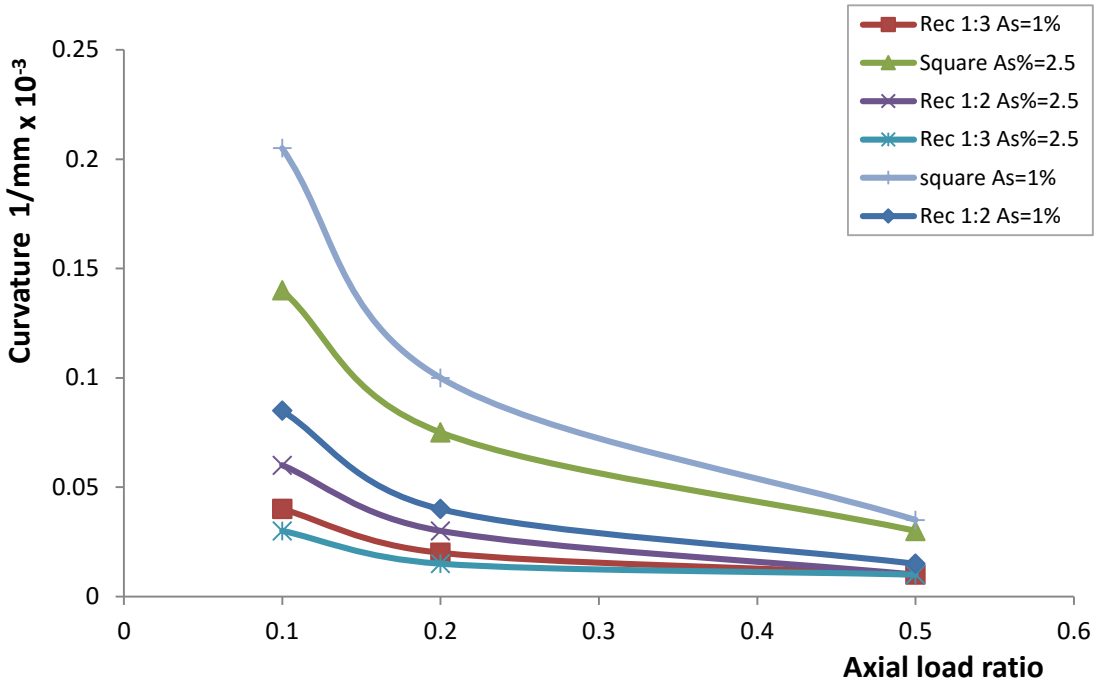

Fig. 5-14 Effect of axial load ratio on normalized plastic curvature for different aspect ratio and steel reinforcement percentage at 1 mm thickness.

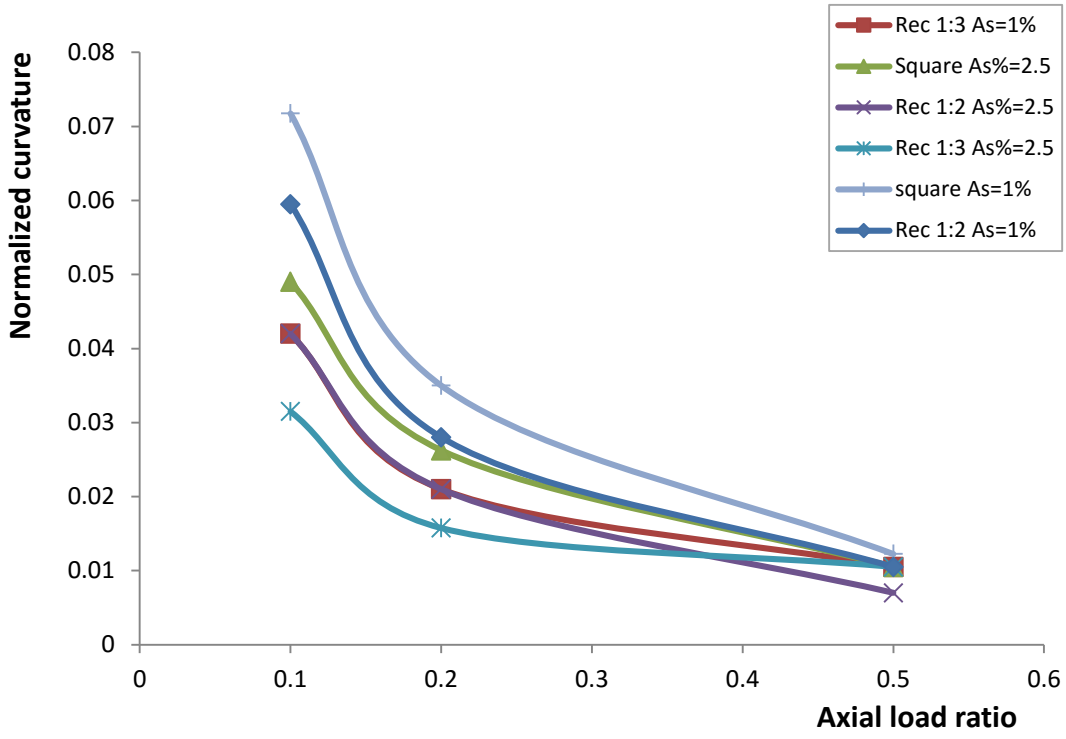

Fig. 5-15 Effect of axial load ratio on normalized ultimate curvature for different aspect ratio and steel reinforcement at 1 mm thickness.

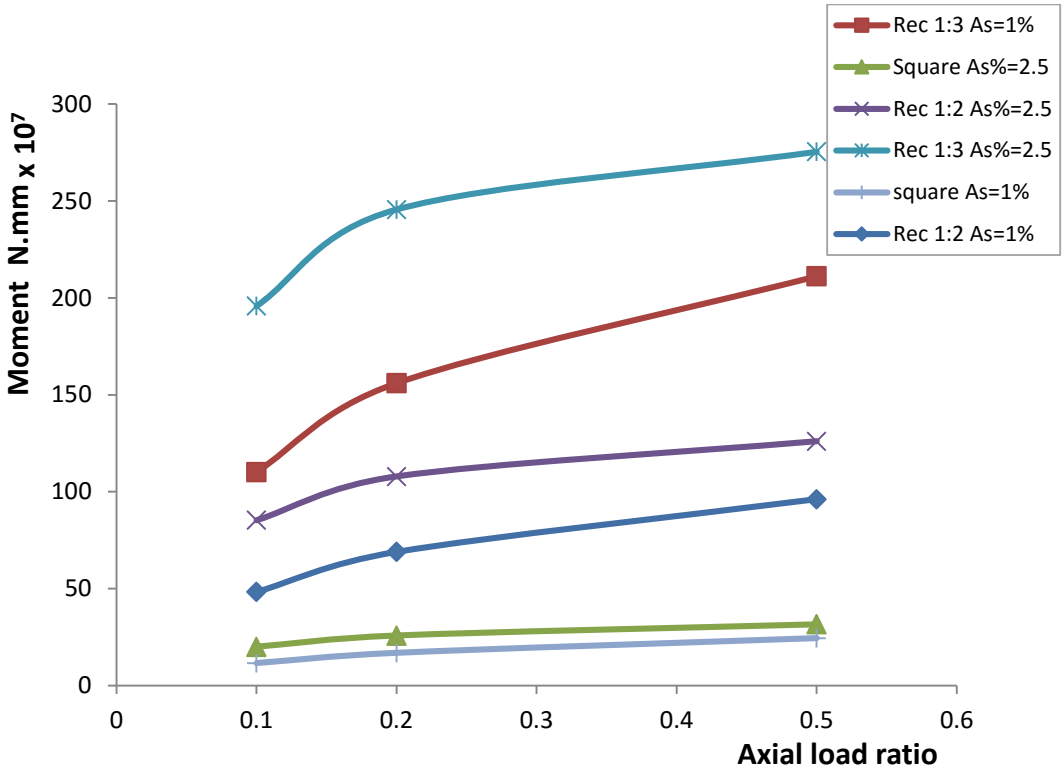

Fig. 5-16 Effect of axial load ratio on ultimate moment for different aspect ratio and steel reinforcement at 1 mm thickness.

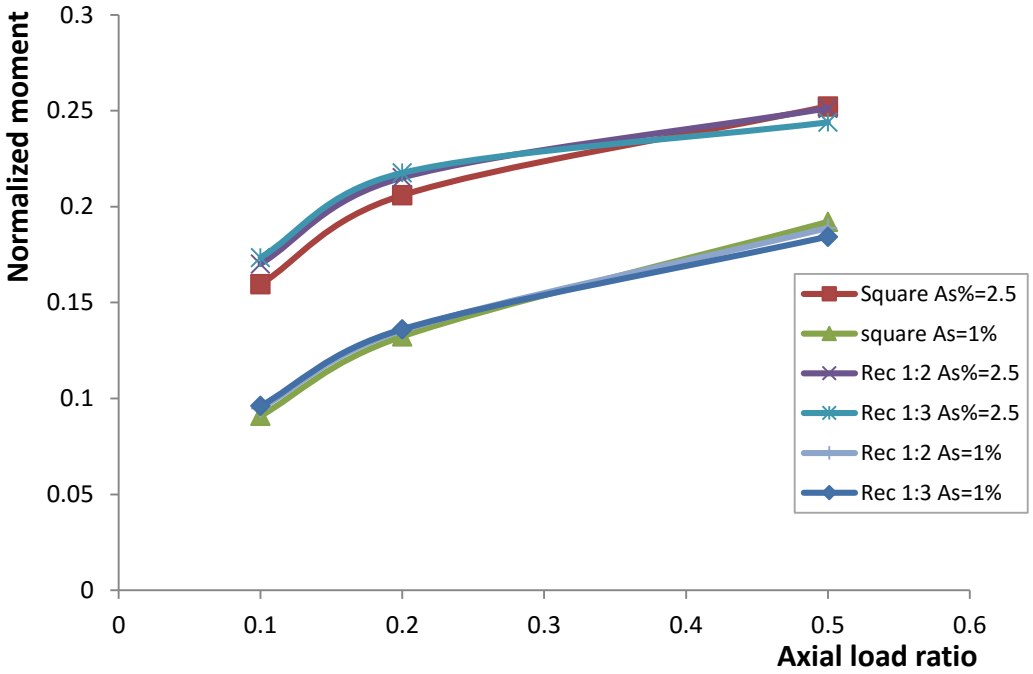

Fig. 5-17 Effect of axial load ratio on normalized ultimate moment for different aspect ratio and steel reinforcement at 1 mm thickness.

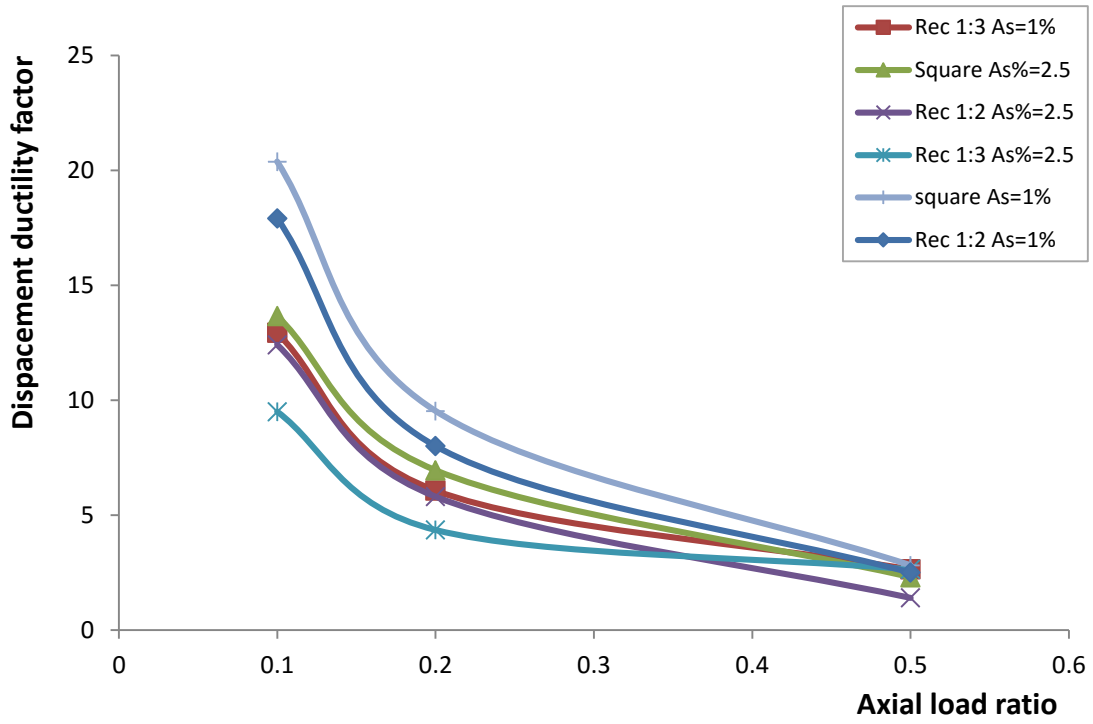

Fig. 5-18 Effect of axial load ratio on displacement ductility factor for different aspect ratio and steel reinforcement at 1 mm thickness.

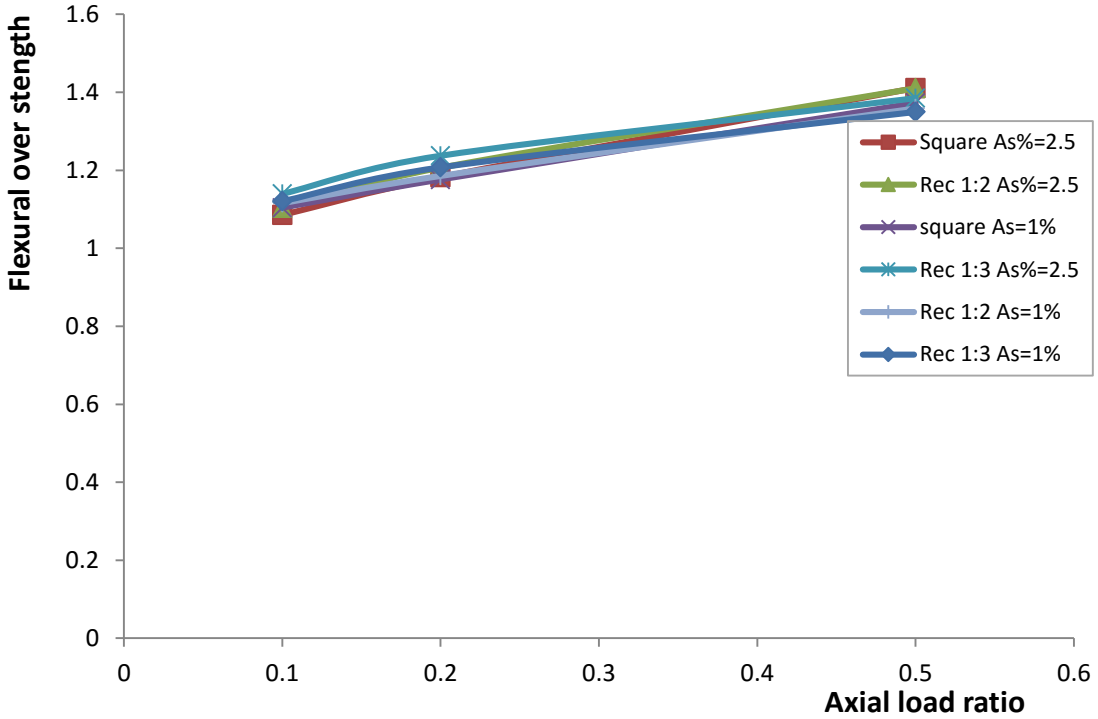

Fig. 5-19 Effect of axial load ratio on flexural over strength for different aspect ratio and steel reinforcement at 1 mm thickness.

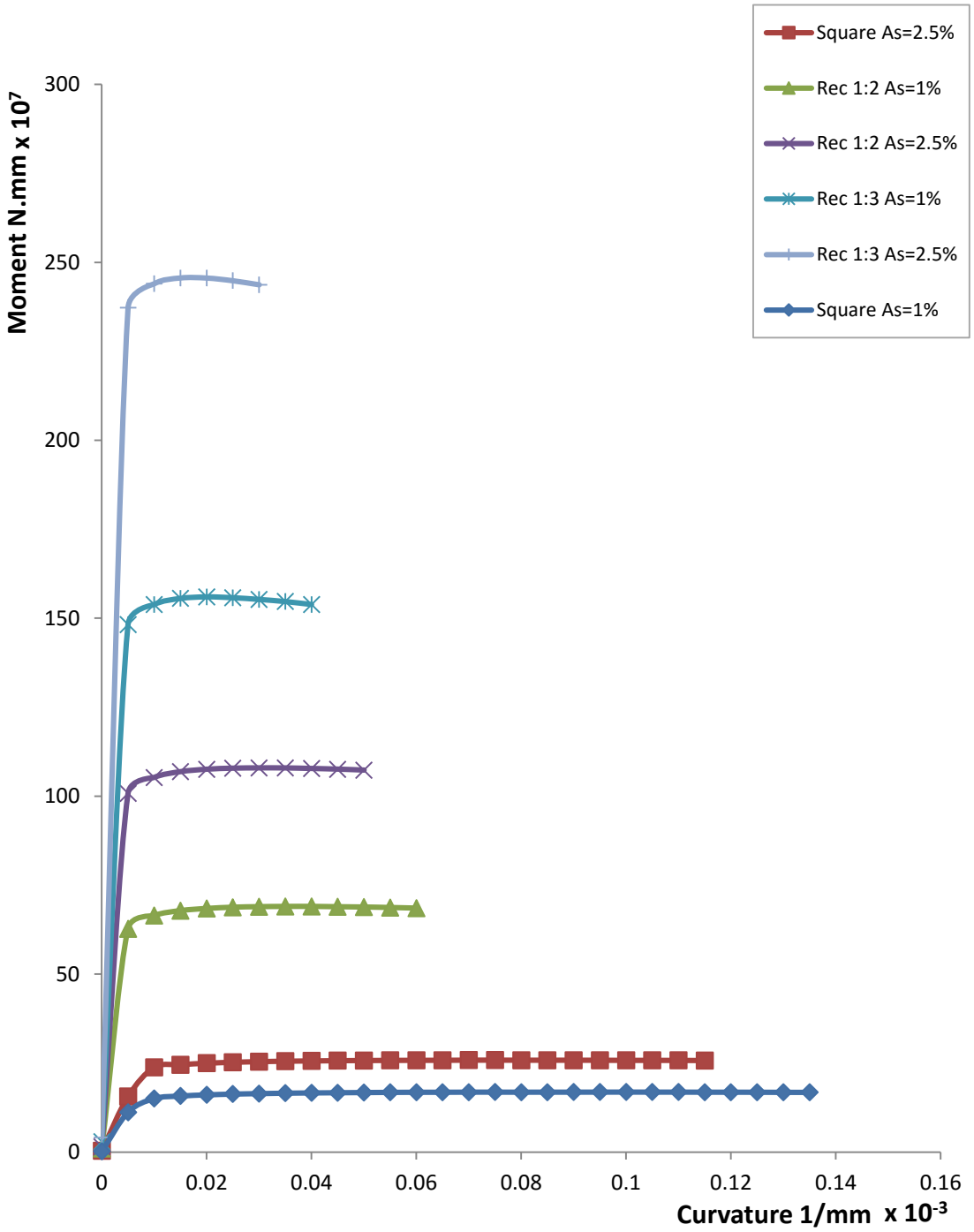

Fig. 5-20 M-phi Diagrams for different steel reinforcement precentage and cross section aspect ratio at axial load ratio = 0.2

5.2.3 Effect of jacket thickness

Tables 5-7, 5-8 and figures 5.20 to 5.28 demonstrates the effect of jacket thickness used for confinement on the seismic behaviour of retrofitted columns. As the jacket becomes thicker, the ultimate and plastic curvature increase, which means the enhancement of the rotational capacity and ductility of columns. However at higher axial loads, this influence is reduced.

It is shown that both the normalized and ultimate moment is weakly enhanced with the increase in jacket thickness. Therefore, increasing the jacket thickness has a small influence on flexural capacity of retrofitted columns. It is noticed that at higher axial loads flexural strength enhancement is amplified.

This influence of the jacket thickness affects square columns more than rectangular columns as rotational capacity is clearly more enhanced; therefore the cross section aspect ratio is of primary concern for inelastic design of confined columns regarding seismic behavior.

Table 5-7 Cross sections configuration used for demonstrating the effect of jacket thickness

Shape	t_x mm	t_y mm	f_{cu} N/mm^2	t_j mm	$A_{S\%}$	System	Stirrups
Square	350	350	30	0	1	CFRP	no
Square	350	350	30	1	1	CFRP	no
Square	350	350	30	3	1	CFRP	no
Rec 1:2	350	750	30	0	1	CFRP	no
Rec 1:2	350	750	30	1	1	CFRP	no
Rec 1:2	350	750	30	3	1	CFRP	no
Rec 1:3	350	1050	30	0	1	CFRP	no
Rec 1:3	350	1050	30	1	1	CFRP	no
Rec 1:3	350	1050	30	3	1	CFRP	no

Table 5-8 Effect of increasing jacket thickness on confined concrete

Section Property	Effect on square	Effect on 1:2 Rec	Effect on 1:3 Rec	Special notes
Plastic Curvature	Large Increase	Moderate Increase	Small Increase	The influence decreases significantly as axial loads increase
Normalized Plastic Curvature	Large Increase	Moderate Increase	Small Increase	The influence decreases significantly as axial loads increase
Ultimate moment	Small Increase	Small Increase	Small Increase	This increase is significant at high axial loads
Normalized Ultimate moment	Small Increase	Small Increase	Small Increase	This increase is significant at high axial loads
Ultimate Curvature	Large Increase	Moderate Increase	Small Increase	The influence decreases significantly as axial loads increase
Normalized Ultimate Curvature	Large Increase	Moderate Increase	Small Increase	The influence decreases significantly as axial loads increase
Flexural Over strength	Increase	Increase	Increase	This increase is significant at high axial loads
Displacement ductility factor	Large Increase	Moderate Increase	Small Increase	The influence decreases significantly as axial loads increase

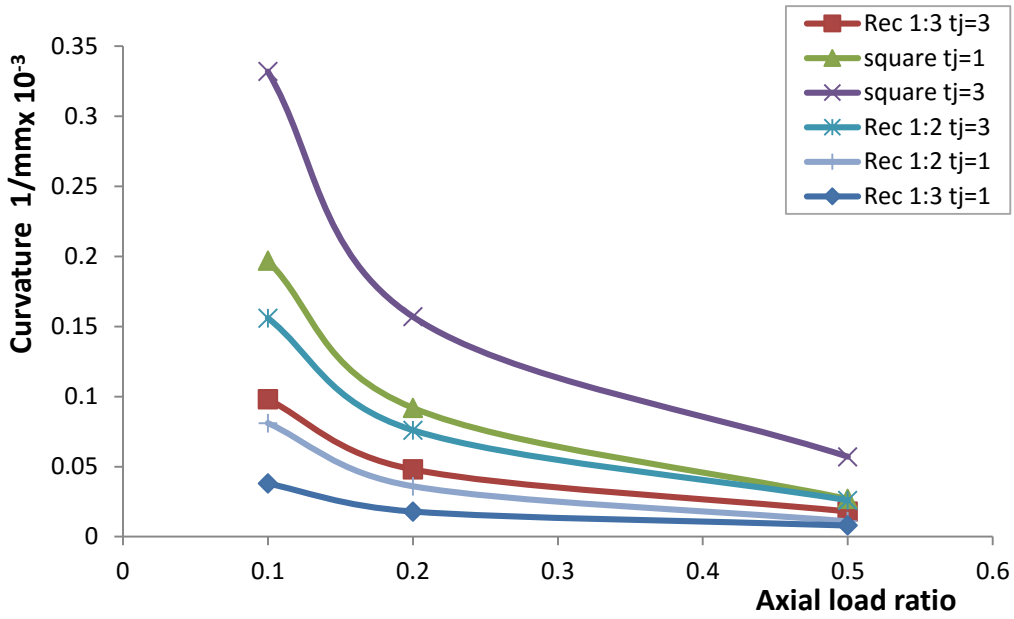

Fig. 5-21 Effect of axial load ratio on plastic curvature for different aspect ratio and FRP thickness.

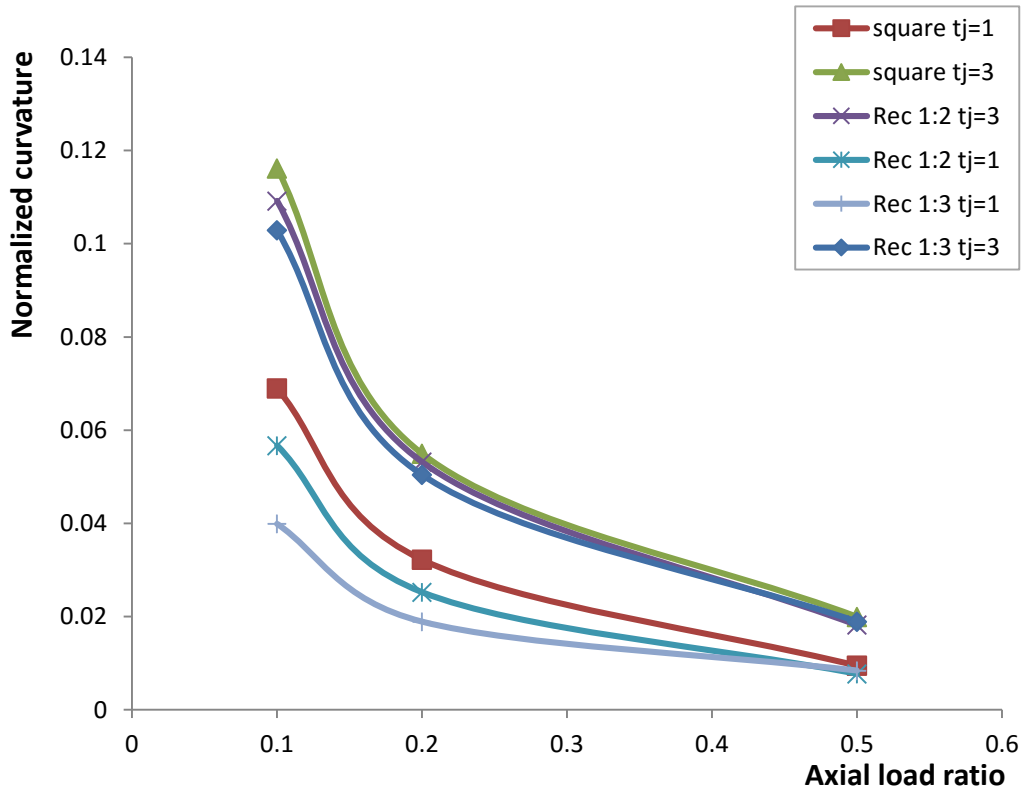

Fig. 5-22 Effect of axial load ratio on normalaized plastic curvature for different aspect ratio and FRP thickness.

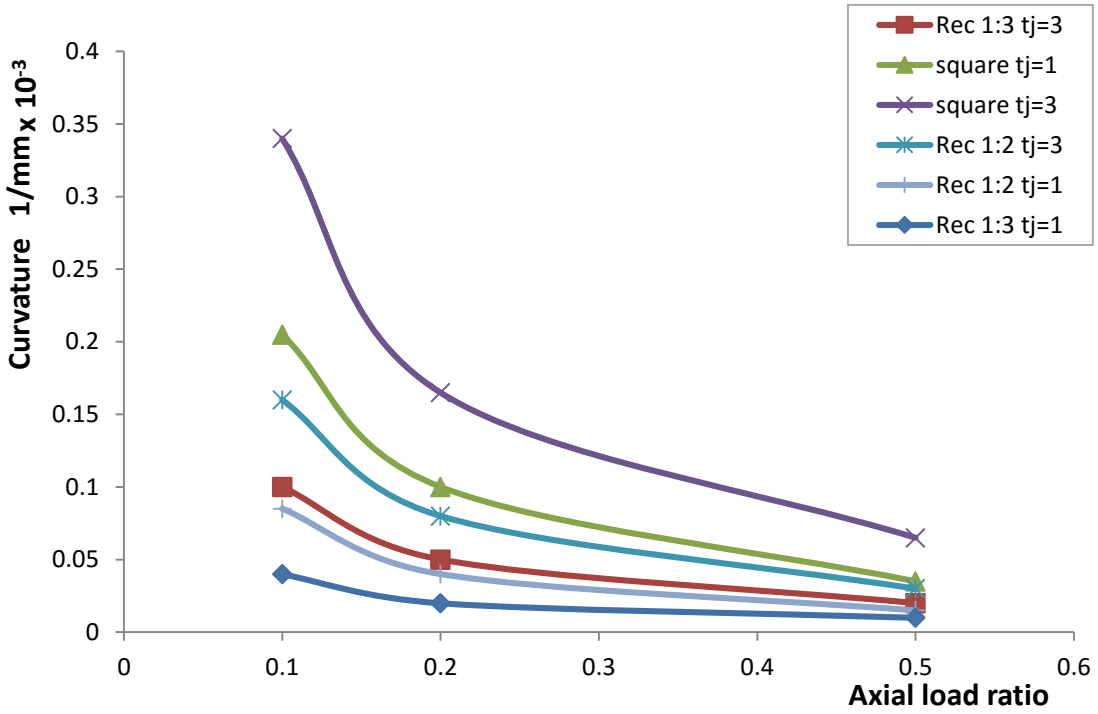

Fig. 5-23 Effect of axial load ratio on ultimate curvature for different aspect ratio and FRP thickness.

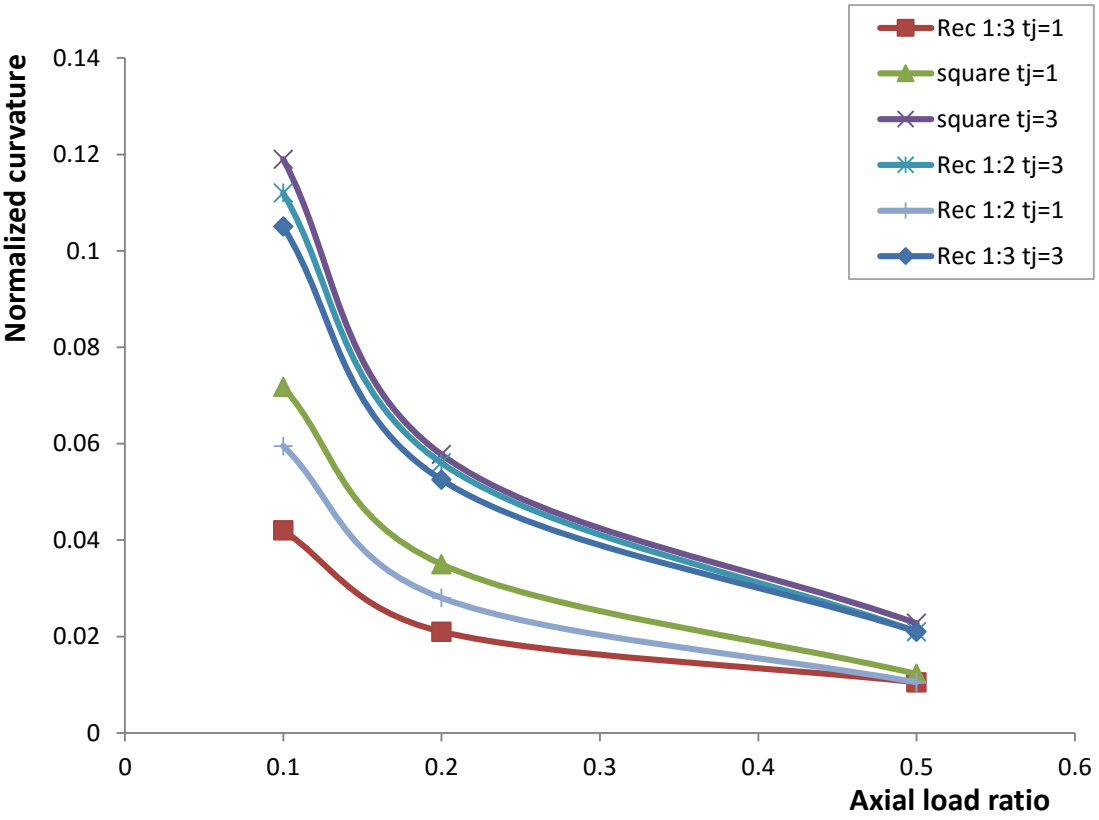

Fig. 5-24 Effect of axial load ratio on normalized ultimate curvature for different aspect ratio and FRP thickness.

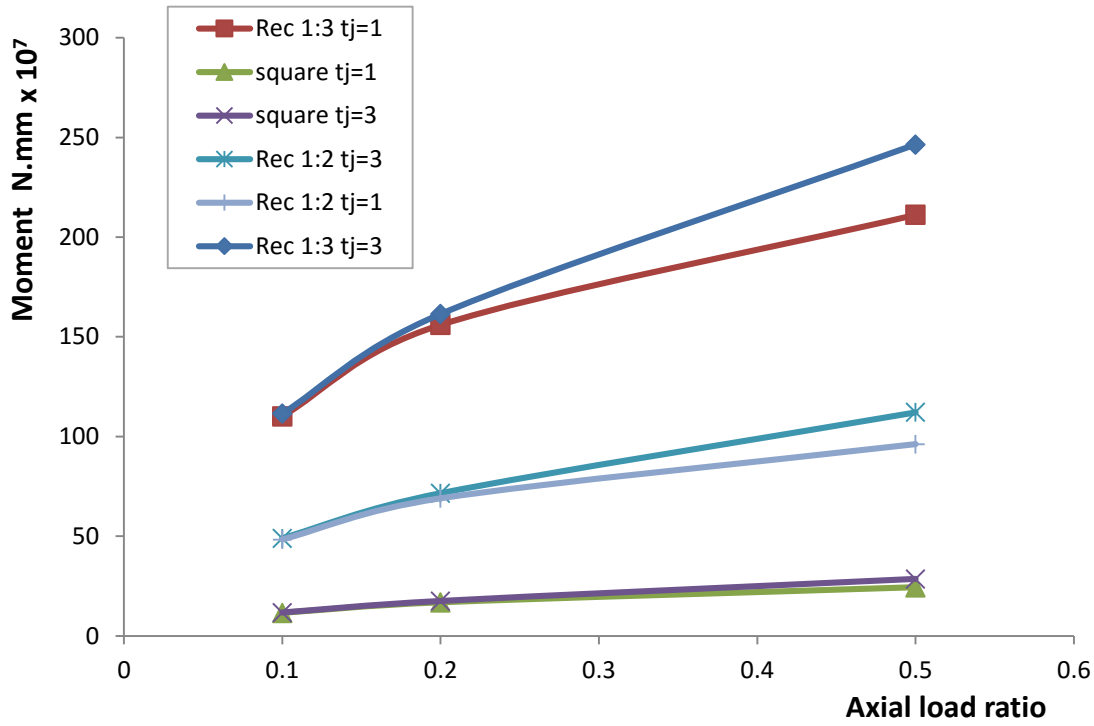

Fig. 5-25 Effect of axial load ratio on ultimate moment for different aspect ratio and FRP thickness.

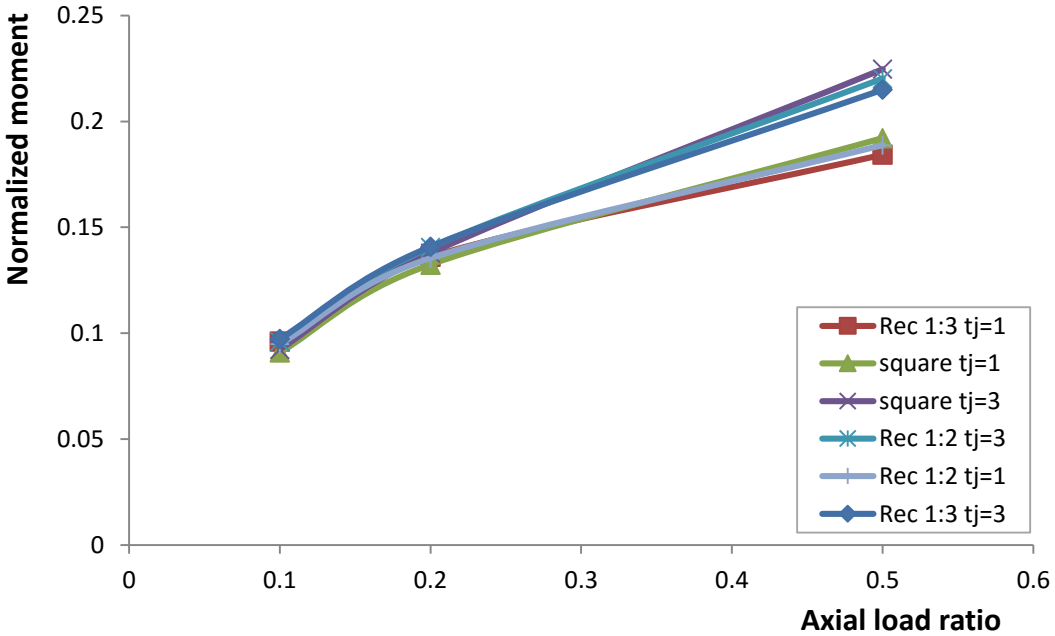

Fig. 5-26 Effect of axial load ratio on normalized ultimate moment for different aspect ratio and FRP thickness.

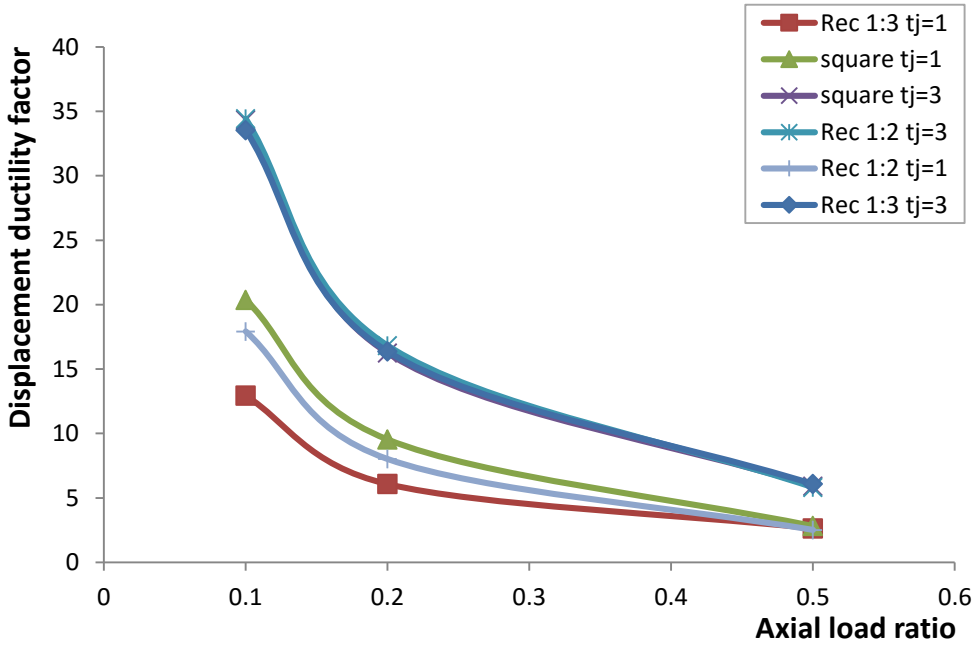

Fig. 5-27 Effect of axial load ratio on displacement ductility factor for different aspect ratio and FRP thickness.

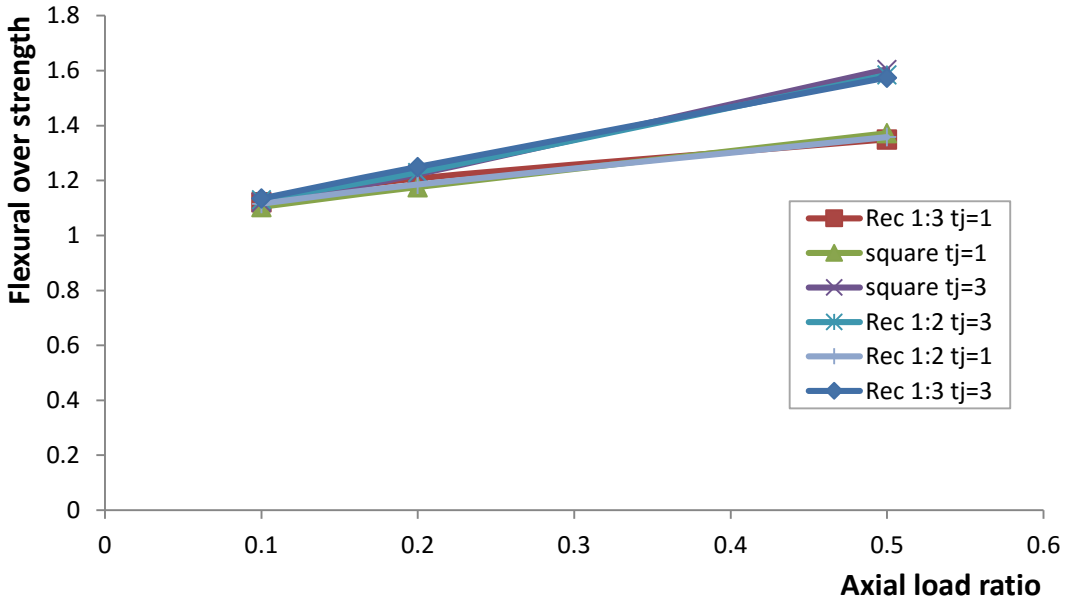

Fig. 5-28 Effect of axial load ratio on flexural over strength for different aspect ratio and FRP thickness.

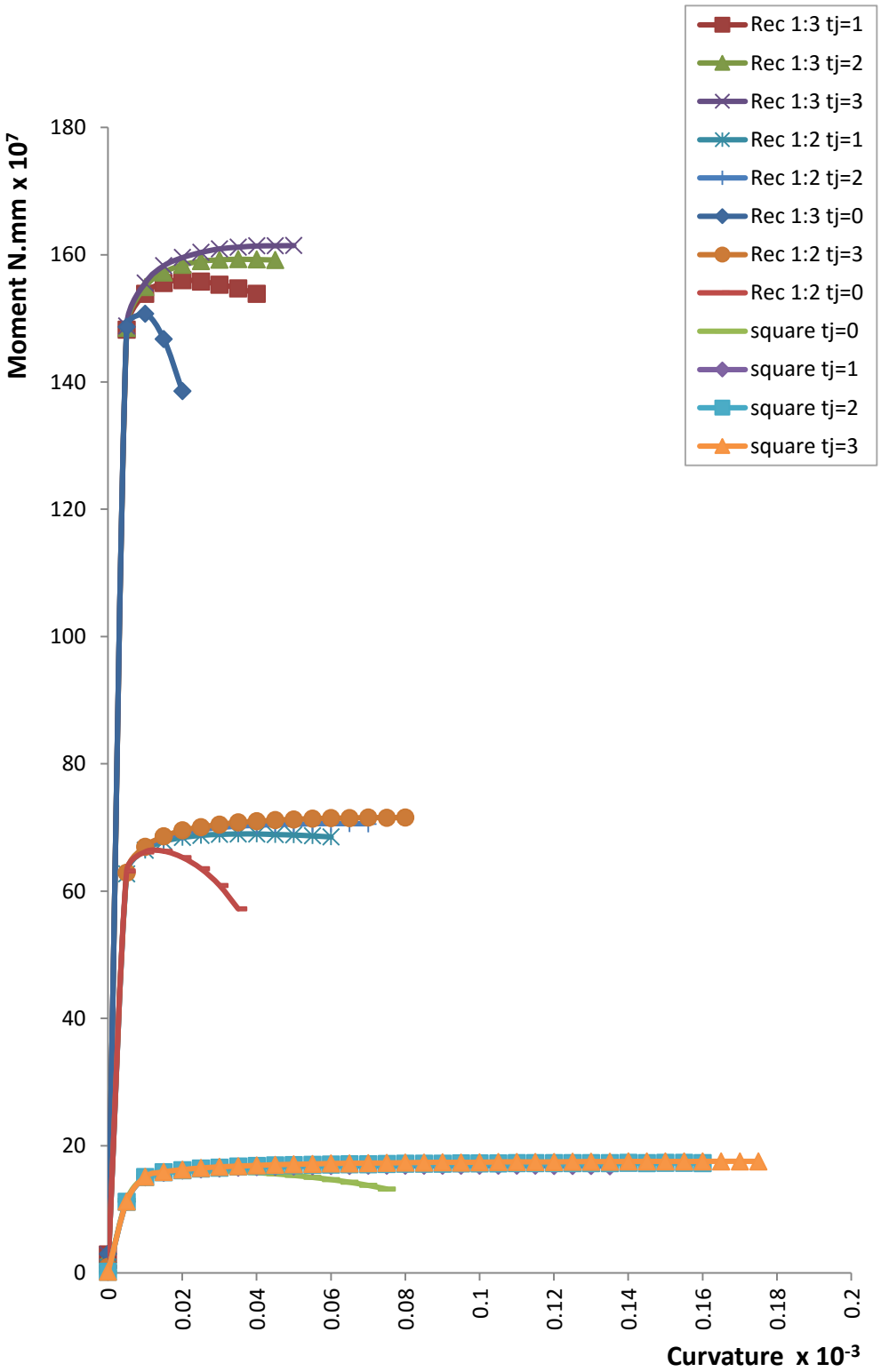

Fig. 5-29 M-phi Diagrams for different FRP thickness and cross section aspect ratio at axial load ratio = 0.2

5.2.4 Effect of FRP System Parameter Study

Tables 5-9, 5-10 and figures 5.29 to 5.37 demonstrate the effect of the type of jacket used for confinement on the seismic behavior of retrofitted columns. The cross sections wrapped with CFRP have larger ultimate and plastic curvature compared to confinement with GFRP. Thus it is shown that the CFRP provides more ductility.

Square columns respond more to enhancement when they are wrapped with CFRP. At higher axial loads, the influence of the jacket is reduced concerning ductility. On the other hand CFRP positive effect on flexural capacity is enhanced.

Table 5-9 Cross sections configuration used for demonstrating the effect of changing the FRP type

Shape	t_x mm	t_y mm	f_{cu} N/mm^2	t_j mm	$A_{S\%}$	**System**	**Stirrups**
Square	350	350	30	1	1	CFRP	no
Rec 1:2	350	750	30	1	1	CFRP	no
Rec 1:3	350	1050	30	1	1	CFRP	no
Square	350	350	30	1	1	GFRP	no
Rec 1:2	350	750	30	1	1	GFRP	no
Rec 1:3	350	1050	30	1	1	GFRP	no

Table 5-10 FRP system property influence on confined concrete

Section Property	Effect on square	Effect on 1:2 Rec	Effect on 1:3 Rec	Special notes
Plastic Curvature	Large Increase	Moderate Increase	Small Increase	The influence decreases significantly as axial loads increase
Normalized Plastic Curvature	Large Increase	Moderate Increase	Small Increase	The influence decreases significantly as axial loads increase
Ultimate moment	Small Increase	Small Increase	Small Increase	This influence is significant at high axial loads
Normalized Ultimate moment	Small Increase	Small Increase	Small Increase	This influence is significant at high axial loads
Ultimate Curvature	Large Increase	Moderate Increase	Small Increase	The influence decreases significantly as axial loads increase
Normalized Ultimate Curvature	Large Increase	Moderate Increase	Small Increase	The influence decreases significantly as axial loads increase
Flexural Over strength	Increase	Increase	Increase	This influence is significant at high axial loads
Displacement ductility factor	Large Increase	Moderate Increase	Small Increase	The influence decreases significantly as axial loads increase

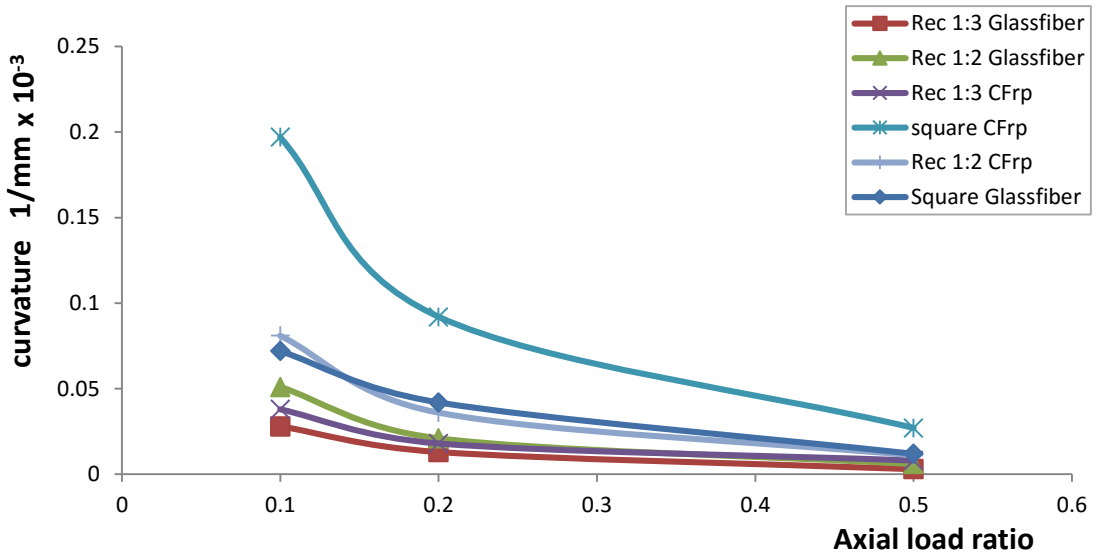

Fig. 5-30 Effect of axial load ratio on plastic curvature for different aspect ratio and FRP types at 1mm thickness.

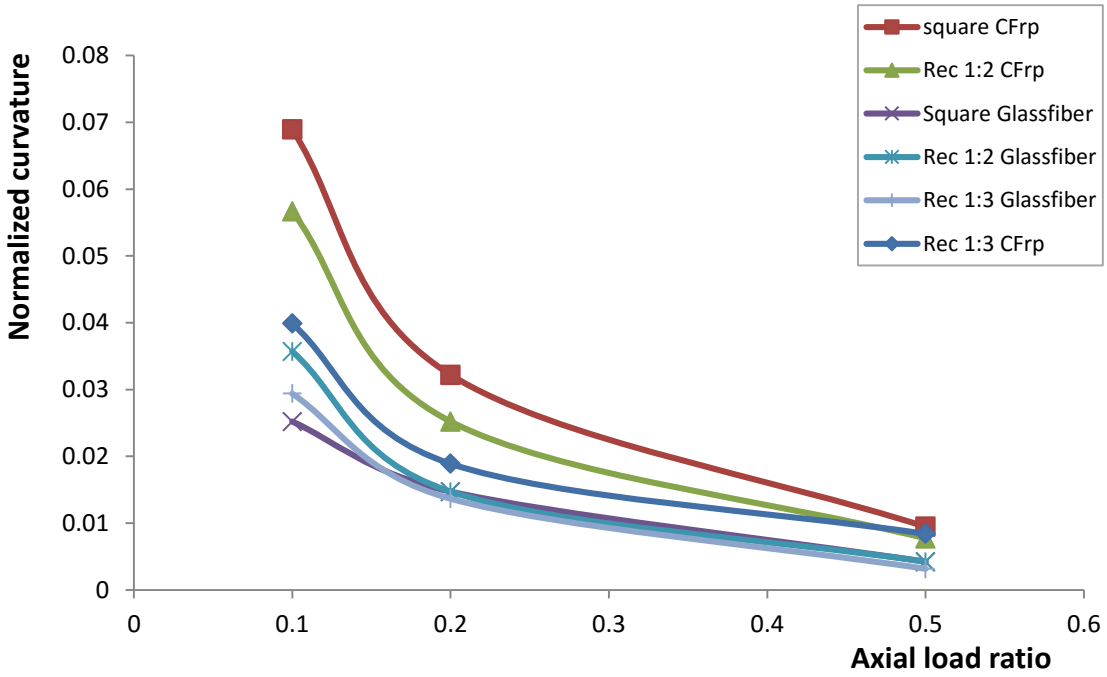

Fig. 5-31 Effect of axial load ratio on normalized plastic curvature for different aspect ratio and FRP types at 1mm thickness.

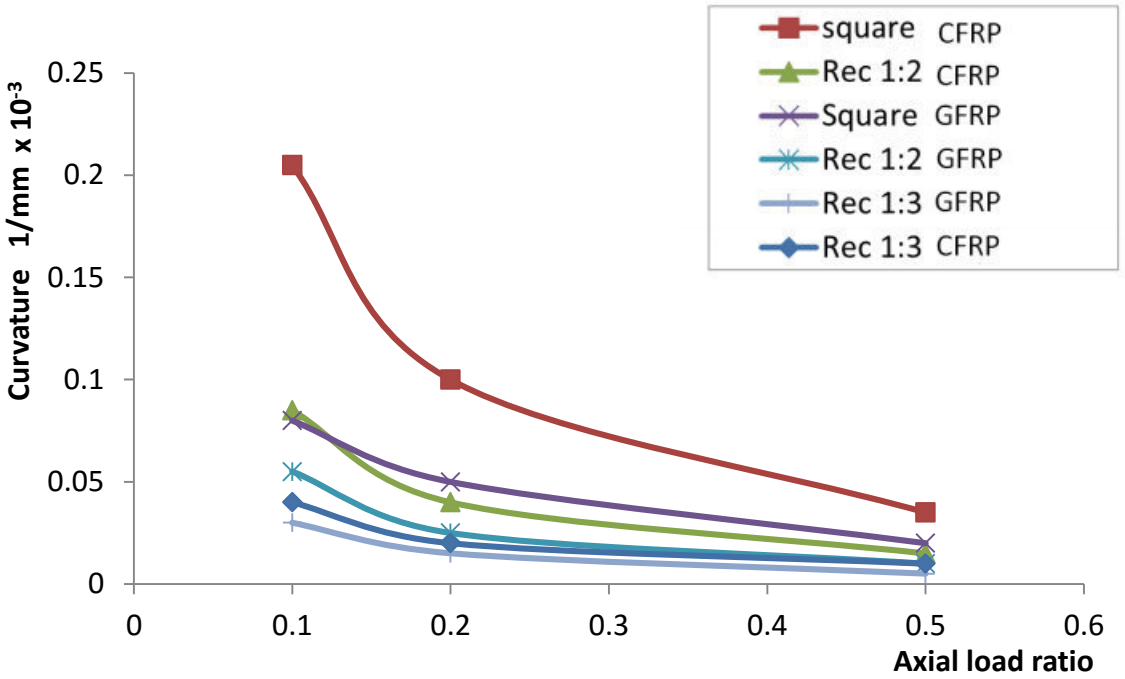

Fig. 5-32 Effect of axial load ratio on ultimate curvature for different aspect ratio and FRP types at 1mm thickness.

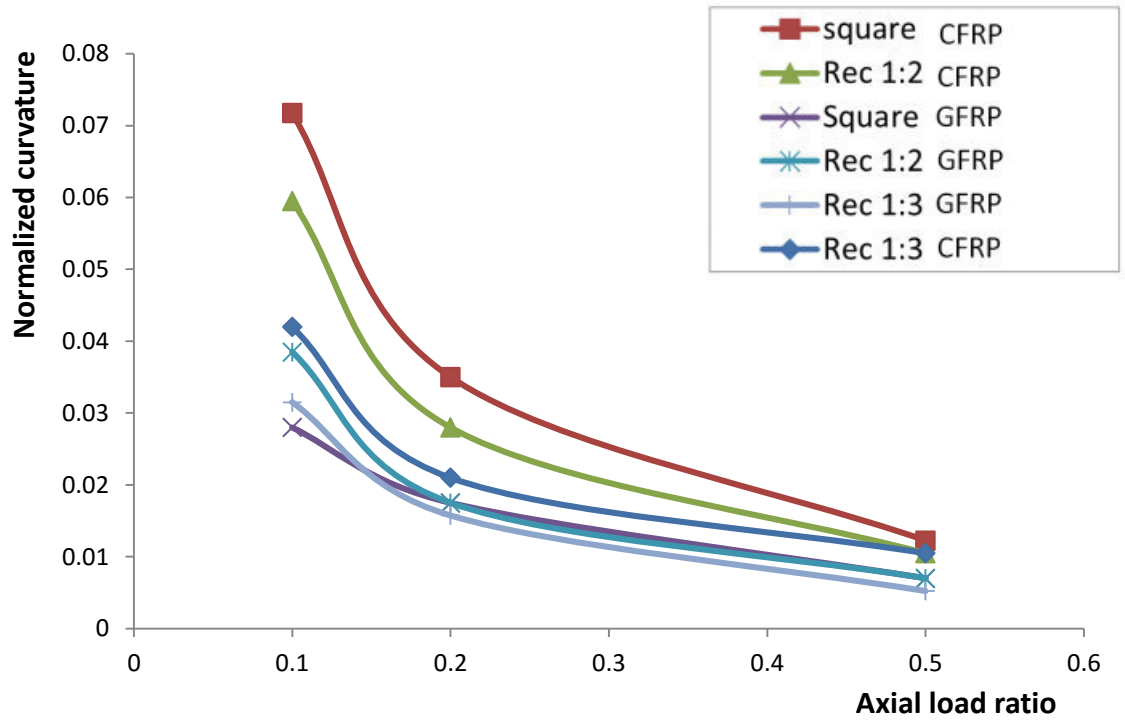

Fig. 5-33 Effect of axial load ratio on normalized ultimate curvature for different aspect ratio and FRP types at 1mm thickness.

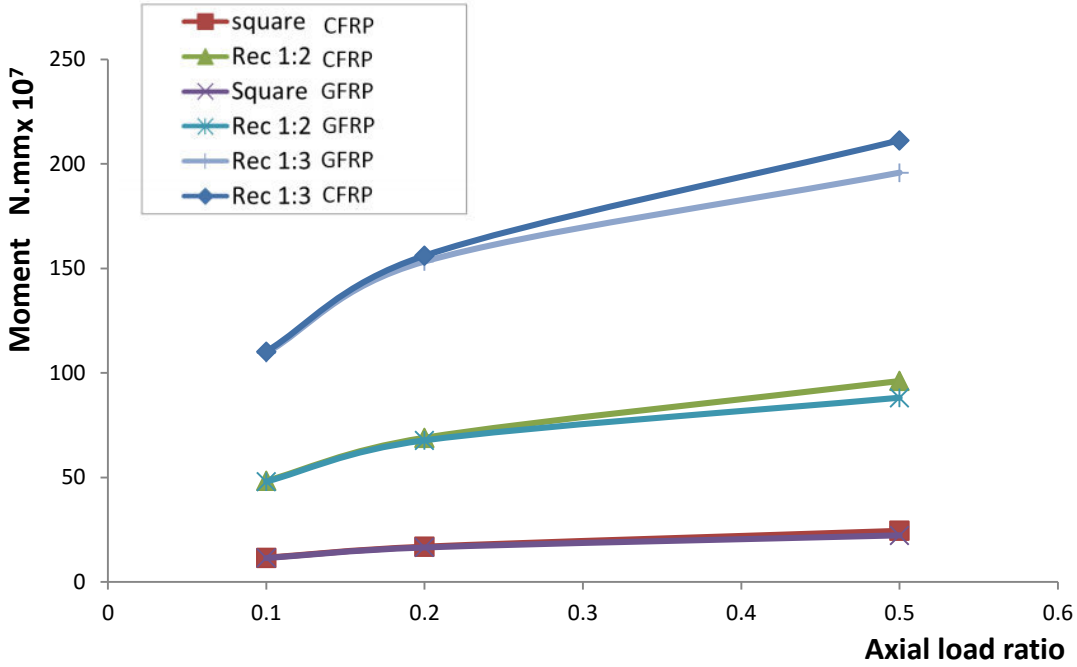

Fig. 5-34 Effect of axial load ratio on ultimate moment for different aspect ratio and FRP types at 1mm thickness.

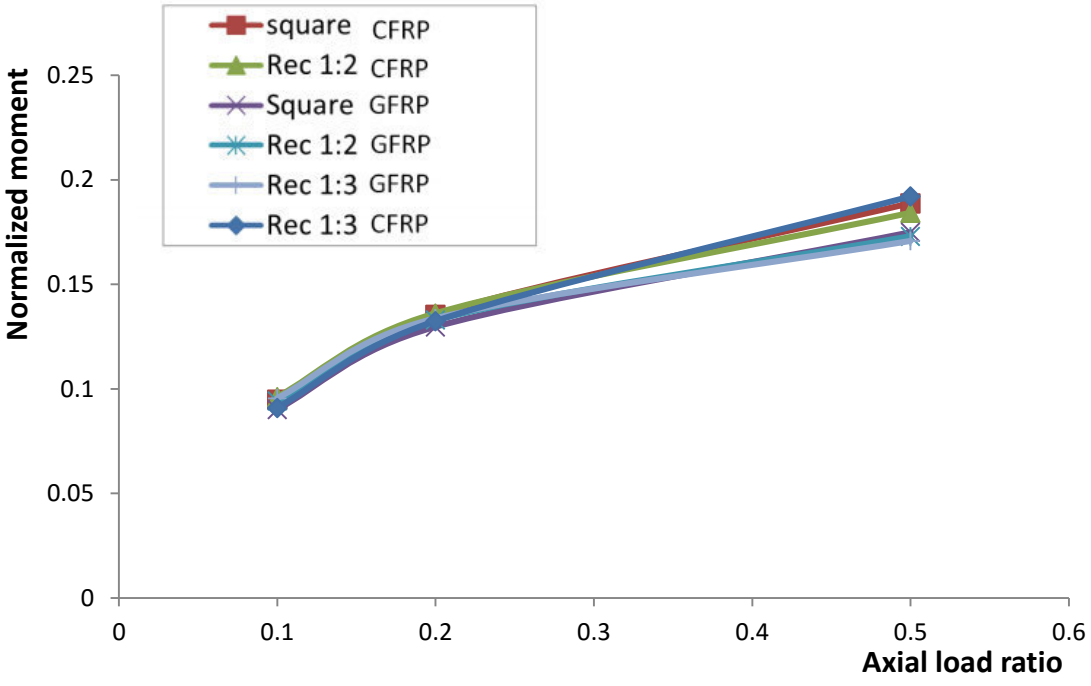

Fig. 5-35 Effect of axial load ratio on normalized ultimate moment for different aspect ratio and FRP types at 1mm thickness.

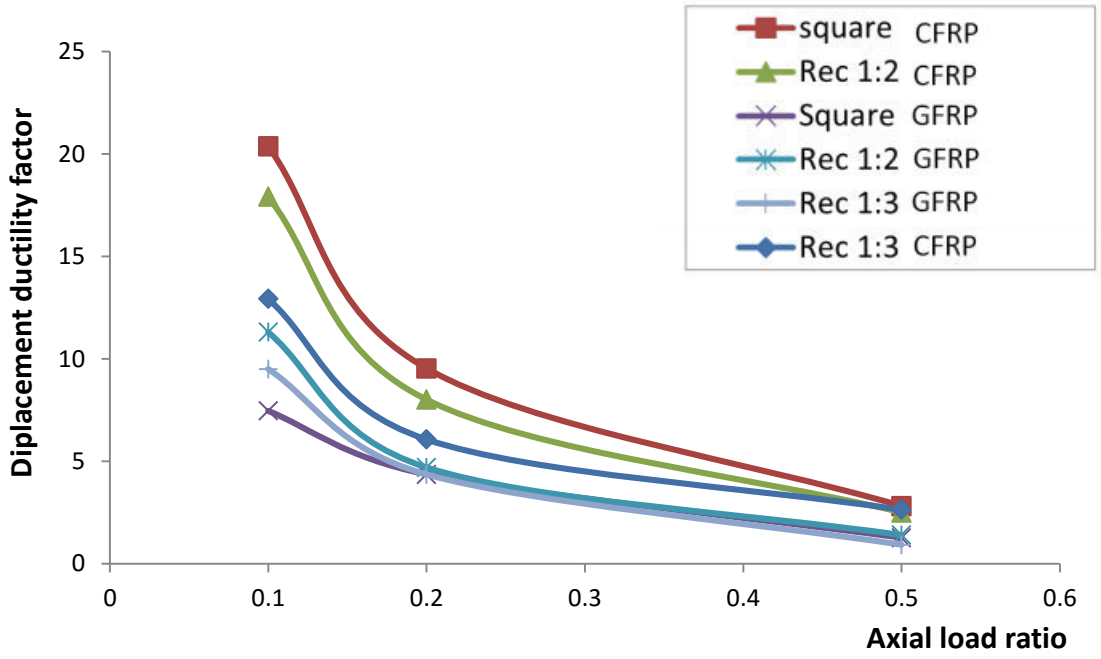

Fig. 5-36 Effect of axial load ratio on displacement ductility factor for different aspect ratio and FRP types at 1mm thickness.

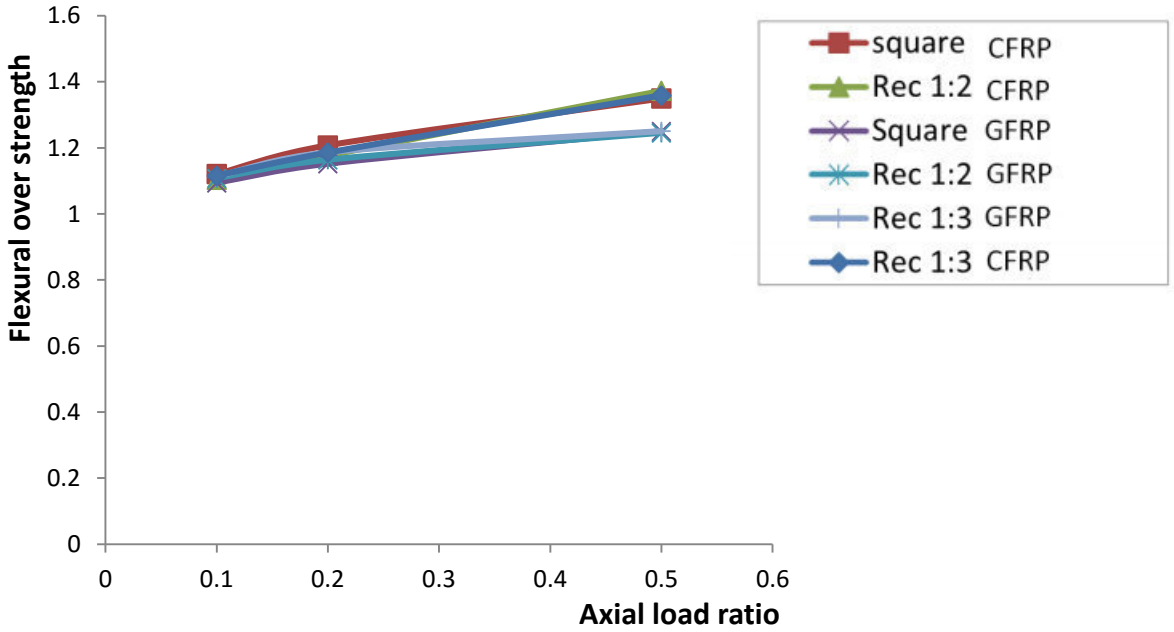

Fig. 5-37 Effect of axial load ratio on flexural over strength for different aspect ratio and FRP types at 1mm thickness.

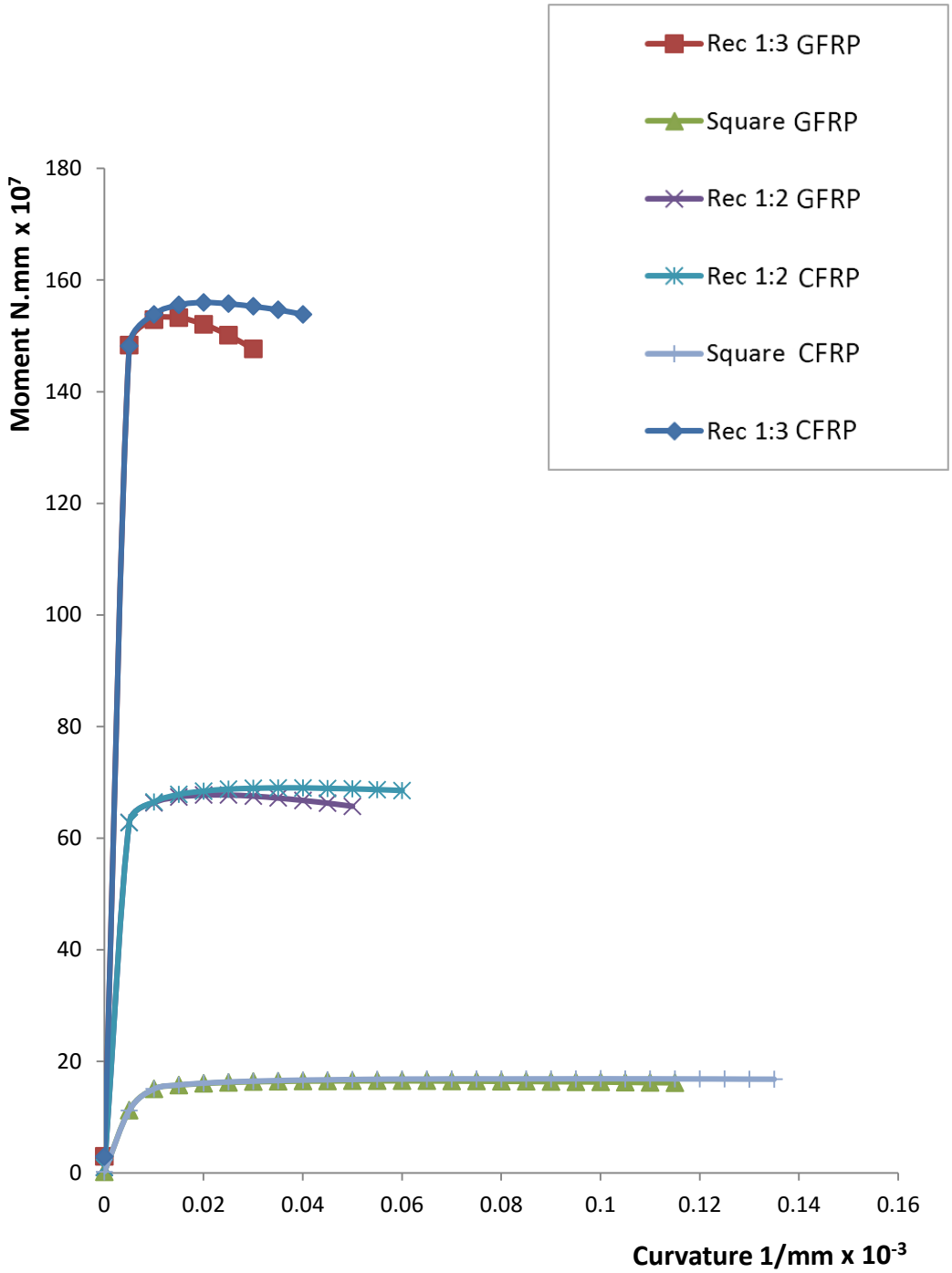

Fig. 5-38 M-phi Diagrams for different FRP types and cross section aspect ratio at axial load ratio = 0.2

Chapter 6

FINITE ELEMENT INVESTIGATION

This chapter presents a finite element investigation of the behavior of columns wrapped with FRP using the general purpose finite element model program ABAQUS. This program enables the construction of models taking into account geometrical and material nonlinearity. This program is used to explore the confinement mechanism in concrete columns wrapped with FRP. Three different configurations are studied. First, a cylindrical short column wrapped with FRP to validate its results with experimental data. Second, a square cross sectioned column wrapped with FRP and subjected to axial loading, as an attempt to explore confinement mechanism in such type of columns. Third, a steel reinforced square cross sectioned column subjected to both axial and lateral loading to compare the results with the numerical model of chapter four.

6.1 Element types

6.1.1 Concrete

Elements used for concrete cylindrical model are C3D6 for the central core and C3D8 for the rest of the cross section. For the other two models, C3D8 is used for the whole model. The C3D8 element is an 8 nodes brick fully integrated general purpose linear brick element .The C3D6 element is a 6 node prism fully integrated element.

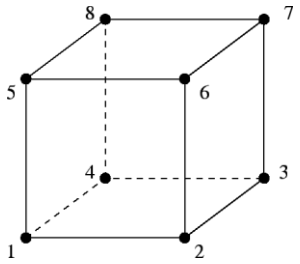

Fig. 6-1 C3D8 3D Brick element structure

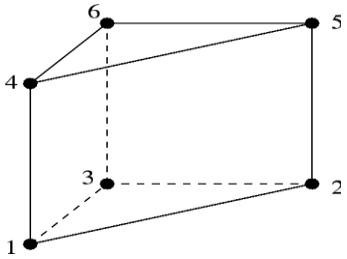

Fig. 6-2 C3D6 3D Prism element

6.1.2 FRP and Steel

FRP is simulated by membrane elements which are used to represent thin surfaces in space that offer strength in the plane of the element but have no bending stiffness. For this purpose M3D4 is chosen which is a 4-node quadrilateral fully integrated membrane element. Steel is simulated using solid C3D8 elements.

6.2 Material properties

6.2.1 Concrete

Modeling of an elastic plastic material, such as concrete is a challenging task. More challenging is to construct a model of confined concrete. Two models were used in the present study to simulate concrete. The first is the smeared cracking material model and concrete damaged plasticity model. The smeared cracking model interprets local cracks effect on a material as a distributed degradation of the material stiffness. This is done by calculations that are performed independently at each integration point of the finite element model. The second model - concrete damaged plasticity model (CDP) is a plasticity theory based model for nonlinear analysis of concrete. The model uses yield criterion. It takes in and considers the change that happens on plastic and elastic stiffness of concrete [3].

6.2.2 FRP and steel

In the first two finite element models (the cylinder and the square specimen), FRP is simulated as an elastic membrane material with an added property to carry no compression as to take into account the orthographic nature of FRP sheet. In The last model, FRP is simulated as a lamina with real FRP orthotropic properties to make sure of an adequate simulation of the FRP as it is compressed and tensioned due to lateral load. Steel used in the third model is simulated as an elastic plastic material.

6.3 Cylinder model wrapped with FRP

The finite element representation is shown in Fig. 6.3. Roller boundary conditions are assigned to the base of the cylinder to make the body free to move radially so confinement comes from only the FRP. The base center is hinged to prevent general body motion. Axial load is applied using displacement control method to the top nodes. This is done to actually simulate the displacement control testing of

concrete samples and to improve convergence.

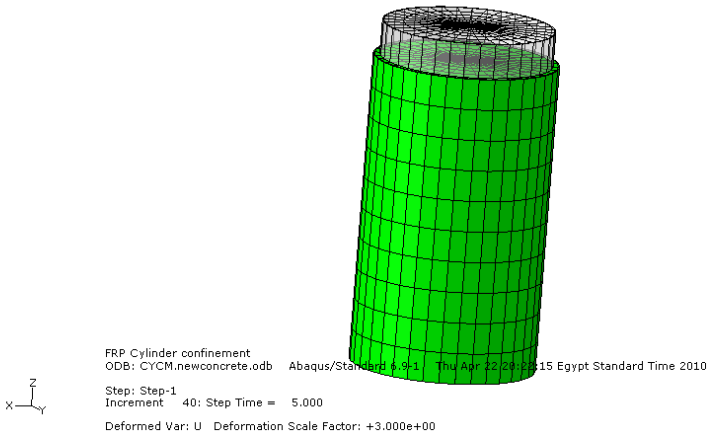

Fig. 6-3 Concrete cylinder wrapped with FRP before and after application of axial load

Results

Stress strain curve of the whole specimen is calculated from ABAQUS results. The stress is calculated by dividing the sum of the reactions of the cylinder by the area of the circular cross section. The strain is extracted by dividing the displacement of the top surface by the total length of the specimen. The comparison is shown in Fig. 6-4.

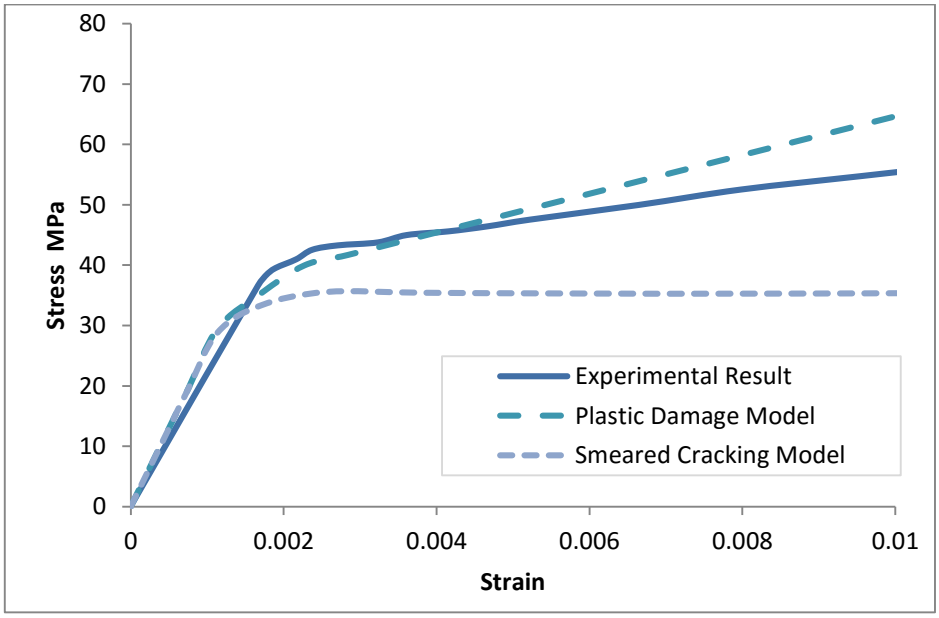

Fig. 6-4 Stress strain curve for the specimen used for validation

The model is compared with published experimental data for a cylinder specimen of 152 mm diameter and 300 mm height. The test specimen is made of concrete with compressive strength of 37 MPa warpped with 2 layers of carbon fibers each of 0.165 mm thickness and modulus of elasticity 230 GPa. It is clear that the CDP model is more accurate in predicting stress strain curve for a concrete cylinder wrapped with FRP.

6.4 Square model wrapped with FRP

Fig. 6-5 shows a square column simulated using ABAQUS for the purpose of investigating and exploring FRP confinement mechanism in rectangular columns. No corner radius is made in order for the sample to be a pure square without shape enhancement.

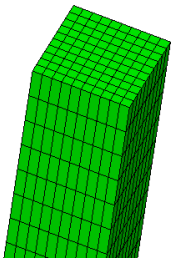

Fig. 6-5 Square column Wrapped with FRP

The concrete is modeled as a CDP material since the cylinder model showed that it is better than smeared cracking model for modeling confined concrete.

Results

Vertical stress distribution is shown in Fig. 6-6 for the confined and unconfined columns. The comparison between the two stress distributions show that the effect of FRP is not only on the stress value but also on stress distribution. While the increase in the vertical load capacity due to confining is also seen in the cylindrical column, the variation in the distribution is seen only on the rectangular column. This is due to the nonuniformity of the confining pressure. This pressure could be represented roughly by the sum of the principal stresses in the plane of the cross-section Fig.6-7. The highly stressed area in the graph represents the effect of the confinement. This roughly matches the effective confinement area used in the developing numerical procedure as shown in Fig.6-8.

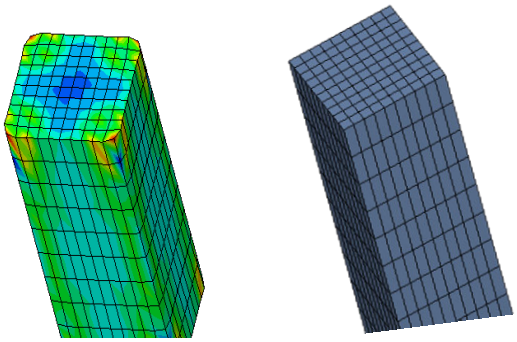

Fig. 6-6 Vertical stress distribution for (a) confined column and (b) unconfined one

This demonstrates the ability of the finite element model to predict the effective confinement area of square concrete columns wrapped with FRP, where the sum of lateral stresses could be plotted to show the regions of high stresses as an indication of the effective confinement area. This could be extended to numerically calculate the efficiency of the confinement.

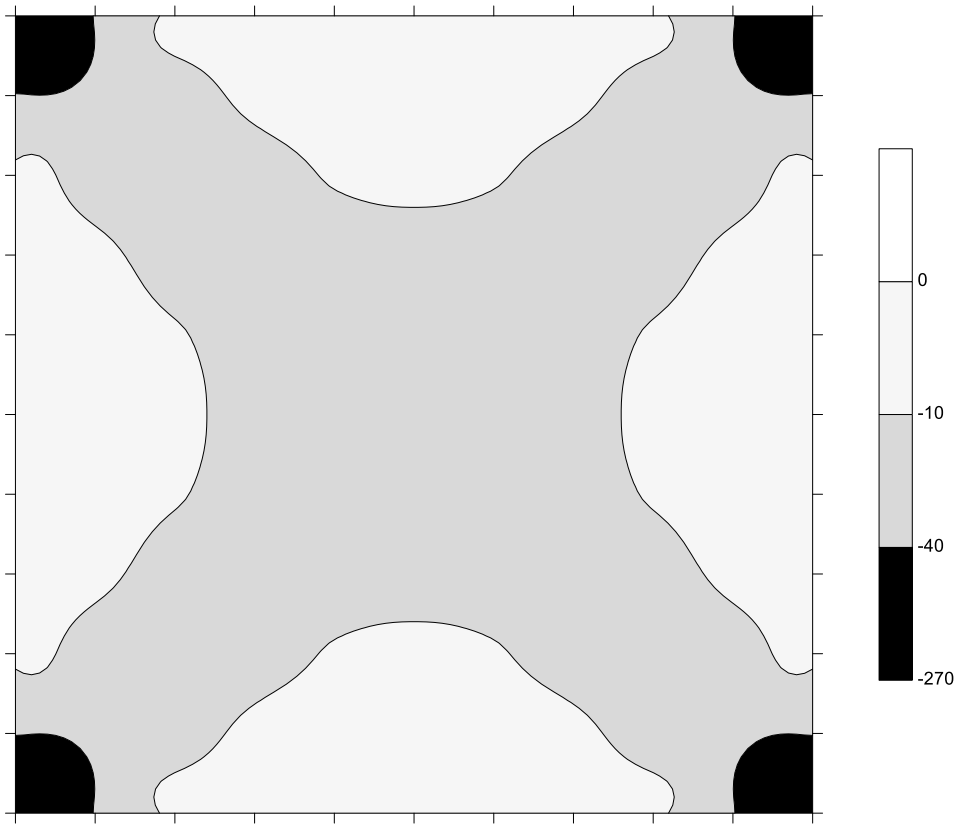

Fig. 6-7 The summation of lateral stresses across the cross section (0➔270 MPa)

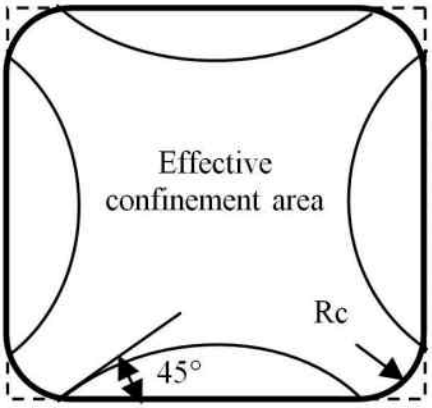

Fig. 6-8 Effectively confined concrete in square column [19]

6.5 Square column subjected to both axial and lateral loads

In this third FE model, a square RC column wrapped with FRP is subjected to axial load first then to lateral displacement to induce bending moment on the column. The FE mesh is partially shown in Fig.6-9 where the four steel reinforcement bars can be seen. The parameters of this column is shown in Table 6-1

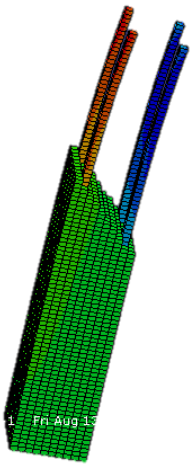

Fig. 6-9 Column subjected to lateral load and confined with FRP

Calculating M-Phi diagram

The M-phi Diagram of the column is plotted in Fig. 6-10 from both the numerical and FE models. The curvature phi is calculated at outer most elements where phi is the difference between axial strain divided by column depth. The bending moment is the lateral load obtained from the base reaction multiplied by column height.

Table 6-1 Proprties of column

Item	quantity	Unit
FRP Young's Modulus	140000	MPa
Steel Young's Modulus	200000	MPa
Concrete compressive strength	39	MPa
Column Side length	250	mm
Column height	1500	mm
Area steel	1250	mm^2
Axial force	70	kN
Steel yield strength	360	MPa
Plastic hinge length	500	mm
FRP thickness	1.5	mm

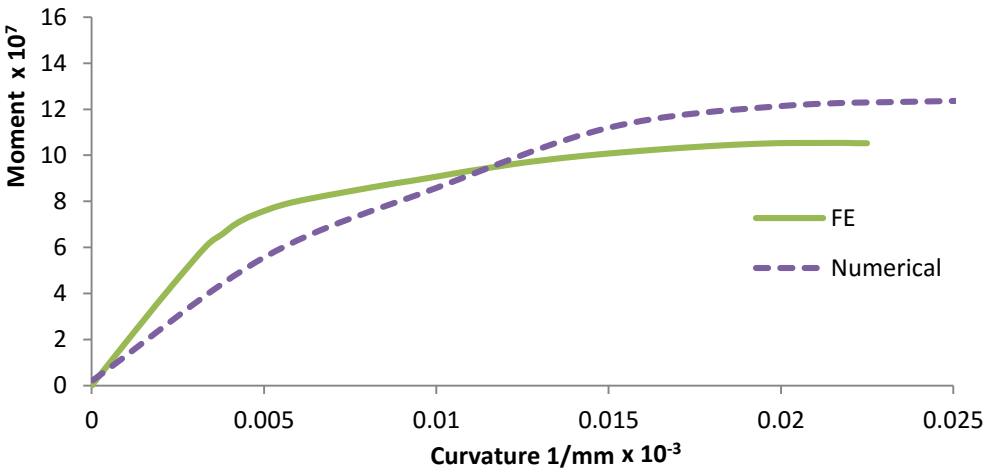

Fig. 6-10 M-phi deduced from numerical and FE element models for the column

The two curves of Fig.6-11 shows a reasonable agreement between the numerical procedure, and FE technique This shows the validity of using either one to obtain an M-phi diagram for a column subjected to axial load and bending moment simultaneously. It should be noted that the concrete mechanical behavior is modeled differently in each technique.

Chapter 7

SUMMARY AND CONCLUSION

7.1 Summary

The retrofit of existing structures has always been a crucial field where civil engineering has to give solutions. In addition to the natural aging and damage of structures and materials, there are many other reasons that make necessary the structural intervention. This research considers FRP as an efficient method of retrofitting.

This research presents an analytical tool to help predicting the level of ductility enhancement of wrapped columns in the form of a computer program written in C language based on Mander's confinement model.

Results are collected from different published experimental analysis performed on rectangular and square columns and used to determine the level of accuracy of the new design approach.

A parametric study is performed to investigate how much ductility and flexural strength is affected by concrete compressive strength, columns cross sectional shape (square-rectangular), thickness of the jacket, longitudinal reinforcement ratio, axial load level and type of FRP (CFRP or GFRP).

A Finite element analysis is performed for three separate models to study and investigate confinement effect on different types of concrete columns wrapped with FRP.

7.2 Conclusion

A numerical analysis model for FRP wrapped rectangular and square columns is presented in this study. The model is capable of predicting the enhancement of the seismic behavior of columns retrofitted using FRP jackets. The model is validated through comparisons with published experimental results. Such comparisons show that the proposed procedure is reliable and can be used as an effective tool in the design of rectangular and square columns confined with FRP.

Results of the parametric study lead to the following conclusions:

- For the same thickness and type of FRP jacket, normal strength confined concrete columns display better flexural ductility than comparable high strength concrete columns subjected to similar axial load level.
- The improved seismic performance of fiber-reinforced polymer-wrapped reinforced concrete results mainly from the ability of the column sections at the plastic hinge zone to develop greater compressive strains in the concrete before failure.
- Columns with high longitudinal steel reinforcement ratio need to be wrapped with more thickness of FRP to maintain same ductility of those with low longitudinal steel reinforcement ratio. This is due to the fact that as the longitudinal steel reinforcement ratio increases; the depth of the neutral axis increases, resulting in failure of the extreme concrete compression fibers at smaller curvatures.
- The FRP composite jacket retrofits for flexural rectangular columns performed very effective in enhancing their seismic performance through confining the plastic hinge region. Due to the fact that the depth of the compression zone in flexural rectangular columns is weakly dependent on the degree of rectangularity of the columns, there was no noticeable difference between rectangular columns of aspect ratio 2 and 3.
- Increasing the thickness of the FRP jacket resulted in improvement in ductility and energy dissipation capacity of the retrofitted columns. The effect of the increase of the jacket thickness on the values was less than proportional.
- Due to the fact that CFRP has higher stiffness and strength than GFRP polymer, columns retrofitted with CFRP exhibited better seismic in terms of ductility and load displacement when compared to GFRP thickness or more.

The higher values of the increasing confinement action of the elastic CFRP limits the lateral strain (concrete dilation), thus delaying degradation.

A Finite element analysis is held to investigate the behavior of columns retrofitted with FRP. This is done through constructing three models:

- Cylindrical model which is validated by comparison with experimental data.
- Square cross sectioned column model done to investigate the behavior of square column confined with FRP regarding confinement effective area. It shows that the model is successful to predict the shape of effective confinement area of square columns wrapped in FRP.
- Concrete column wrapped with FRP to the height of the plastic hinge subjected to axial and lateral displacement is modeled as an attempt to predict moment curvature diagram and compare it to the moment curvature diagram predicted by the numerical procedure where the two approaches shows reasonable agreement.

Recommendations

Based on the study presented in this thesis it is recommended for further studies to:

Develop the numerical procedure to include various column shapes and different ties configurations.

Experimental analysis must be made to identify values of different parameters needed for the accurate simulation of concrete columns wrapped with FRP.

REFERENCES

1. Konstantinos Georgiou Megalooikonomou, Modelling Of Frp-Confinement Of Rectangular Rc Sections (2007) Master thesis European School Foradvanced Studies In Reduction Of Seismic Risk

2. ACI Code, "Building Code Requirements for Reinforced Concrete (ACI-318-02)," American Concrete Institute, Detroit, (2002).

3. Dassault Systèmes Simulia Corp., Abaqus Analysis User's Manual, Version6.9

4. Gabor Lorant, FAIA (2012) "Seismic Design Principles" whole building design guide"

5. Richart, F.E., Brandtzaeg, A., and Brown, R.L. (1928). "A Study of the Failure of Concrete under Combined Compressive Stresses." Bulletin No. 185, Univ. of Illinois, Engineering Experimental Station, Urbana, Illinois.

6.Kupfer, H., H. K. Hilsdorf, and H. Rusch [1969]"Behaviour of concrete Under Bi-axial stress" journal, American Concrete institute, Vol 66

7. Priestley, M.J.N., Seible, F. and Calvi, G.M. (1996), Seismic Design and Retrofit of Bridges, John Wiley and Sons, Inc.,.

8. Sun, Z., F.seible , and M.j.n. priestley , Flexural Retrofit of Rectangular Reinforced Concrete Bridge Column by Steel Jacketing , Structural Systems Research Project Report SSRP-90/07 , University of California , San Diego February 1993 ,215 pp.

9. Hatem Mohamed Abdel-Aal Seliem [2002]"Seismic retrofit of reinforced concrete columns Using Fiber-Reinforced polymers" Master thesis Cairo university

10. Memon, M., and Sheikh, S., (2005), "Seismic Resistance of Square Concrete Columns Retrofitted with Glass Fiber-Reinforced Polymer," ACI Structural Journal, V. 102, No. 5, Sept.-Oct., pp. 774-783.

11. Richard D. Iacobucci, Shamim A. Sheikh, and Oguzhan Bayrak (2003) , Retrofit of Square Concrete Columns with Carbon Fiber-Reinforced Polymer for Seismic Resistance . Aci Structural journal V. 100 issue 6.

12. Priestley, M.J.N.,F.Seible, Design of Seismic Retrofit Measures for concrete and Masonary Structures .1995

13. Priestley, M.J.N., Seible, F. and Fyfe, E. (1993b). Column Retrofit Using Pre-stressed Fiberglass/Epoxy Jackets, In: Proceedings of 1993 FIP Symposium, pp. 147–160, Kyoto, Japan.

14. Hossam Sherif Alalily [2011] "Retrofit of reinforced concrete columns by composite jacketing" Master thesis Arab Academy for scince and technology and maritime transport.

15. Mander, J. B., Priestley, M. J. N., and Park R., (1988a) “Theoretical Stress-Strain Model for Confined Concrete,” Journal of the Structural Engineering, ASCE, Vol. 114, No. 8, pp. 1804-1826.

16. Wang, Y. C., and Restrepo, J. I., (2001)“Investigation of Concentrically Loaded Reinforced Concrete Columns Confined with Glass FRP Jackets,” ACI Structural Journal, , Vol. 9, No. 3, 377-385.

17. Pantazopoulou, S. J., and Mills, R. H., (1995)“Microstructural Aspects of the Mechanical Response of Plain Concrete,” ACI Material Journal Vol. 92, , pp. 605-616.

18. Spoelstra, M. R., and Monti G., (1999) “FRP-Confined Concrete Model,” Journal of Composites for Construction, ASCE, Vol. 3, No. 3, , pp. 143-150.

19. Benzaid, R Mesbah, H & chick, N.E (2010). FRP confined concrete cylinders: Axial compression experiments and strength model .journal of reinforced plastics and composites, 29(16), 2469-2488